Inaugural dissertation

for

obtaining the doctoral degree

of the

Combined Faculty of Mathematics, Engineering and Natural Sciences

of the

Ruprecht - Karls - University

Heidelberg

Presented by

M.Sc. Fabian Rose

born in: Frankfurt am Main

Oral Examination: 15th February 2023

A pan-cancer long non-coding RNA (lncRNA) signature defines oncogene activity in blood serum of cancer patients

Referees: Prof. Dr. Peter Angel

PD Dr. Kai Breuhahn

Abstract

Tumor-derived material in blood samples is informative concerning molecular alterations in respective tumor tissues. Thus, biomarkers detected by liquid biopsy can guide clinicians in designing personalized therapies and moreover may serve as a proxy for treatment response and success. However, robust biomarkers for the detection of aberrant oncogene activity in tumor cells and the identification of druggable target structures are difficult to define.

To illustrate the applicability of RNA signatures as cancer-spanning biomarkers, I established an *in vitro* screening approach integrating RNA-seq data from siRNA screens, publicly available ChIP-seq data as well as patient expression data from different tumor entities. As exemplified for the Hippo pathway, a 4-gene long non-coding RNA (lncRNA) signature consisting of CYTOR, MIR4435-2HG, SNHG1, and SNHG17 was defined that is transcriptionally controlled by the YAP/TAZ/TEAD complex. This 4-lncRNA signature represents a robust predictor of YAP activity in several tumor types such as liver or lung cancer and its overexpression is statistically associated with poor clinical outcome. *In vitro* experiments showed that lncRNA signature constituents themselves contribute to the tumor-promoting properties of the Hippo/YAP/TAZ pathway. Furthermore, murine orthologues of these lncRNAs were overexpressed in YAP^{S127A} transgenic mouse livers and lncRNA signature levels were elevated in a subgroup of human cancer tissues and serum samples. Importantly, nuclear YAP accumulation in human liver cancer tissues is significantly associated with YAP-dependent lncRNA abundance in the serum of these patients. Moreover, the signature defines responsiveness of tumor cells to YAP-directed-pharmacological inhibition.

These results let me draw the following conclusions: First, lncRNA-based approaches broaden previous liquid biopsy concepts by allowing the detection of potential druggable oncogene activity in the tumor. Second, lncRNAs represent robust and sensitive biomarkers to identify patients eligible for specific oncogene-directed therapies and to monitor treatment response. Third, the lncRNA signature constituents themselves support tumorigenesis in a multi-modal manner. Fourth, the YAP/TAZ/TEAD complex represents a promising target structure to inhibit YAP/TAZ activity. Lastly, YAP and TAZ may play different roles in regulating lncRNA expression depending on the cellular context.

Thus, my data underline that liquid biopsy-based detection of pan-cancer lncRNA signatures can define oncogene activity in tumor cells. I therefore conclude that serum lncRNA signatures represent novel and powerful tools for diagnostics, therapy design, as well as for monitoring treatment success.

Zusammenfassung

Blutproben können Aufschluss über molekulare Veränderungen in den Tumorzellen des Krebspatienten geben. Somit kann eine auf Blut-basierende Analytik Ärzte bei der Zusammenstellung personalisierter Therapien unterstützen und darüber hinaus als Indikator für das Ansprechen auf eine Behandlung genutzt werden. Zurzeit gibt es jedoch keine robusten (Serum-) Biomarker für den Nachweis einer erhöhten Aktivität von z.B. Onkogenen in Tumorzellen.

Um die Anwendbarkeit von langen nicht-kodierenden RNA (lncRNA)-Signaturen als Biomarker für verschiedene Tumorentitäten zu untersuchen, habe ich einen *in-vitro* Screening Ansatz entwickelt, der experimentelle RNA-Seq Daten, öffentlich verfügbare ChIP-Seq-Resultate sowie Expressionsdaten von Patienten verschiedener Tumorentitäten kombiniert. Am Beispiel des Hippo-Signalwegs habe ich eine 4-lncRNA-Signatur bestehend aus CYTOR, MIR4435-2HG, SNHG1 und SNHG17 identifiziert, welche durch den Hippo Signalweg kontrollierten YAP/TAZ/TEAD-Komplex transkriptionell reguliert wird. Diese 4-lncRNA-Signatur stellt einen robusten Prädiktor für YAP-Aktivität in verschiedenen Tumortypen wie z.B. Leber- und Lungenkrebs dar. Zusätzlich ist das Vorhandensein dieser Signatur in Patientenproben statistisch mit einer schlechten klinischen Prognose verbunden. *In vitro*-Experimente zeigen, dass die einzelnen lncRNAs der Signatur selbst z.B. die Tumorzellproliferation unterstützen. Darüber hinaus sind murine Orthologe einzelner lncRNAs in einem transgenen Mausmodell mit Zelltyp-spezifischer Überexpression von konstitutiv aktivem YAP^{S127A} nachweisbar. In einer Subgruppe von Leberkrebspatienten liegt die lncRNA-Signatur in vitalem Leberkrebsgewebe als auch in Serumproben erhöht vor. Ein zentrales Resultat dieser Arbeit ist, dass das Vorhandensein der lncRNA-Signatur im Serum von Leberkrebspatienten mit der Aktivität des Onkogens YAP im zugehörigen Tumorgewebe korrelierte. Außerdem charakterisiert das Vorhandensein der lncRNA Signatur die Sensitivität von Tumorzellen gegenüber einer pharmakologischen Inhibierung des von YAP.

Diese Ergebnisse lassen mich die folgenden Schlussfolgerungen ziehen: Erstens erweitern lncRNA-basierte Ansätze die bisherigen Konzepte der „liquid biopsy", indem sie den Nachweis potenziell behandelbarer Onkogenaktivität im Tumor ermöglichen. Zweitens stellen lncRNAs robuste und empfindliche Biomarker dar, um Patienten zu identifizieren, die für spezifische Onkogen-gerichtete Therapien in Frage kommen, und um das Ansprechen auf die Behandlung zu überwachen. Drittens unterstützen die einzelnen Signatur lncRNAs selbst die Onkogenese auf vielfältige Weise. Viertens stellt der YAP/TAZ/TEAD-Komplex eine vielversprechende Zielstruktur zur Hemmung der YAP/TAZ-Aktivität dar. Und schließlich können YAP und TAZ je nach zellulärem Kontext unterschiedliche Rollen bei der Regulierung der lncRNA-Expression spielen.

Zusammengenommen unterstreichen diese Daten, dass der „liquid biopsy"-basierte Nachweis von lncRNA-Signaturen in verschiedenen Tumorentitäten als robustes Korrelat für die Aktivität eines Onkogens in Tumorzellen darstellen kann. Daraus schließe ich, dass eine sensitive Messung von lncRNA-Serumsignaturen eine neuartige und leistungsstarke Technik für Diagnostik, die Anpassung von Therapien als auch die Überwachung des Behandlungserfolgs darstellen kann.

Table of Contents

List of abbreviations

ACC	Adrenocortical carcinoma
ANKRD1	Ankyrin repeat domain 1
APS	Ammonium persulfate
ASAP	Automated Slide Analysis Platform
ATCC	American Type Culture Collection
BSA	Bovine serum albumin
CCLE	Cancer Cell Line Encyclopedia
ChIP	Chromatin immunoprecipitation
ChIP-seq	ChIP sequencing
cfDNA	Cell-free DNA
cfRNA	Cell-free RNA
CIN25	Chromosomal instability gene signature
CL	Cirrhotic liver
COAD	Colon adenocarcinoma
CSC	Cancer Stem cells
CTC	Circulating tumor cells
ctDNA	Circulating tumor DNA
CTGF	Connective tissue growth factor
CYR61	Cysteine-rich angiogenic inducer 61
CYTOR	Cytoskeleton regulator RNA
DLEU1	Deleted in lymphocytic leukemia 1
DMEM	Dulbecco's Modified Eagle's Medium
DMSO	Dimethyl sulfoxide
DSMZ	German Collection of Microorganisms and Cell Cultures
ESCA	Esophageal carcinoma
FCS	Fetal calf serum
FDA	Food and Drug Administration
FFPE	Formalin-fixed paraffin-embedded
FTX	FTX transcript XIST regulator
GPCR	G protein-coupled receptor
HCC	Hepatocellular carcinoma
HE	Hematoxylin and eosin
IHC	Immunohistochemistry
JCRB	Japanese Collection of Research Biosources
KIRC	Renal clear cell carcinoma

LATS1/2	Large tumor suppressor kinase 1/2
LLC	Large-cell lung carcinoma
lncRNA	Long non-coding RNA
LUAD	Lung adenocarcinoma
MEM	Minimum Essential Medium
MIR4435-2HG	MIR4435-2 host genes
miRNA	MicroRNA
MST1/2	Mammalian STE20-like protein kinase 1/2
ncRNA	Non-coding RNA
NGS	Next-generation sequencing
NL	Normal liver
NSCLC	Non-small cell lung cancer
PAGE	Polyacrylamide gel electrophoresis
PBS	Phosphate buffered saline
Pei	Polyethylenimine
qPCR	Semi-quantitative real-time PCR
RPMI	Rosewell Park Memorial Institute 1640
RNAi	RNAinterference
RNA-Seq	RNA sequencing
ROC	Receiver operating characteristics
SCC	Lung squamous cell carcinoma
SDS-PAGE	Sodium dodecyl sulfate polyacrylamide gel electrophoresis
siCo	Nonsense siRNA
siRNA	Small interfering RNA
SNHG1/17	Small nucleolar RNA host gene 1/17
snoRNA	Small nucleolar RNA
TAZ/WWTR1	WW domain containing transcription regulator 1
TBS	Tris buffered saline
TCGA	The Cancer Genome Atlas
TEAD	TEA domain family
TKI	Tyrosine kinase inhibitor
TMA	Tissue microarray
UCEC	Uterine endometrial carcinoma
WT	Wildtype
YAP	Yes-associated protein

List of Figures

List of Tables

1 Introduction

1.1 Precision Medicine

1.1.1 Overview

In recent years, precision medicine has received increasing attention regarding diagnostic sensitivity and personalized treatment. The term was introduced and shaped by The National Research Council[1] and describes how disease taxonomy at higher resolution can enable the design of more customized treatment strategies for individuals and patient groups[2]. For this, precision medicine focuses on the patient's specific genetic/molecular, clinical, and environmental background[3].

Although disease-causing mechanisms have been studied for many years, most clinical practice still follows a "one-size-fits-all" strategy. For example, in oncology, histopathological methods are used to diagnose and estimate the prognosis of patients, while treatment often relies on surgical tumor resection with subsequent radiation and/or chemotherapy to prevent tumor recurrence[4,5]. Nevertheless, the development of highly sensitive "next-generation" technologies, thereby leading to more accurate classification of diseases has facilitated the introduction of first precision medicine techniques to the clinics[6]. For instance, the tyrosine kinase inhibitor mobocertinib has recently been approved by the US Food and Drug Administration (FDA) to target non-small cell lung cancer (NSCLC) patients with EGFR exon 20 insertion mutations[7]. Another example is the combinational therapy using ivacaftor and lumacaftor to treat cystic fibrosis patients with the common Phe508del mutation[8]. Lastly, olaparib has been approved for the treatment of BRCA1- or BRCA2-mutated breast cancer patients[9].

1.1.2 Identification and detection of biomarkers

The accurate stratification of patients is essential to enable personalized treatment with therapeutic success. To achieve this, there is a need for robust and sensitive biomarkers. By definition, a biomarker represents a read-out that defines specific biological/pathogenic processes or is an indicator for the response to certain exposures[10].

The introduction of "next generation" technologies has facilitated and accelerated the identification of novel biomarkers. Large-scale genomic studies advanced the molecular characterization of diseases and identified proteomic, transcriptomic, and genomic aberrations. Here, data repositories, such as the Geo database, made these data publicly

accessible for integrative data analyses[11]. In addition, consortia e.g., the Cancer Genome Atlas (TCGA) research network, have provided high-dimensional data, which enables patient classification and the identification of novel disease biomarkers in tumor tissue[12].

Considering the detection of these biomarkers, tissue biopsy still represents the gold standard for diagnostics. However, tissue-based approaches face multiple biological and technological challenges, which substantially hamper their applicability in precision medicine[13]. First, the analysis of multiple tumor specimens obtained from the same patient revealed spatial and temporal heterogeneity of the tumor, which complicates the stratification of patients[14]. Second, monitoring disease dynamics and treatment response is not feasible due to the invasive procedures necessary to repeatedly sample tumor tissue[15]. Lastly, limitations such as poorly accessible tumors, high total costs of the medical procedure and patient recovery, and bad clinical condition of patients may hinder the application of tissue biopsy[13,16].

1.1.3 Liquid biopsy

To overcome these challenges, liquid biopsy has recently gained increasing attention as a novel diagnostic and molecular tool in the field of precision medicine. Liquid biopsy describes the sampling and analysis of tumor-derived components in biological fluids intending to capture a broader picture of the genomic landscape of a patient's tumor[17]. In contrast to tissue biopsy, it is a minimally invasive and highly sensitive technique that can be used to serial monitor treatment response and disease dynamics[18,19]. Tumor-derived material that can be assessed by liquid biopsy include circulating tumor cells (CTCs)[20]; cell-free DNA (cfDNA)[21]; and less frequently cell-free RNA (cfRNA), mainly microRNAs (miRNAs) and long non-coding RNAs (lncRNAs)[22]; extracellular vesicles, such as exosomes[23]; proteins; and metabolites[24] (Figure 1). Here, liquid biopsy research has mainly focused on the detection of blood-based biomarkers[25]. However, recent studies indicate that other biological fluids, such as urine[26], stool[27], saliva[28], and cerebrospinal fluid[29] also contain tumor-derived components.

Among the first liquid biopsy markers that were introduced to routine diagnostics were alpha-fetoprotein for the early diagnosis of hepatocellular carcinoma (HCC)[30] and prostate-specific antigen for the early detection of prostate cancer[31]. However, concerns about their sensitivity and specificity, highlight the demand for more robust and reliable liquid biopsy markers[32,33]. Since then, only a few approaches have been implemented in clinical practice e.g., the detection of RAS/BRAF/EGFR mutations in plasma cfDNA from colorectal cancer patients[34]; screening for methylated Septin 9 cfDNA in plasma from colorectal cancer patients[35]; and monitoring the mutational status of EGFR cfDNA in lung cancer patients[36]. Regarding the latter, the FDA recently approved the first diagnostic test combining next generation sequencing (NGS) and liquid biopsy for the identification of EGFR mutations in lung cancer

patients[37]. Unfortunately, several liquid biopsy approaches could not demonstrate clinical utility due to their lack of robustness and predictive power[38]. This illustrates the necessity to develop reliable and cost-effective methods and techniques that are suitable for the detection of biomarkers in body fluids.
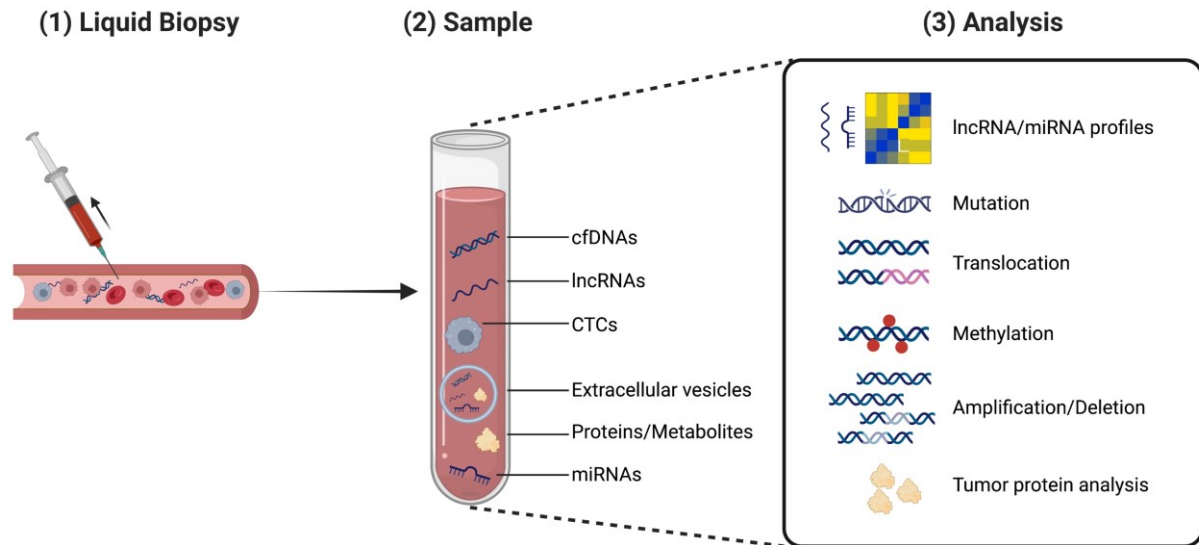
Figure 1 | Liquid biopsy markers. Liquid biopsy encompasses the detection of different tumor-derived materials, including cfDNA, cfRNA (lncRNAs and miRNAs), CTCs, extracellular vesicles, proteins, and metabolites. Each of these biomarkers can provide different levels of information: cfDNA, especially circulating tumor DNA, contains information about mutations, deletion and amplifications, translocations, and methylation patterns; lncRNA/miRNA expression patterns represent a proxy for tumor-specific aberrations; CTCs provide genomic, transcriptomic, and proteomic information; extracellular vesicle components represent a "molecular fingerprint" of tumor cells; and quantitative measurement of single tumor-derived proteins or protein panels provides valuable prognostic and diagnostic information. For further details see text[39].

1.2 Long non-coding RNAs (lncRNAs)

1.2.1 Definition, classification, and function

In the early 2000s, studies demonstrated that approximately 70% of the human genome is transcribed, but only around 2% of the genome has protein-coding capabilities[40-42]. The larger share of transcribed sequences can be divided into classical housekeeping RNA species and regulatory non-coding RNAs (ncRNAs). Housekeeping ncRNAs include transfer RNAs, ribosomal RNAs, small nuclear RNAs, and small nucleolar RNAs (snoRNAs), which are constitutively expressed and are involved in many cellular processes. The group of regulatory

ncRNAs is subdivided according to their size into short ncRNAs (< 200 nt) and lncRNAs (> 200 nt)[43]. Among the group of small ncRNAs are miRNAs, small interfering RNAs (siRNAs)[44], and Piwi-associated RNAs[45], which have been extensively studied concerning their biogenesis, cellular function as well as role in cancer development[46,47].

In contrast, lncRNAs represent the most transcribed regulatory ncRNA species but have only recently emerged as a major class of eukaryotic transcripts[48]. Due to their broad definition, lncRNAs constitute a large and heterogeneous group of RNA molecules that are usually spliced, capped, and polyadenylated similar to mRNAs[49]. But in comparison to protein-coding RNAs, the majority of lncRNAs (78%) are considered highly tissue-specific[50]. In addition, lncRNAs show a low degree of conservation among mammalian species. For example, only 39% and 38% of orthologous transcripts were found in cows and mice, respectively[51]. Based on their chromosomal location, lncRNAs are classified into five broad categories: (1) divergent; (2) sense; (3) intergenic; (4) intronic; or (5) antisense[52] (Figure 2).

The number of functional lncRNAs is still unclear. However, increasing evidence regarding disease- and tissue-specific expression of lncRNAs indicates that they play an important role in cellular processes. Indeed, their mode of action can be divided into four categories: signal, scaffold, guide, and decoy[53]. As signal molecules, lncRNAs alone or in combination with proteins, such as transcription factors, mediate target gene expression. For instance, the p53-dependent lncRNA-p21 interacts with hnRNP to repress p53-induced transcriptional responses[54]. As scaffolding molecules, lncRNAs can enable the assembly of macromolecule complexes by facilitating the recruitment and interaction of proteins[55]. One example is the Xist lncRNA, which interacts with the PRC1 and PRC2 complexes to inhibit the expression of one X chromosome in females[56]. In their role as guiding molecules, lncRNAs aid specific proteins to find their target location so that they can exert their biological functions. This mainly applies to the recruitment of transcription factors to the promotor region of a specific gene. For example, LINC00649 recruits TAF15 to the MAPK6 promotor inducing MAPK6 gene expression, which leads to the activation of MAPK signaling[57]. Lastly, lncRNAs can also act as decoy molecules to impair the function of specific proteins, such as transcriptional regulators or chromosome-folding proteins. For instance, the lncRNA PANDA interacts with the nuclear transcription factor NF-YA thereby limiting the expression of pro-apoptotic genes[58]. In addition, lncRNAs can affect mRNA abundance on a post-transcriptional level by sponging miRNAs. As a result, miRNAs can no longer bind to their target mRNAs, which indirectly upregulates their expression. For example, the pseudogene PTENP1 shows decoy activity by competing for the same miRNAs as its corresponding protein-coding gene PTEN[59].
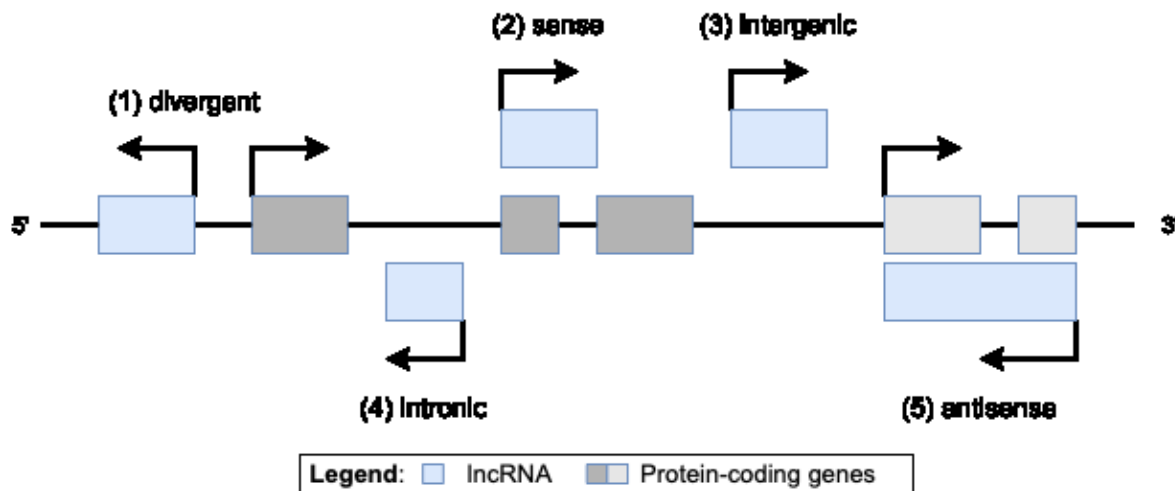
Figure 2 | Classes of lncRNAs. lncRNAs are classified according to their chromosomal location and orientation. (1) Divergent lncRNAs are in proximity of the promoter region of a protein-coding gene but are transcribed in the opposite direction. (2) Sense lncRNAs are transcribed from the same strand and in the same direction as protein-coding genes. (3) Intergenic lncRNAs are located between two protein-coding genes. (4) Intronic lncRNAs are located in intronic regions of a protein-coding gene. (5) Antisense lncRNAs are transcribed from the opposite strand and in the opposite direction as protein-coding genes. Adapted from[52].

According to the lncRNADisease v2.0 database, which is a comprehensive repository of experimentally supported lncRNA-disease associations, there are more than 500 diseases associated with lncRNAs[60]. For instance, the lncRNA BACE1-AS is upregulated in patients with Alzheimer's disease. Elevated levels of BACE1-AS results in increased abundance of the corresponding protein BACE1, which is a crucial enzyme driving Alzheimer's disease pathophysiology[61]. Another example is the aberrant expression of lncRNA in patients with diabetes mellitus. Transcriptomic profiling revealed > 1100 pancreatic islet-specific lncRNAs, of which some are dysregulated in type 2 diabetes and relevant to β cell programming and diabetes pathophysiology[62].

Taken together, lncRNAs play a crucial role in many cellular processes and their deregulation is associated with different disease phenotypes.

1.2.2 lncRNAs in cancer

Studies have demonstrated that many lncRNAs are aberrantly expressed in tumors and are directly involved in oncogenic processes, such as resisting cell death, sustaining proliferation, and activating invasion[63]. As described in the previous part, they can impact gene expression at an epigenetic, transcriptional, and post-transcriptional level and thus can play important roles in the development and progression of cancer.

Introduction

As epigenetic modulators, lncRNAs have two modes of action how to induce tumor cell formation: *cis*- and *trans*-gene regulation[63]. *Cis*-acting lncRNAs affect the expression of proximally located genes. One example is the silencing of the INK4b/ARF/INK4a tumor suppressor locus by the corresponding antisense lncRNA ANRIL leading to increased cell proliferation. ANRIL is required for the recruitment of the PRC1 and PRC2 complexes, which leads to the repression of this gene cluster by histone 3 trimethylation[64,65]. Accordingly, aberrant expression of ANRIL is associated with several types of cancer[66]. In contrast, *trans*-acting lncRNAs regulate the expression of genes located on different chromosomes. For instance, the lncRNA HOTAIR likewise interacts with the chromatin repressor complex PRC2 and LSD1 to silence specific distantly located genes, leading to metastasis[67]. HOTAIR is deregulated in multiple cancer types[68] and represents an adverse prognostic marker in breast cancer patients[69].

While some lncRNAs directly affect the expression and activity of oncogenes and tumor suppressor genes, they themselves can support/prevent tumor cell progression via tumor-cell intrinsic mechanisms. An example for the former is the tumor suppressor p53, which regulates the expression of numerous lncRNAs[54]. These p53-dependent lncRNAs are a part of a positive feedback loop that modulates and enhances the p53 transcriptional network promoting apoptosis signaling upon DNA damage. Their expression is downregulated in colorectal cancer and thereby displays a tumor suppressor signature with high predictive power[70]. An example for oncogene activity-modulating lncRNAs represents CCAT1, which enhances the expression of the proto-oncogene MYC by chromatin looping[71]. In addition, MYC-dependent lncRNAs, such as ELFN1-AS1, are upregulated in colorectal cancer and are involved in the silencing of cell-cycle-relevant genes[72].

Furthermore, lncRNAs can induce tumor formation on a post-transcriptional level by regulating the splicing, export, and translation of mRNAs and by directly modifying proteins[73]. An example is the natural antisense transcript of ZEB2 (NAT ZEB2), which promotes the splicing of a ZEB2 mRNA transcript with an additional internal ribosome entry site (IRES). This alternative mRNA isoform leads to enhanced ZEB2 protein translation and thus decreased E-cadherin expression, which causes impaired cell proliferation and invasion. Increased NAT ZEB2 expression has been associated with tumors that show aberrant ZEB2 activity[74].

As previously reported, lncRNA can also act as miRNA sponges, thereby reducing their effect on target mRNAs. One example is the regulation of the tumor suppressor PTEN by its pseudogene lncRNA PTENP1[59]. PTENP1 is downregulated in melanoma, which leads to increased repression of PTEN resulting in profound consequences on tumor progression[75].

Together, these findings demonstrate that aberrant expression of lncRNAs is detectable in many cancer types and that these molecules can directly and indirectly affect tumor development and progression.

6

1.2.3 lncRNAs in liquid biopsy

The differential expression of lncRNAs in tumor tissues makes them a valuable tool for the diagnosis and prognosis of cancer. In addition, due to their tumor- and tissue-specific expression, lncRNAs can be used to identify unknown primary tumors or to distinguish between subtypes of the same cancer entity[76]. Especially in the field of liquid biopsy, they represent promising circulating biomarkers: First, they exhibit high stability while circulating in body fluids due to extensive secondary structures[67], stabilizing post-translational modifications, poor sensitivity towards nuclease-mediated degradation, and protection by exosomes[77]. For instance, it has been shown that plasma-derived lncRNAs remain stable despite multiple freeze-thaw cycles and prolonged exposure to RT or 45°C[78]. Second, the dysregulation of lncRNA in primary tumor tissues is mirrored in corresponding body fluids[79]. For example, the lncRNA MALAT1 is overexpressed in multiple cancer entities, including liver, breast, lung, and prostate[80,81]. It was later shown that this upregulation of MALAT1 was reflected in plasma samples and could predict the presence of NSCLC and prostate cancer with a specificity of 96% and 84.8%, respectively[82,83]. So far, liquid biopsy research has mainly focused on the detection of CTCs and cfDNAs. However, because of their relatively low abundance in body fluids, especially in the early stages of cancer development, as well as their heterogeneity, lncRNAs may represent a more reliable type of circulating biomarker[84].

Individual prognostic circulating lncRNAs, such as HOTAIR for colorectal cancer[85], GIHCG for renal cell carcinoma[86], and UCA1 for HCC[87], have been identified and can distinguish cancer patients from healthy individuals with high specificity. However, their diagnostic potential remains limited due to relatively poor sensitivity. As one example, circulating MALAT1 can identify NSCLC patients with high specificity of 96%, but only correctly identifies cancer patients with a sensitivity of 56%[82]. Thus, MALAT1-based liquid biopsy tests may create numerous false-negative results as cancer samples may not be detected. In contrast, other circulating lncRNAs, such as H19[88], HULC[89], and GACAT2[90] for gastric cancer, have shown great sensitivity but poor specificity in the detection of cancer. This implies that liquid biopsy testing may result in many false positive results as samples from healthy individuals may be labeled cancer samples.

To improve the diagnostic power of circulating lncRNAs and to compensate for the moderate sensitivity/specificity, studies have integrated the diagnostic performance of several lncRNA into one lncRNA signature. For instance, the 3-lncRNA panel of SPRY4-IT1, ANRIL, and NEAT1 identified NSCLC cancer patients with a sensitivity of 82.8% and a specificity of 92.3%[91]. Another example is the lncRNA signature consisting of UCA1, POUF3, ESCCAL-1, and PEG10, which can detect esophageal squamous cell carcinoma patients with a specificity of 80.2% and a sensitivity of 80.2%[92].

So far, the identification of biomarkers in body fluids is exclusively based on the direct comparison of samples derived from healthy individuals and patients[93]. In this way, biomarker studies try to create comprehensive maps of aberrantly expressed lncRNAs in different cancer entities. However, analyses solely based on patient-derived specimens have limitations: First, tumor cell-specific alterations may be diluted or concealed by "interfering noise" from non-tumorous cells. Second, the molecular alterations responsible for aberrant lncRNA expression in body fluids remain unnoticed, which hinders the design of novel drugs against these potential target structures. Last, comparative analysis of patient specimen only results in a "snapshot" of lncRNA levels in body fluids and do not allow the measurement of lncRNA dynamics in response to specific treatments or genetic manipulations.

Together these findings show, that circulating lncRNAs represent a valuable tool for the diagnosis and prognosis of cancer. Especially, the integration of individual lncRNA into a signature significantly increases their diagnostic performance. So far, no circulating lncRNA-based approach has reached the stage of clinical applicability due to its persistent lack of robustness and predictive power.

1.3 The Hippo pathway

1.3.1 Overview

The Hippo pathway plays a central role in development and organ size control[94]. It was first discovered in *Drosophila melanogaster* using genetic mosaic screens designed to identify drivers of tissue growth[95,96]. Since the Hippo pathway and its core components are highly conserved in *Drosophila* and mammals, this section will focus only on the mammalian Hippo pathway.

A central role in Hippo signaling represents the core kinase cascade, consisting of the serine-threonine kinases mammalian STE20-like protein kinase 1/2 (MST1/2) and large tumor suppressor kinase 1/2 (LATS1/2)[97] (Figure 2). Upon activation, MST1/2 phosphorylates the adaptor proteins SAV1 and MOB1, which is required for the recruitment and subsequent phosphorylation of LATS1/2[98-100]. In the next step, active LATS1/2 phosphorylates the transcriptional co-activators yes-associated protein (YAP) and its paralog WW domain containing transcription regulator 1 (WWTR1; synonym: TAZ) leading to their cytoplasmic retention and degradation, thus preventing target gene expression[101,102].

YAP and TAZ represent the major effectors of the Hippo pathway. Their phosphorylation by LATS1/2 occurs at multiple serine/threonine residues, of which some are more important than others in regulating YAP/TAZ nuclear translocation (S127/S381 for YAP and S89/S311 for TAZ). First, phosphorylated S127/S89 serves as a binding site for 14-3-3 proteins, which

mediates the cytoplasmic retention of YAP and TAZ[101,102]. Second, phosphorylation of S381/S311 recruits CK1δ/ε that further phosphorylates YAP/TAZ resulting in the activation of a phosphodegron. The activated phosphodegron is recognized by the SCF[β-TRCP] E3 ubiquitin ligase leading to the ubiquitination and subsequent proteasomal degradation of YAP and TAZ. Thus, YAP/TAZ activity is controlled by the Hippo pathway via both spatial (nuclear-cytoplasmic shuttling) and temporal (degradation) regulation[103,104]. In addition, recent studies have shown that YAP is phosphorylated on tyrosine 357 (Y357) independent of LATS activity leading to its cytoplasmic sequestration[105]. This illustrates the diversity of YAP/TAZ regulatory mechanisms with regard to their phosphorylation sites.

Inactivation of the Hippo kinase cascade results in the nuclear accumulation of hypo-phosphorylated YAP/TAZ, where they interact with transcription factors to mediate target gene expression[101,102] (Figure 2). Several DNA-binding partners of YAP/TAZ have been identified e.g., SMAD2/3[106], p73[107], FOXM1[108], and TEA domain family members (TEADs)[109]. Among those, the four highly homologous TEAD transcription factors (TEAD1-4) represent the major mediators of YAP/TAZ activity[109,110]. Well-characterized target genes of YAP/TAZ/TEAD are summarized in a 22-gene signature published by Wang et al., including connective tissue growth factor (CTGF), cysteine-rich angiogenic inducer 61 (CYR61), and ankyrin repeat domain 1 (ANKRD1)[111]. In addition, a chromosomal instability gene signature (CIN25) can be used as a surrogate for YAP activity in liver cancer cells[108].

Hippo pathway activity can be regulated in response to several intrinsic and extrinsic signals (Figure 2). First, cell polarity and cell-cell contact induced by adherens and tight junctions can directly affect YAP/TAZ subcellular localization[112]. For instance, cell culture experiments showed that the Hippo kinase cascade is activated at high cell density concentrations resulting in the nuclear exclusion of YAP/TAZ, which indicates that YAP/TAZ silencing is crucial for cell contact inhibition[113,114]. Second, studies have demonstrated that YAP/TAZ can serve as mechanotransducers and mechanosensors as their activity is tightly correlated with factors such as extracellular matrix stiffness, polarity, cell stretching, and cell geometry[115,116]. Here, Rho-GTPase signaling and actin cytoskeleton organization are essential for the regulation of YAP/TAZ activity by mechanical signals[117]. Third, the Hippo pathway can integrate signals from extracellular molecules, including hormones and growth factors via G protein-coupled receptors (GPCRs). Mechanistically, $G_{α12/13}$- and $G_{αq/11}$-coupled GPCRs activate Rho-GTPases leading to the silencing of LATS1/2 by F-actin assembly[118]. Lastly, stress signals, including energy stress[119], oxidative stress[120], and hypoxia[121] can modulate YAP/TAZ activity.
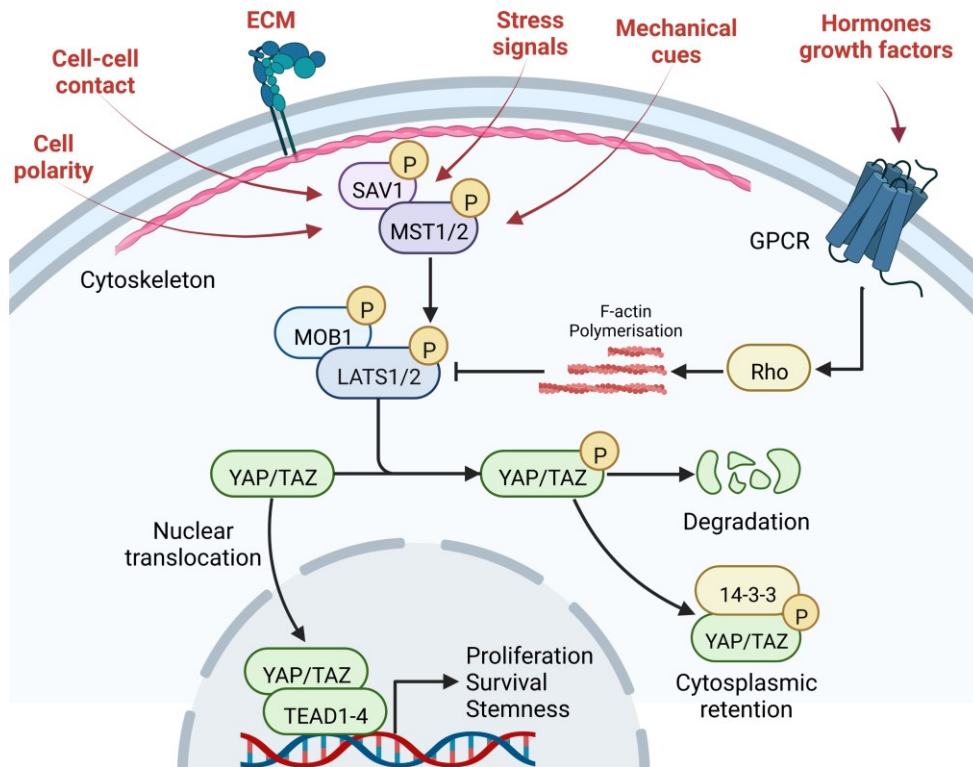
Figure 3 | Scheme of the Hippo pathway. The Hippo pathway is regulated by several intrinsic and extrinsic signals, including cell polarity, cell-cell contract, ECM, stress signals, mechanical cues, and signaling molecules. Upon activation, the central Hippo kinase cascade consisting of MST1/2, LATS1/2, and their respective adaptor proteins SAV1 and MOB1, phosphorylates the Hippo pathway effector proteins YAP/TAZ leading to their cytoplasmic retention and degradation. Inactivation of the kinase cascade results in the nuclear translocation of YAP/TAZ, where they interact with the TEAD family transcription factors driving target gene expression. For further details see text.

Taken together, Hippo signaling is based on the integration of a complex network of input signals, which affect the subcellular localization and activity of its effector proteins YAP/TAZ. In the nucleus, YAP/TAZ predominantly interact with TEAD1-4 resulting in the expression of target genes associated with cell proliferation and survival.

1.3.2 The role of the Hippo pathway in cancer development

Hippo pathway dysregulation/inactivation and thus increased nuclear YAP/TAZ abundance has been associated with the development of many solid tumor entities, including breast, liver, lung, colorectal, and pancreatic cancer[122]. Indeed, tissue analysis of human colorectal cancer samples revealed that 72% and 58% of patients exhibit nuclear enrichment of YAP and TAZ, respectively[123]. In addition, 77% of pancreatic cancer patients are positive for nuclear YAP expression[124]. This increased YAP/TAZ activity correlates with poor patient prognosis and

histological grade[125]. In contrast to the tumor suppressive function of the Hippo kinase cascade, YAP/TAZ predominantly act as oncogenes, which promote several key features of cancer cells, such as proliferation, survival, invasion, and stemness[125,126].

Aberrant cell proliferation is caused by YAP/TAZ-mediated transcription of genes involved in cell cycle progression e.g., the transcription factor FOXM1 and its target genes MCM2, CCNB1, and CCND1[108,127]. In addition, YAP/TAZ/TEAD colocalize with the transcription factor complex AP-1 to regulatory sites of the genome, which drives cell cycle transcriptional programs[101,128]. Furthermore, YAP/TAZ promote cancer cell survival by suppressing pro-apoptotic pathways as well as adapting to a nutrient-poor environment[129,130]. Lastly, it has been demonstrated that YAP/TAZ are constitutively active in cancer stem cells (CSCs), are required for CSC expansion, and are even able to transform "normal" tumor cells in cells with CSC characteristics[131-133]. In this context, additional cancer-related attributes, such as tumor initiation, drug resistance, metastasis, and cell plasticity can be associated with YAP/TAZ-dysregulation[125,134].

Interestingly, despite the common dysregulation of Hippo signaling in cancer cells, mutations of components within the pathway are relatively rare. One exception is the upstream regulator NF2 (synonym: merlin), which is frequently mutated in schwannomas, meningiomas, and malignant mesotheliomas[135], but also less frequently mutated in HCC (2%) and intrahepatic cholangiocarcinoma (5%)[136]. So far, activating mutations of YAP/TAZ/TEAD have not been reported[137]. However, activating fusions of YAP and TAZ have been detected in various rare cancer types e.g., TAZ-CAMTA1 (in ~90% of patients) and the less frequent YAP-TFE3 fusion proteins in epithelioid hemangioendothelioma[138,139] and YAP-MAMLD1 fusion (in ~10% of patients) in a rare subtype of glioma[140]. Additional mechanisms leading to aberrant Hippo pathway activity include rare genomic amplification of the YAP locus at chromosome 11q22 (e.g. in breast and liver cancer patients)[141,142], and deletions as well as epigenetic silencing of core Hippo components. An example of the latter is the LATS1/2 promotor, which is methylated in several types of cancer resulting in its downregulation[143]. Interestingly, this high number of different genetic, epigenetic, and cellular mechanisms cause a very similar phenotype, which is the nuclear enrichment and activation of YAP and/or TAZ.

Taken together, these findings demonstrate the crucial role of the Hippo/YAP/TAZ pathway in cancer development and progression. Moreover, the frequent nuclear accumulation of the transcriptional effectors YAP and TAZ qualify these proteins as potential therapeutic targets in anti-cancer treatment. Indeed, recent advances in the development of novel drugs targeting both transcriptional regulators suggest that Hippo pathway-directed therapies will be available in the future[144,145]. This illustrates the necessity to develop robust and highly sensitive techniques to identify patients who could benefit from such treatment.

1.3.3 The Hippo pathway in HCC

The Hippo pathway effector YAP has been identified as a driver of human hepatocarcinogenesis[142]. Indeed, tissue analysis of human HCC samples revealed that around 67% of HCC patients exhibit nuclear YAP enrichment and that elevated YAP or TAZ levels correlate with poor tumor differentiation and worse overall survival[146-148]. Furthermore, a meta-analysis, including 391 HCC cases and 334 controls, showed significant overexpression of YAP in HCC in comparison to adjacent non-tumorous tissue, which was associated with vascular invasion, tumor size, and tumor staging[149]. These findings were confirmed by independent mRNA expression analysis with 224 HCC patients and 220 healthy controls[150].

The implication of YAP in HCC formation has been well documented in various animal models. First, a rat model of liver cancer showed increased levels of YAP already at precancerous lesions, however nuclear enrichment of YAP was only detected in fully developed HCC[151]. Second, liver-specific overexpression of constitutively active YAP (S127A mutant) in transgenic mice results in hepatomegaly and the formation of tumors with HCC characteristics[101,152]. Third, hydrodynamic tail vein injection of a YAP-5SA mutant (mutations at all 5 phosphorylation sites) induced large tumors in the liver 100 days post injection[153]. Last, heterozygous YAP deletion in NF2 deficient mice completely rescued the NF2 knockout-mediated liver overgrowth and tumor formation, highlighting the role of YAP and the Hippo pathway in liver carcinogenesis[154].

In line with these experimental findings, first data illustrate that TAZ may play a similar role in HCC development. For instance, silencing of YAP and also TAZ decreases subcutaneous tumor growth of human HCC cell lines[155,156]. Furthermore, comprehensive expression profiling identified genes that are exclusively regulated by TAZ, such as ITGAV, which contributes to YAP/TAZ-driven hepatocarcinogenesis[157]. In addition, hydrodynamic tail vein injection of a constitutively activated form of TAZ (TAZ[S89A]) and the EGFR/HER2 pathway effector molecule BRAF caused HCC development[158]. Moreover, it was shown that TAZ is required for c-MYC-driven hepatocarcinogenesis as deletion of Taz completely prevented tumor growth in c-Myc induced murine HCCs[159].

Lastly, genetic manipulation of components of the Hippo pathway demonstrates their involvement in tumor development. For example, Mst1/2 knock-out in mice (Mst1−/−Mst2+/−) leads to liver overgrowth and tumor formation after 15 months[160].

To conclude, the Hippo/YAP/TAZ pathway plays a crucial role in the development of HCC. However, little is known about the mechanisms that lead to YAP/TAZ activation and their subsequent effect on tumor cell formation.

1.3.4 The Hippo pathway in lung cancer

The term lung cancer comprises several histo-morphological subtypes of lung cancer, including lung squamous cell carcinomas (SCC), large-cell lung carcinomas (LLC), and lung adenocarcinomas (LUAD), all summarized as non-small-cell lung cancer (NSCLC). Many studies do not discriminate between different types of NSCLC. However, the following part considers only research, which exclusively focused on the role of the Hippo pathway in LUAD development and progression.

Immunohistochemical (IHC) studies on human tissue samples showed that YAP is overexpressed in 87.8% of LUAD patients and that YAP's elevated expression and nuclear localization is associated with poor prognosis and tumor staging[161,162]. In addition, lower protein and transcript levels of the Hippo pathway kinase LATS2 are observed in LUAD patients and increased LATS2 expression contributes to better prognosis and overall survival[163].

These patient analyses were complemented by several experimental studies that highlight the relevance of YAP/TAZ in LUAD formation. First, silencing of YAP or TAZ impaired tumor formation in a LUAD xenograft mouse model[164,165]. Second, increased nuclear localization of YAP/TAZ was observed in metastatic in comparison to nonmetastatic tumors in mice[164,165]. Third, the genetic loss of YAP decreased the number of experimentally induced tumors in mice, while the remaining tumors were benign and did not progress to poorly differentiated LUAD[166]. Taken together, these findings underline the involvement of YAP/TAZ in LUAD development and progression. Due to the relatively high incidence of patients with aberrant YAP/TAZ activity (HCC, LUAD, and more), the Hippo pathway represents a promising target for future therapies.

1.4 Objectives

Precision medicine techniques aim to provide individualized treatment strategies for cancer patients. A prerequisite for this is the availability of robust and sensitive biomarkers for accurate patient stratification. In this context, body fluids are highly informative regarding disease conditions in tumor tissues. Especially lncRNAs, whose aberrant expression in tumors is reflected in body fluids, represent valid prognostic liquid biopsy markers for tumor-relevant signaling pathways and/or activity of respective oncogenic transcription factors. However, previous liquid biopsy studies that aim to identify pathways/oncogene-specific biomarkers cannot define the cellular source of information and therefore often suffer from a lack of reproducibility.

As showcase, I here investigate the Hippo pathway, which is dysregulated in many cancer types and for which novel drugs can be expected in the future. Thus, techniques are required to identify patients eligible for such Hippo/YAP/TAZ-directed therapies. However, it is unclear whether YAP/TAZ regulates the expression of specific lncRNAs and whether their serum levels can be used as a proxy for YAP/TAZ activity in the tumor.

Therefore, the aim of this thesis was to provide answers to the following questions:

1. Do YAP/TAZ regulate the expression of a common set of lncRNAs in HCC and LUAD cells?
2. Does a tumor-spanning lncRNA signature that defines YAP/TAZ activity in different cancer entities exist and does its expression correlate with relevant clinicopathological features?
3. Do YAP/TAZ-dependent lncRNAs contribute to pro-tumorigenic functions of the Hippo pathway effectors in HCC cells?
4. Are YAP/TAZ-regulated lncRNAs detectable in serum samples of HCC patients?
5. Does the abundance of lncRNAs in the serum of HCC patients correlate with YAP/TAZ activation in the corresponding tumor tissues?
6. Is the expression of YAP/TAZ-dependent lncRNAs a marker for the responsiveness of tumor cells to Hippo pathway-directed therapy?

2 Materials

2.1 Chemicals and consumables

2.1.1 Chemicals

All chemicals were purchased from the following manufacturers if not stated differently:

- AppliChem (Darmstadt, Germany)
- Carl Roth (Karlsruhe, Germany)
- Merck Millipore (Darmstadt, Germany)
- SERVA (Heidelberg, Germany)
- Sigma-Aldrich (Taufkirchen, Germany)

UltraPure™ DNase/RNase-free distilled water was obtained from Thermo Fisher Scientific (Darmstadt, Germany)

2.1.2 Consumables

Table 1 | General consumables

Consumables	Supplier
Amersham™ Protran™ 0.45 µm Nitrocellulose Blotting Membrane	GE Healthcare, Solingen, Germany
Cell culture plates (96-well, 6-well, 10 cm, 15 cm)	NeoLab, Heidelberg, Germany Orange Scientific (Braine-l'Alleud, Belgium)
Cell scrapers	Corning, New York, USA
Cryovials	Greiner-Bio-One, Frickenhausen, Germany
DISTRITIP (micro, mini, maxi)	Gilson, Limburg, Germany
Falcon tubes (15 ml, 50 ml)	Greiner-Bio-One
MicroAmp® fast 96-well reaction plate (0.1 ml)	Thermo Fisher Scientifc
MicroAmp® optical adhesive film	Thermo Fisher Scientific
Microcentrifuge tubes (0.2 ml, 0.5 ml, 2.5 ml, 2 ml, 5 ml)	Eppendorf, Hamburg, Germany Sarstedt, Nürnbrecht, Germany
Microscope cover glasses	Marienfeld, Lauda Königshofen, Germany
Microscope slides "Menzel Gläser"	Thermo Fisher Scientific
Millex-HA filter (0.45 µm)	Merck Millipore
Parafilm	Pechiney, Düsseldorf, Germany

Pasteur Pipettes	Wilhelm Ulbrich, Bamberg, Germany
Pipette tips	Sarstedt Greiner-Bio-One
Sterile stripettes®	Corning
SuperFrost Plus™ microscope slides	Thermo Fisher Scientific
Whatman™ 3MM Chr	GE Healthcare

2.2 Reagents

2.2.1 General reagents

Table 2 | General reagents

Reagents	Supplier
Albumin fraction V, biotin-free (BSA)	Carl Roth
Ammonium persulfate (APS)	Bio-Rad, Munich, Germany
Bradford reagent	Sigma-Aldrich
Cell lysis buffer 10x	Cell Signaling Technology, Frankfurt, Germany
Cristal violet	Sigma-Aldrich
DAPI Fluoromount-G	Southern Biotech, Birmingham, USA
Dynabeads® Protein G	Thermo Fisher Scientific
Fisher's EZ-Run™ pre-stained *Rec* protein ladder	Thermo Fisher Scientific
PhosStop 10x	Roche, Mannheim, Germany
Protease-Inhibitor Mix G 1000x	SERVA
Salmon sperm DNA	Thermo Fisher Scientific
TED-347	Selleck Chemicals GmbH, Planegg, Germany
Verteporfin	Sigma-Aldrich

2.2.2 Transfection Reagents

Table 3 | Transfection reagents

Reagents	Supplier
Lipofectamine™ RNAiMAX	Thermo Fisher Scientific
Oligofectamine™	Thermo Fisher Scientific
Polyethylenimine (Pei)	Polysciences, Warrington, USA

2.2.3 Immunohistochemistry reagents

Table 4 | Immunohistochemistry reagents

Reagents	Supplier
AP-Polymer Detection Line	DCS, Hamburg, Germany
Enhancer Detection Line	DCS
Epredia™ Richard-Allan Scientific™ Cytoseal™ 60	Thermo Fisher Scientific
Mayer's Hematoxylin solution for clinical diagnostics	AppliChem
Mouse and Rabbit Specific HRP/DAB IHC Detection Kit	Abcam, Cambridge, UK
Permanent AP-Red-Kit	Zytomed, Berlin, Germany
POLYVIEW® PLUS AP (anti-rabbit) reagent	Enzo Life Sciences, Lörrach, Germany
Target Retrieval Solution pH 6	DAKO, Hamburg, Germany

2.3 Assays and kits

Table 5 | Assays and kits

Reagents	Supplier
Cell proliferation ELISA Biotrak™ system	GE Healthcare/Amersham, Buckinghamshire, UK
ExtractMe Total RNA Kit	7BioSciences, Neuenburg, Germany
miRNeasy Serum/Plasma Advanced Kit	Qiagen, Hilden, Germany
NE-PER™ Nuclear and Cytoplasmic Extraction Reagents kit	Thermo Fisher Scientific
NucleoSpin® Gel and PCR Clean-up Kit	Machery-Nagel, Düren, Germany
NucleoSpin® RNA II kit	Machery-Nagel
Prelude PreAmp Master Mix	TakaraBio, Saint-Germain-en-Laye, France
primaQuant 2x qPCR-SYBR-Green-Mastermix	Steinbrenner Laborsysteme, Wiesenbach, Germany
PrimeScript RT Master Mix	TakaraBio
Resazurin Assay Kit	Bio-Techne GmbH, Wiesbaden, Germany
RNAscope® 2.5 Reagent Kit-brown	Advanced Cell Diagnostics, Newark, USA
RNAscope® Positive Control Probe- Hs-PPIB	Advanced Cell Diagnostics
RNAscope® Negative Control Probe-DapB	Advanced Cell Diagnostics
RNAscope® Probe-Hs-CYTOR-O1	Advanced Cell Diagnostics

RNAscope® Probe-Hs-SNHG1	Advanced Cell Diagnostics
RNAscope® Probe-Mm-Morrbid	Advanced Cell Diagnostics
RNA subcellular isolation kit	Active Motif, Carlsbad, USA

2.4 Cell culture

2.4.1 Cell lines

All cell lines were obtained from the listed suppliers if not otherwise indicated:

- American Type Culture Collection (ATCC; LGC Standards GmbH, Wesel, Germany)

- German Collection of Microorganisms and Cell Cultures GmbH (DSMZ; Braunschweig, Germany

- Japanese Collection of Research Biosources (JCRB; via Tebu-Bio, Offenbach, Germany)

Table 6 | Cell lines and corresponding background information

Cell line	Gender	Age	Ethnicity	Origin	Supplier
A549	male	58	Caucasian	NSCLC/LUAD	ATCC
Calu-1	male	47	Caucasian	NSCLC/SCC	ATCC
Calu-6	female	61	Caucasian	NSCLC	ATCC
NCI-H1299	male	43	Caucasian	NSCLC/LCC	ATCC
NCI-H1650	male	27	Caucasian	NSCLC/LUAD	ATCC
NCI-H1975	female	NA	NA	NSCLC/LUAD	ATCC
NCI-H2009	female	68	Caucasian	NSCLC/LUAD	ATCC
NCI-H358	male	NA	NA	NSCLC/LUAD	ATCC
Hep3B	Male	8	Black	HCC	DSMZ
HHT4	hTERT-immortalized human liver epithelial cells (kindly provided by AG Roessler, Institute of Pathology, Heidelberg, Germany)				
HLE	male	68	Asian	HCC	JCRB
HLF	male	68	Asian	HCC	JCRB
Huh1	male	53	Asian	HCC	JCRB
Huh7	male	57	Asian	HCC	JCRB
SNU182	male	24	Asian	HCC	JCRB
SNU449	male	52	Asian	HCC	ATCC
SNU475	male	43	Asian	HCC	ATCC

2.4.2 Cell culture media and additives

Table 7 | Cell culture media and additives

Reagents	Supplier
Blasticidin	Thermo Fisher Scientific
Defined Trypsin Inhibitor	Thermo Fisher Scientific
Dimethyl sulfoxide (DMSO)	Sigma-Aldrich
Dulbecco's Modified Eagle's Medium (DMEM)	Sigma-Aldrich
Dulbecco's Phosphate Buffered Saline (PBS)	Sigma-Aldrich
Fetal Calf Serum (FCS)	Thermo Fisher Scientific
FNC Coating Mix®	AthenaES, Baltimore, USA
HCM™ Hepatocyte Culture Medium BulletKit™	Lonza, Basel, Switzerland
HEPES Buffer Solution (1M)	Thermo Fisher Scientific
Knockout Serum Replacement	Thermo Fisher Scientific
L-Glutamine	Sigma-Aldrich
Minimum Essential Medium (MEM)	Sigma-Aldrich
MEM Non-Essential Amino Acids	Thermo Fisher Scientific
Opti-MEM®	Reduced Serum Medium	Thermo Fisher Scientific
Penicillin/Streptomycin	Thermo Fisher Scientific
Rosewell Park Memorial Institute 1640 (RPMI)	Sigma-Aldrich
Sodium pyruvate (100 mM)	Thermo Fisher Scientific
Trypsin-EDTA solution	Sigma-Aldrich

2.5 Buffers and Solutions

All buffers and solutions were prepared in deionized water.

Table 8 | List of buffers and solutions with respective recipes

Solution/Buffer	Recipe
Blocking solution	5% BSA in TBST
Borate buffer (Blotting buffer) (pH 8.8)	20 mM Boric acid, 1.27 mM EDTA
Crystal violet staining solution	1% Crystal violet, 25% methanol
IP wash buffer	100 mM Tris pH 8.5, 500 mM LiCl, 1% Igepal CA 630, 1% Na-Deoxycholate; sterile filtered
PBS (pH 7.4)	140 mM NaCl, 2.7 mM KCl, 10 mM $Na_2HPO_4x2H_2O$, 1.8 mM KH_2PO_4
Protein loading buffer (4x)	250 mM Tris HCl pH 6.8, 8% SDS, 40% glycerol, 0.04% bromphenol blue, 100 mM DTT

RIPA buffer	150 mM NaCl, 0.1% SDS, 0.5% Na-Deoxycholate, 1% Igepal CA 630, 5 mM EDTA, 50 mM Tris pH 8; sterile filtered
SDS-Running buffer	25 mM Tris, 192 mM Glycine, 0.1% SDS
SDS-Polyacrylamide gel	30% acrylamide mix, 1 M Tris pH 6.8, 10% SDS, 10% APS, TEMED
TAE-Buffer (pH 8.0)	40 mM Tris-Acetate, 1 mM EDTA
Talianidis elution buffer	70 mM Tris pH 8, 1 mM EDTA, 1.5% SDS
TBST	0.1% Tween-20 in TBS
TE buffer	70 mM Tris pH 8, 1 mM EDTA
Tris buffered saline (TBS) (pH 7.6)	20 mM Tris-HCl, 140 mM NaCl

2.6 Oligonucleotides

2.6.1 Primers for semi-quantitative real-time PCR (qPCR) for human genes

Primers for qPCR analysis were designed using Primer-BLAST and were obtained from Thermo Fisher Scientific.

Table 9 | List of qPCR primers for human genes with mRNA accession number

Gene	RNA accession number	Sequence (5'-3')
ANKRD1	NM_014391	For: AGTAGAGGAACTGGTCACTGG Rev: TGGGCTAGAAGTGTCTTCAGAT
CTGF	NM_001901	For: CCAAGGACCAAACCGTGG Rev: CTGCAGGAGGCGTTGTCAT
CYR61	NM_001554	For: CCAAGGACCAAACCGTGG Rev: CTGCAGGAGGCGTTGTCAT
CYTOR_1	NR_024204	For: ATGCCCAAAGTTACGGAGGA Rev: TATTCGAGGGATGCAGACGG
CYTOR_2	NR_024206	For: CCACCAGCCTCTCCTTGAATA Rev: GGCTGAGTCGTGATTTTCGG
DLEU1	NR_109973	For: TTACCAGATGAGGACACCTGAG Rev: AAGAATGGCTGGCAAAGGCT
FTX	NR_028379	For: TCCTGTGCCTGCTGTCCATT Rev: TGTGGCATCACCTCCTGGTT
GAPDH	NM_002046	Rev: CTGGTAAAGTGGATATTGTTGCCAT

		For: TGGAATCATATTGGAACATGTAAACC
MIR4435-2HG	NR_015395	For: GTCATTAAGGTGGTCCTGCC Rev: AGTGTCCTTTTCAGCGAGTGA
RPL41	NM_001035267	For: AAACCTCTGCGCCATGAGAG Rev: AGCGTCTGGCATTCCATGTT
SNHG1	NR_003098	For: ACGTTGGAACCGAAGAGAGC Rev: GCAGCTGAATTCCCCAGGAT
SNHG17	NR_01536	For: AGCGTAGCTTCCTTGTCGTG Rev: GAGACCTGACAGACAGCGTG
Spike In	artificial oligo	For: GAGCGCCCGCTGCATTTA Rev: GTAGGCATCCGCTGCATTTA
SRSF4	NM_005626	For: TGCAGCTGGCAAGACCTAAA Rev: TTTTTGCGTCCCTTGTGAGC
TAZ/WWTR1	NM_015472	For: CAGAGAATCCAGATGGAGAG Rev: GTTGACAGCAGCCTGAACTG
TEAD1	NM_021961	For: GACAGTCACCTGTTCCACCAAAG Rev: CCATTCTCAAACCTTGCATACTCCG
TEAD2	NM_001256658	For: CTCACCTGTTCCTCCAAGGTC Rev: CACCAGGTACTCGCACATGG
TEAD3	NM_003214	For: TTCATGGAGGTGCAGCGAGAC Rev: CGCACATCTACTGCCTCCAG
TEAD4	NM_201443	For: TGGAGTTCTCTGCCTTCCTG Rev: GGACTGGCCAATGTGCACGA
YAP	NM_006106	For: CCTGCGTAGCCAGTTACCAA Rev: CCATCTCATCCACACTGTTC

2.6.2 Primers for semi-quantitative real-time PCR (qPCR) for murine genes

Table 10 | List of qPCR primers for murine genes with mRNA accession number

Gene	RNA accession number	Sequence (5'-3')
Actb	NM_007393	For: GCTTCTTTGCAGCTCCTTCGT Rev: ACCAGCGCAGCGATATCG
Gapdh	NM_008084	For: TGTCCGTCGTGGATCTGAC Rev: CCTGCTTCACCACCTTCTTG
Hprt	NM_013556	For: TCCTCCTCAGACCGCTTTT Rev: CCTGGTTCATCATCGCTAATC
Morrbid	NR_028589	For: CAAAGCAAACCAGAGGACCAG Rev: TCAACCCAACAGGTTGTCATCA
Ppia	NM_008907	For: GCATACAGGTCCTGGCATCT Rev: AGCTGTCCACAGTCGGAAAT
Tubb5	NM_011655	For: TCACTGTGCCTGAACTTACC Rev: GGAACATAGCCGTAAACTGC
Snhg1	NR_002896	For: GCTTGTAGTCAGGGTGCTGT Rev: AAACCTGCACTCATCCTGGG
Snhg17	NR_015463	For: TGAAGGTGAGCCACTTCGGA Rev: AGCGACACGTTACTTCCTCTG

2.6.3 PCR primer for Chromatin immunoprecipitation (ChIP)

PCR primers for ChIP analysis were designed based on transcription factor binding sites identified by ChIP-sequencing (ChIP-Seq) data analysis in combination with the prediction of transcription factor binding sites using the JASPAR database[167].

Table 11 | List of qPCR primers for ChIP analysis

Gene	Sequence (5'-3')
CYTOR promotor	For: TACCTGTGTGTGTTTTGGAGAGT Rev: CATCTGCATGCTCTTTCCCCA
MIR4435-2HG promotor	For: AGACCTACCGGAAGGATCAGA Rev: ACTGGAAAAATGTAGGTTGCACG
SimpleChIP® Human CTGF Promoter Primers	Commercial primers (Cell Signaling Technology)

SimpleChIP® Human CTGF Upstream Primers	Commercial primers (Cell Signaling Technology)
SNHG17 promotor	For: GTTACCCGCTGTGCATCTCT Rev: AATGAATTCTACCCCCGCCC

2.6.4 Oligonucleotides for RNA interference

siRNAs were designed and synthesized at Microsynth AG (Balgach, Switzerland).

Table 12 | siRNA sequences with respective accession number

siRNA	RNA accession number	Sequence (5'-3')
Control	NA	UGG UUU ACA UGU CGA CUA A
CYTOR#1	NR_024204	CAG UCU CUA UGU GUC UUA A dTdT
CYTOR#2		CAC ACU UGA UCG AAU AUG A dTdT
MIR4435-2HG#1	NR_015395	GGC ACA AUU UAA UCC AUA A dTdT
MIR4435-2HG#2		GGA UCA CCG CUA AAG AAA A dTdT
SNHG17#1	NR_01536	UUA CCC ACC CAU UCA AUA A dTdT
SNHG17#2		GGU GAC GUG UCU UCA AGA A dTdT
TAZ#2	NM_015472	AAA CGU UGA CUU AGG AAC UUU dTdT
TAZ#3		AGG UAC UUC CUC AAU CAC A dTdT
TEAD#1*	NM_021961	AUG AUC AAC UUC AUC CAC A dTdT
TEAD#2*	NM_003214 NM_201443	UCA ACU UCA UCC ACA AGC U dTdT
YAP#1	NM_006106	CCA CCA AGC UAG AUA AAG A dTdT
YAP#2		GGU CAG AGA UAC UUC UUA A dTdT

* - siRNAs recognize the TEAD family members TEAD1, TEAD3, and TEAD4

2.6.5 Additional oligonucleotides

A custom Spike-In oligonucleotide was designed to account for variances introduced during RNA isolation procedures.

Sequence (5'-3'):

TGCTGTTGACAGTGAGCGCCCGCTGCATTTATAAAGAATATAGTGAAGCCACAGATGTA
TATTCTTTATAAATGCAGCGGATGCCTACTGCCTCGGA

2.7 Antibodies

2.7.1 Primary antibodies

Table 13 | Primary antibodies

Antigen (clone)	Species	Application	Dilution	Company
β-Actin	rabbit	WB	1:1,000	Cell Signaling Technology
GAPDH	chicken	WB	1:5,000	Merck Millipore Darmstadt, Germany
Ki67	rabbit	IHC	1:500	Abcam
Rabbit serum	rabbit	ChIP	2 µg	Agilent Technologies Waldbronn, Germany
Pan-TEAD (D3F7L)	rabbit	WB	1:1,000	Cell Signaling Technology
TEAD4	mouse	ChIP	2 µg	Abcam
TAZ	rabbit	IHC	1:50	Abcam
TAZ XP (E9J5A)	rabbit	WB ChIP	1:1,000 2 µg	Cell Signaling Technology
YAP XP (D8H1X)	rabbit	IHC WB IF ChIP	1:200 1:400 1:60 2 µg	Cell Signaling Technology

2.7.2 Secondary antibodies

Table 14 | Secondary antibodies

Antigen	Isotype	Application	Company
anti-goat 488	donkey IgG	IF	Jackson ImmunoResearch Newmarket, UK
IRDye® 680RD anti-chicken	donkey IgG	WB	LI-COR Biosciences Bad Homburg, Germany
IRDye® 680RD anti-rabbit	donkey IgG	WB	LI-COR Biosciences
IRDye® 800CW anti-chicken	donkey IgG	WB	LI-COR Biosciences
IRDye® 800CW anti-rabbit	donkey IgG	WB	LI-COR Biosciences

2.8 Equipment

2.8.1 General equipment

Table 15 | List of general laboratory equipment

Equipment	Supplier
12-Tube Magnet	Qiagen
Aperio® AT2 scanner	Leica Mikrosysteme Vertrieb GmbH, Wetzlar, Germany
D-6010 magnetic stirrer	Neolab, Heidelberg, Germany
DISTRIMAN repetitive pipette	Gilson
Dri-Block® heater DB 100/4	Techne/Thermo Fisher Scientific
EV202 power supply	Consort, Turnhout, Belgium
EV231 power supply	Consort, Turnhout, Belgium
C-MAG MS 7 magnetic stirrer	IKA, Staufen im Breisgau, Germany
FluorChem™ M	Bio-Techne GmbH
FLUOstar Omega Microplatereader	BMG Labtech, Ortenberg, Germany
HybeEZ oven	Advanced Cell Diagnostics
Intelli-mixer overhead shaker	Neolab
Kern EG scale	Kern, Balingen-Frommern, Germany
Mini Trans-Blot Cell	Bio-Rad, Munich, Germany
Mini-PROTEAN® 3 Cell SDS-gel electrophoresis systems	Bio-Rad
Mini-PROTEAN® Tetra Cell Casting Module	Bio-Rad
NanoDrop ND-1000 Spectrophotometer	Thermo Fisher Scientific
Odyssey Sa Infrared imaging system	LI-COR Biosciences
Olympus CKX31 microscope	Olympus, Hamburg, Germany
Olympus IX81 microscope	Olympus
ORCA-R2 camera	Hamamatsu Photonics, Herrsching, Germany
pH 210 Microprocessor pH-Meter	Hanna Instruments, Kehl am Rhein, Germany
Photometer	Eppendorf
PIPETBOY acu 2	INTEGRA Biosciences, Zizers, Switzerland
Pipettes Research Plus	Eppendorf
PR224M analytical balance	Ohaus Corporation, Nänikon, Switzerland
Precellys® 24 Homogenizer	Peqlab Biotechnologie GmbH, Erlangen, Germany

Roll shaker CAT RM5	Neolab
S-4000 ultrasonic liquid processor	Qsonica, Newton, USA
Secuflow fume hood	Waldner, Wangen, Germany
Thermomixer compact	Eppendorf
Transsonic T460/H ultrasound waterbath	Elma, Singen, Germany
Vacusafe pump system	INTEGRA Biosciences
Vortexer	VWR International, Darmstadt, Germany

2.8.2 Centrifuges

Table 16 | List of centrifuges

Equipment	Supplier
5424 R	Eppendorf
5415 R	Eppendorf
Labnet Spectrafuge™ Mini Centrifuge	Sigma-Aldrich
Megafuge 16R	Thermo Fisher Scientific
Mikro 200	Hettich, Tuttlingen, Germany
Universal 32 R	Hettich

2.8.3 Cell culture

Table 17 | List of cell culture equipment

Equipment	Supplier
BIOWIZARD Silver Line safety cabinet	Ewald, Bad Nenndorf, Germany
Heracell™ VIOS 250i CO2 Incubator	Thermo Fisher Scientific
Neubauer counting chamber	Brand, Frankfurt, Germany

2.8.4 PCR devices

Table 18 | List of PCR devices

Equipment	Supplier
Arktik Thermal Cycler	Thermo Fisher Scientific
Cyclone Thermal Cycler	Peqlab Biotechnologie GmbH
DNA Engine® Thermal Cycler	Bio-Rad
PTC-200 Thermal Cycler	Biozym, Hessisch Oldendorf, Germany
QuantStudio™ 5 Real-Time PCR System, 96-well	Thermo Fisher Scientific

2.9 Software

Table 19 | Software and online tools

Software	Provider
Adobe® Photoshop® CS6	Adobe Systems, Munich, Germany
ApE v2.0.61	https://jorgensen.biology.utah.edu/wayned/ape/
Aperio ImageScope v12.4.3.7001	Leica Biosystems, Nussloch, Germany
Automated Slide Analysis Platform	https://computationalpathologygroup.github.io/ASAP/
BioRender	https://biorender.com
CellSens Dimension	Olympus
DepMap Portal	https://depmap.org/portal/
ENCODE portal	https://www.encodeproject.org/
FIJI/Image J v1.53	www.fiji.sc
Human Protein Atlas	https://www.proteinatlas.org
GraphPad Prism 9	GraphPad Software, San Diego, USA
Ilastik v1.3.3	https://www.ilastik.org/
Image Studio Lite v5.2	LI-COR Biosciences
Omega v.3.00 R2 and MARS	BMG Labtech, Ortenberg, Germany
QuantStudio™ Design & Analysis Software v1.4.3	Thermo Fisher Scientific
QuPath	https://qupath.github.io/
R-4.1.0	www.R-project.org
RStudio v1.4.1717	www.rstudio.com
UCSC Xena Browser	https://xena.ucsc.edu

2.10 R packages and other tools

- biclust (https://CRAN.R-project.org/package=biclust)
- Bioconductor packages
- Boruta[168]
- ChIPseeker[169]
- ColonyArea[170]
- ComplexHeatmap[171]
- EnhancedVolcano (https://github.com/kevinblighe/EnhancedVolcano)
- FastQC (https://www.bioinformatics.babraham.ac.uk/projects/fastqc/)
- kallisto v0.46.1[172]
- limma[173]
- pheatmap (https://CRAN.R-project.org/package=pheatmap)

- pROC[174]

- systemPipeR[175]

- trackplot[176]

- trim_galore v0.6.4 (www.bioinformatics.babraham.ac.uk/projects/trim_galore/)

- VennDiagram[177]

2.11 Deposited data

Table 20 | Deposited data used in this study

Deposited data	Accession number
Raw and normalized RNA-Seq data from HLF and A549 cells upon YAP/TAZ silencing	GSE207724 (this thesis)
TEAD1/TEAD4 ChIP-Seq data from HuCCT1 cells	GSE68296[178]
TEAD1 ChIP-Seq data from HepG2 cells	GSE96195[179]
TEAD3 ChIP-Seq data from HepG2 cells	GSE96302[179]
TEAD4 ChIP-Seq data from HepG2 cells	GSE170161[179]
TEAD4 ChIP-Seq data from A549 cells	GSM1010868[180]

3 Methods

3.1 Cell Culture

3.1.1 Cultivation of cells

All cell lines used in this study are adherent cell lines of human origin (additional information in Table 6). The HCC cell lines HLE, HLF, Huh1, and Huh7 as well as the NSCLC cell lines A549, NCI-H1299, and NCI-H2009 were cultured in DMEM supplemented with 10% FCS and 1% penicillin/streptomycin. The HCC cell lines SNU475, SNU449, and SNU182 as well as the NSCLC cell lines NCI-H1650, NCI-H1975, and NCI-H358 were cultured in RPMI supplemented with 10% FCS and 1% penicillin/streptomycin. Medium for SNU449 and SNU182 cells was additionally supplemented with 1% HEPES, 1% L-glutamine, and 1% sodium pyruvate. The HCC cell line Hep3B and the NSCLC cell lines Calu-1 and Calu-6 were cultured in MEM supplemented with 10% FCS and 1% penicillin/streptomycin. Medium for Calu-1 and Calu-6 was additionally supplemented with 1% non-essential amino acids and 1% sodium pyruvate. The hTERT-immortalized human liver epithelial cell line HHT4 was cultivated in HBM basal medium supplemented with SingleQuots (HCM BulletKit), 20% knockout serum replacement, 1% L-glutamine, and 1% penicillin/streptomycin. Cells were cultured at 37°C and 5% CO_2 in a humidified incubator. Cells were routinely checked for mycoplasma contamination and authenticity by short tandem repeat analysis (DSMZ, Braunschweig, Germany).

All cell lines were passaged twice a week by washing with PBS, trypsinizing with trypsin-EDTA, and seeding into new cell culture dishes containing the corresponding medium. HHT4 cells require the addition of 0.3 ml defined trypsin inhibitor after trypsinization and are seeded onto FNC pre-coated dishes (coating at 37°C for 1 h).

3.1.2 Cryopreservation of cells

To preserve cells for long-time storage, cells from a subconfluent 10 cm culture dish were trypsinized and pelleted at 1000 rpm for 5 min. The cell pellet was resuspended in 1.8 ml respective medium supplemented with 10% DMSO. The cells were slowly cooled down at -80°C and then transferred into the vapor phase of a liquid nitrogen tank. Cells were thawed quickly at 37°C, resuspended in pre-warmed medium, and centrifuged at 1,000 rpm for 5 min to remove DMSO residuals. The pellet was resuspended in medium and the cells were seeded onto cell culture dishes.

3.1.3 Transfection of small interfering RNAs (siRNAs)

siRNAs were transfected using Lipofectamine RNAiMAX or Oligofectamine following the manufacturer's protocol. Transfection reagents and siRNAs were diluted in Opti-MEM according to Table 21. For Lipofectamine RNAiMAX transfections, the solutions were mixed and incubated at RT for 20 min. Cells were covered with 1.5 ml antibody-free medium and the siRNA-lipid complexes were added. For Oligofectamine transfections, the solutions were incubated at RT for 10 min, mixed, and subsequently incubated at RT for 15 min. Cells were washed and covered with 800 µl Opti-MEM and the transfection complexes were added. After 4 h of incubation at 37°C, 1 ml culture medium was added and the medium was replaced after 24 h. siRNAs were used at a final concentration of 20 nM (CYTOR) or 40 nM (YAP/TAZ, TEAD, MIR4435-2HG, SNHG17). Equimolar 'nonsense' siRNA (siCo) without detectable gene-specificity was used as a negative control. Cells were seeded 24 h prior to transfection and harvested at indicated time points.

Table 21 | siRNA transfection protocols

		Oligofectamine		Lipofectamine RNAiMAX	
		20 nM	**40 nM**	**20 nM**	**40 nM**
A	Opti-Mem	181 µl	180 µl	248 µl	246 µl
	siRNA [20µM]	1 µl	2 µl	2 µl	4 µl
B	Opti-Mem	15 µl	15 µl	245 µl	245 µl
	Transfection reagent	3 µl	3 µl	5 µl	5 µl

3.1.4 Viral infection of cells

Lentiviral particles containing CYTOR-pLV-EF1a-IRES-Blast vector or an empty vector as control were kindly provided by Dr. Rossella Pellegrino (Institute of Pathology, Heidelberg, Germany). CYTOR-overexpressing HLF cells were generated as previously described[181]. In brief, HLF cells were seeded in 6-well plates 24 h prior to infection. For retroviral infection, cells were washed twice with PBS, and subsequently, a mix, consisting of 1.5 ml DMEM, 2 µl polybrene, and 1 ml virus suspension, was added onto the cells. The next day, the cells were washed twice with PBS and 2 ml culture medium was added. After 48 h, positive cells were selected with 2 µg/ml blasticidin for 3 days.

3.1.5 Treatment with Verteporfin and TED-347

For treatment with the YAP/TEAD inhibitors Verteporfin and TED-347 cells were seeded into 6-well plates one day before treatment. Cells were incubated with the indicated concentrations (0.5-2 µM for Verteporfin; 1-10 µM for TED-347) and at indicated time points (24 h for Verteporfin; 48 h for TED-347), protein and RNA were isolated for further analysis. Respective concentrations of the solvent DMSO served as control.

3.2 Methods in molecular biology

3.2.1 RNA isolation and cDNA synthesis

Total RNA was isolated using the ExtractMe Total RNA Kit or the NucleoSpin® RNA II kit according to the manufacturer's instructions. RNA was stored at -80°C for further downstream analysis.

cDNA was synthesized using up to 500 ng of total RNA with the PrimeScript RT Master Mix following the manufacturer's protocol. In this process, random hexamer primers were used for the reverse transcription reaction. cDNA was stored at -20°C for further downstream analysis.

3.2.2 Semi-quantitative real-time PCR (qPCR)

Gene expression levels were analyzed using qPCR. qPCR reactions were set up using the primaQuant 2x qPCR-SYBR-Green-Mastermix according to Table 22 with the following cycling conditions: 95°C for 15 min, followed by 40 cycles of 95°C for 15 s and 60°C for 60 s. Subsequent melting curve analysis was applied to assure product specificity (95°C for 15 s, 60°C for 30 s, 60-95°C 0.5 °C/second).

Table 22 | qPCR master mix (1 rxn)

Reagent	Volume	Final concentration
SYBR Green Mix	5 µl	50%
Forward primer [10 µM]	0.3 µl	0.3 µM
Reverse primer [10 µM]	0.3 µl	0.3 µM
cDNA (1:50)	2 µl	
dH$_2$O	2.4 µl	

Relative gene expression was calculated using standard curve formulas, which were determined for each primer pair based on serial dilutions of cDNAs (1:12.5 – 1:400). For human samples, the housekeeping genes GAPDH, RPL41, or SRSF4 were used for normalization. The housekeeping genes Actb, Gapdh, Hprt, Ppia, and Tubb5 were used for murine samples.

3.2.3 Expression profiling

For the identification of YAP and TAZ-regulated mRNAs and lncRNAs, HLF cells and A549 cells were transfected with two different combinations of YAP and TAZ-specific siRNAs (siYAP/TAZ #1, siYAP/TAZ #2). Total RNA was isolated 24 h after transfection. Quality control and RNA-sequencing (RNA-seq) were performed at BGI (Hongkong, China). In this process, only samples with an RNA integrity number (RIN) > 7 were considered for RNA-seq. For the library preparation, the rRNA removal method was utilized to ensure the sequencing of lncRNAs lacking a poly(A) tail.

RNA-seq data were analyzed with R and Bioconductor using the package systemPipeR[175]. Quality control of raw sequencing reads was performed using FastQC (https://www.bioinformatics.babraham.ac.uk/projects/fastqc/). Here, low-quality reads were removed using trim_galore (version 0.6.4). The resulting reads were aligned to human genome version hg19 (HLF) and GRCh38.p13 (A549) from GeneCode and counted using kallisto version 0.46.1[172]. The count data was transformed to log2-counts per million (logCPM) and differential expression analysis was performed using the R package limma[173]. A false positive rate of $\alpha = 0.05$ after false discovery rate (FDR) correction was taken as the level of significance. For a visual representation of the data, heatmaps, volcano plots, and Venn diagrams were created using the R packages ComplexHeatmap[171], EnhancedVolcano (https://github.com/kevinblighe/EnhancedVolcano), and VennDiagram[177], respectively. Raw and normalized data were deposited in the Gene Expression Omnibus database (https://www.ncbi.nlm.nih.gov/geo/;GSE207724).

3.2.4 Expression data analysis

Cancer Cell Line Encyclopedia (CCLE) expression data were downloaded from the depmap portal[182] and filtered for HCC and LUAD cell lines. Expression values were z-scaled and visualized using the R packages pheatmap (https://CRAN.R-project.org/package=pheatmap) and ComplexHeatmap[171], respectively.

3.2.5 ChIP-Seq data analysis

TEAD1, TEAD3, and TEAD4 ChIP-Seq data from liver cancer cells (HepG2) and TEAD4 ChIP-Seq data from A549 cells were obtained from the ENCODE project (GSE96195, GSE96302, GSE170161, and GSM1010868, respectively)[179,180]. TEAD1 and TEAD4 Chip-Seq data from HuCCT1 cells were retrieved from GEO (GSE68296)[178]. BED files, containing peak information, were used for ChIP-Seq data analysis. In this process, peak positions were annotated to the genes in closest proximity using the Bioconductor package ChIPseeker[169]. For each peak, a score was calculated, which consisted of both the peak height and the peak width (height/width). To account for background noise, peaks with a score lower than the first quartile were excluded from subsequent analysis. Intersection analysis was performed using the R package VennDiagram[177]. To visualize the ChIP-Seq data, BigWig files containing the information about a transcription factor binding event at each base pair of the genome were binned and the corresponding ChIP-Seq tracks were plotted using the function trackplot[176].

3.2.6 Chromatin immunoprecipitation (ChIP)

For ChIP experiments, HLF cells were seeded onto 15 cm dishes and incubated until reaching about 80% confluency. Formaldehyde crosslinking was achieved by fixing the cells with 1% formaldehyde in PBS at RT for 15 min, followed by quenching with 125 mM glycine for 5 min. Subsequently, the cells were washed twice with cold PBS. Cells were harvested in 1 ml RIPA buffer supplemented with 1x Protease Inhibitor Mix G and sonicated to generate fragments of genomic DNA < 500 bp. Cell debris were removed via centrifugation at 16,000 g at 4°C for 15 min. For preclearing of the protein lysates, Dynabeads® Protein G were resuspended in RIPA buffer and incubated with 1 ml of the protein lysates at 4°C for 1.5 h under rotation. In the meantime, Dynabeads were prepared for IP by washing with RIPA buffer and blocking with BSA (1 mg/ml) and salmon sperm DNA (0.3 mg/ml) at 4°C for 1.5 h under rotation. After preclearing, samples were mixed with 2 µg of a specific antibody or IgG as control and blocked Dynabeads flowed by incubation at 4 °C under rotation overnight. The next day, the beads were then washed several times (4 x RIPA, 4 x IP wash buffer, 2 x TE) with a 5 min rotation in between. Subsequently, the beads were shortly washed with and resuspended in TE buffer. The protein-DNA complexes were eluted from the Dynabeads with Talianidis elution buffer at 65°C for 10 min. Crosslinking reversal of the supernatant was achieved by adding 4 M NaCl and incubation at 65°C for 5 h. DNA was purified using the NucleoSpin® Gel and PCR Clean-up Kit according to the manufacturer's protocol. Finally, promoter binding was analyzed with qPCR using a serial dilution of genomic DNA as a reference standard curve.

ChIP primers were designed based on the TEAD4 binding sites identified by ChIP-Seq data analysis in combination with the prediction of TEAD4 binding sites using the JASPAR

database[167]. Commercially available primers covering the human CTGF promoter and primers covering the CTGF upstream region without transcription factor binding sites served as positive and negative controls, respectively.

3.3 Methods of protein and RNA biochemistry

3.3.1 Protein isolation and quantification

Total protein extracts were isolated from cultured cells using 1x Cell Lysis Buffer, supplemented with 1x PhosStop and 1x Protease Inhibitor Mix G. For complete disruption of cellular membranes, samples were sonicated 3x 20 s in an ultrasound waterbath and cooled on ice in between. Cell debris were removed by centrifugation at 18,000 x g at 4°C for 10 min. Protein concentration of the supernatant was determined by either measuring the absorption at 280 nm using a NanoDrop device or performing a Bradford Assay. Regarding the latter, 1.25 µl protein lysate was mixed with 11.25 µl H_2O and 625 µl Bradford Reagent. The optical density was measured at 595 nm using a photometer and the protein concentration was calculated based on a BSA standard curve. Protein lysates were stored at -20°C.

3.3.2 SDS-Polyacrylamide gel electrophoresis (PAGE) and Western immunoblotting

Protein lysates were separated according to their molecular weight using 8%-10% sodium dodecyl sulfate-polyacrylamide gel electrophoresis (SDS-PAGE). Before loading onto the gels, protein samples were mixed with 4x protein sample buffer and were boiled at 95°C for 5 min. Electrophoresis was carried out at 120 V for 2 h in SDS-running buffer and separated proteins were blotted to a nitrocellulose membrane using ice-cold borate buffer at 130 V and 600 mA/chamber for 1.5 h. Subsequently, the membranes were blocked in 5% BSA in TBS-T for 30 min, followed by primary antibody incubation in blocking solution at 4°C overnight (Table 13). Membranes were washed three times with TBST and incubated with the corresponding secondary antibody (Table 14) in blocking solution at RT for 1 h. The next step, membranes were washed three times with TBST and fluorescence signals were detected and quantified using Odyssey-CLx Infrared Imaging system with the ImageStudio Lite software. GAPDH or β-Actin served as loading controls.

3.3.3 Subcellular protein fractionation

Subcellular protein fractionation was performed using the NE-PER™ Nuclear and Cytoplasmic Extraction Reagents kit. For this, cells were seeded at low cell density concentrations (150,000 cells/10 cm dish). The next day, cells were harvested and treated according to the manufacturer's instructions. Fractionation success was assessed by SDS-PAGE and Western immunoblotting. GAPDH and PARP served as cytoplasmic and nuclear loading control, respectively.

3.3.4 Immunofluorescence

For immunofluorescence stains, HLF cells were seeded on coverslips under different cell density concentrations ranging from low (100,000 in 6-well plate) to high density conditions (500,000 in 6-well plate). The next day, fixation of cells was performed with 4% paraformaldehyde in PBS for 15 min, followed by 7 min permeabilization in 0.2% Triton X-100/PBS. After two washing steps with PBS, coverslips were blocked in 1% BSA/PBS for 30 min and incubated with primary antibodies overnight. After 24h, coverslips were washed three times with PBS, followed by Alexa-488 conjugated secondary antibody incubation at RT in a wet chamber for 1 h. Subsequently, coverslips were washed three times with PBS, rinsed with aqua dest. and incubated in 100% ethanol for 5 min. After drying, the coverslips were mounted on microscope slides with DAPI Fluoromount-G®. Images were conducted at 40x magnification with an Olympus IX81 microscope using the Olympus CellSens Dimension software. Image processing and analysis was performed using ImageJ[183].

3.3.5 Immunohistochemistry (IHC)

Immunohistochemical staining was performed on formalin-fixed, paraffin-embedded (FFPE) tissue sections. For this, FFPE tissues were cut into 3 μm sections using a microtome, mounted on microscope slides and dried overnight. Slides were deparaffinized and rehydrated by a series of washing steps: xylene (3 x 5 min), 100% ethanol (2 x 2 min), 96% ethanol (2 x 2 min), 70% ethanol (2 x 2 min), and rinsed with aqua dest. Antigen retrieval was performed in a pressure cooker (YAP, 8 min; Ki-67, 15 min) or steamer (TAZ, 30 min) with Target Retrieval Solution Citrate pH 6. After cooling down, slides were washed with TBS (YAP, Ki-67) or TBS-T (TAZ) for 10 min and subsequently incubated with primary antibodies in a wet chamber at 4°C overnight (YAP) or for 1 h (Ki-67, TAZ). Slides were washed twice with TBS or TBS-T for 5 min and incubated with Enhancer Detection Line for 25 min, followed by 2 x 5 min TBS washing steps, and AP-Polymer Detection Line incubation (YAP, 20 min; TAZ 1 h) or incubated with POLYVIEW® PLUS AP (anti-rabbit) reagent for 45 min (Ki-67). Subsequently the slides

were washed twice with TBS or TBS-T for 5 min and developed using the Permanent AP Red Kit for 5 min. IHC staining was performed by the IHC research facility at the Institute of Pathology, Heidelberg (CMCP, head: Dr. Tanja Poth). Tissue slides from cohort 2 were stained using Mouse and Rabbit Specific HRP/DAB IHC Detection Kit (Abcam, Cambridge, UK) according to manufacturer's protocol. Slides were digitalized using the digital slide scanners Aperio AT2 at 40x magnification.

3.3.6 RNA *in situ* hybridization

Detection of RNA molecules on FFPE tissue slides was performed using an RNAscope 2.5HD kit according to the manufacturer's instructions. In brief, FFPE tissues were cut into 5 μm sections using a microtome, mounted on microscope slides (SuperFrost® Plus) and dried overnight. Sections were baked at 60°C for 1 h and subsequently deparaffinized and rehydrated by a series of washing steps: xylene (2 x 5 min) and 100% ethanol (2 x 1 min). Tissues were dried and hydrogen peroxide was added at RT for 10 min. The slides were washed twice with aqua dest and treated with boiling target retrieval solution for 15 min. After a series of washing steps in aqua dest. (2x) and 100% ethanol, the tissue section was encircled with a hydrophobic barrier pen and dried at RT overnight. The next day, the sections were incubated with protease plus at 40°C for 45 min in a humidified oven. The slides were washed and hybridization with specific probes was performed at 40°C for 2 h. Afterwards, the signal was amplified in 6 consecutive steps (AMP 1-6) exactly following the manufacturer's instructions. In between each hybridization/amplification step, the slides were washed twice in wash buffer for 5 min. The signal was detected by incubating the slides with 3,3′-diaminobenzidine (DAB) at RT for 10 min. For counterstaining, the slides were incubated in 50% hematoxylin for 1 min and subsequently washed in 0.02% ammonia water for 10 s. In a last step, the slides were dehydrated and mounted by a series of washing steps: 70% ethanol (1 x 2 min), 95% ethanol (2 x 2 min), and xylene (1 x 5 min). Probes for SNHG1, CYTOR and Morrbid were designed and obtained from the manufacturer. PPIB and DapB genes served as positive and negative controls, respectively. Slides were digitalized using the digital slide scanners Aperio AT2 at 40x magnification.

3.3.7 RNA subcellular isolation

Total, nuclear and cytoplasmic RNA was isolated from cultured cells using the RNA subcellular isolation Kit according to the manufacturer's instructions.

3.4 Functional assays

3.4.1 Cell viability assay

To measure cell viability, cells were seeded and transfected with gene-specific siRNAs and control siRNA or treated with respective concentrations of TED-347 as described. At indicated time points, 1 ml Resazurin agent (1:10 dilution in cell culture medium) was added onto the cells and incubated at 37°C for 1 h. Subsequently, the supernatant was transferred to a 96-well plate (5 technical replicates) and light emission was measured using a FLUOstar Omega microplate reader. RNA was isolated for downstream analysis.

3.4.2 BrdU-ELISA cell proliferation assay

To measure the effect of gene-specific knockdown on cell proliferation, BrdU-ELISA assay was performed. In brief, cells were seeded and transfected with gene-specific siRNAs and control siRNAs as described. 72 h post transfection BrdU-ELISA assay was performed according to the manufacturer's instructions.

3.4.3 Colony formation assay

To investigate colony formation, cells were seeded and transfected with gene-specific siRNAs and control siRNAs as described. 24 h post transfection, cells were seeded at low cell numbers (1,000-2,000 cells/well) into 6-well plates (3 technical replicates) and cultured for 10-14 days. Cells were then washed with PBS, 0.5% crystal violet solution was added, and the cells were incubated for 1 h. Subsequently, cells were washed with water to remove any crystal violet residues. Colony area was assessed using the ImageJ plugin ColonyArea[170].

3.5 Mouse work

3.5.1 Mouse model

All experiments were performed in accordance with the institutional regulations of the IBF (Interfakultäre Biomedizinische Forschungseinrichtung, University of Heidelberg) under pathogen-free conditions. The mouse colony was housed under a 12-hour light/dark cycle with free access to water and food. Exclusion and termination criteria were defined in the ATBW criteria (officials for animal welfare).

The LAP-tTA/Col1A1-YAP^{S127A} transgenic mouse models for the inducible expression of constitutively active human YAP^{S127A} were used for this study[108,152]. Liver tissue samples and

RNA samples from control mice and animals with YAP[S127A] expression (6 weeks after transgene induction) were kindly provided by Dr. Sofia Weiler (Institute of Pathology, Heidelberg, Germany)[108].

3.5.2 Mouse tissue analysis

For a visual quantification of stained mouse liver sections, a score was derived for each tissue sample from the following scoring system: quantity (1, ≤1% positive; 2, 1%–5% positive; 3, 6%–20%; and 4, ≥20% positive cells) and intensity (1, low/not detected; 2, moderate; and 3, high). The product of quantity and intensity was calculated (range: 1-12). For YAP, only the nuclear staining scores were evaluated. For Ki-67 stains, only quantity scores were determined (range 1-4).

To quantify in situ hybridization of the murine lncRNA Morrbid, stained mouse liver tissue sections were digitalized using the digital slide scanners Aperio AT2 at 40x magnification. The digital whole slide images were then divided into tiles (1 mm^2 size) using OpenSlide bindings to python via open source Automated Slide Analysis Platform (ASAP) software. Tiles containing scanning artifacts or less than 50% tissue content were excluded from further analysis. A random forest machine learning algorithm was trained to recognize Morrbid signals using Ilastik software (v1.3.3)[184]. The trained algorithm was afterwards applied to all tiles to generate probability maps of detected classes. The probability maps were thresholded and the Morrbid signals were quantified per tissue area with ImageJ scripts (v1.53q)[185].

3.6 Human patient data analysis

3.6.1 Patient samples

This study comprises paraffin-embedded HCC samples and matched serum samples from different sources: Hannover Medical School (n=10), University Hospital Heidelberg (n=7), and National Liver Institute, Menoufiya University, Egypt (n=8). The use of patient material for research purposes was approved by the respective institutional ethics committees of Hannover (3434-2016, 1818-2013), Heidelberg (S-206/2005, S-428/2013, S-359/2018), and Cairo (00163/2019). Cohort features are listed in Table 23.

Table 23 | HCC patient cohort features.

Nr.	Age	Gender	Time between blood collection and tissue collection (TC) (Months; +: after TC, -: before TC)	Cancer diagnosis	Grading	Staging
cohort1_1	75	m	+136	HCC	NA	NA
cohort1_2	44	m	+3	HCC	G3	pT1a, Nx
cohort1_3	49	m	+18	HCC	G2	NA
cohort1_4	50	m	+23	HCC	G1	pT1, Nx
cohort1_5	60	f	+19	HCC	G2	pT1, N1
cohort1_6	72	m	+12	HCC	G1	NA
cohort1_7	60	m	+11	HCC	G2	pT1, N0
cohort1_8	62	m	-1	HCC	G3	pT2, N0, Mx
cohort1_9	69	m	-0,5	HCC	G2	pT1, NX
cohort1_10	65	f	-0,5	HCC	G2	pT1, Nx
cohort1_11	61	f	+42	HCC	G2	pT2, Nx
cohort1_12	61	m	+2	HCC	G2	pT3a, Nx
cohort1_13	65	m	+3	HCC	G2	pT1, Nx
cohort1_14	70	m	+5	HCC	G3	pT1, NX
cohort1_15	75	f	0	HCC	G2	pT2, Nx, Mx
cohort1_16	69	m	+16	HCC	G2	pT3a, N0
cohort1_17	74	m	+57	HCC	G2	pT2, Nx, pMx
cohort2_1	55	m	0	HCC	G2	pT2, N0, M0 (stage II)
cohort2_2	60	m	0	HCC	G2	pT2, N0, M0 (stage II)
cohort2_3	57	m	0	HCC	G1	pT1b, N0, M0 (stage IB)
cohort2_4	59	m	0	HCC	G2	pT1a, N0, M0 (stage IA)
cohort2_5	74	m	0	HCC	G2	pT2, N0, M0 (stage II)
cohort2_6	53	f	0	HCC	G2+3	pT4, N0, M0
cohort2_7	55	m	0	HCC	G2	pT2, N0, M0 (stage II)
cohort2_8	66	m	0	HCC	G2	pT2, N0, M0 (stage II)

Tumor samples used for the HCC tissue microarray (TMA) analysis were surgically resected at the University Hospital of Heidelberg and histologically classified according to established

criteria by two experienced pathologists. The TMA contained 40 non-tumorous liver tissues, 174 cirrhotic liver tissues, and 476 HCCs (grading: G1 = 87, G2 = 311, G3/4 = 78). The study was approved by the institutional ethics committee of the Medical Faculty of Heidelberg University (S-206/2005).

Expression data from TCGA cohorts and related clinical features were downloaded from the UCSC Xena database (https://xena.ucsc.edu)[186].

3.6.2 TCGA data analysis and signature score calculation

To analyze TCGA expression data, ENSEMBL IDs were mapped to respective gene IDs. In case multiple ENSEMBL IDS mapped to the same gene ID, the expression values were averaged. Subsequently, gene expression values were z-scaled and discretized into 10 bins using the R packages pheatmap and biclust (https://CRAN.R-project.org/package=biclust). K-mean clustering was applied to stratify patients into two groups (lncRNA high and lncRNA low) using the R package ComplexHeatmap. The Random Forest-based Boruta method[168] was used to rank genes according to their importance for patient subclustering.

For each patient, scores for different signatures were calculated: lncRNA signature (described here) and a YAP target gene signature that contributes to chromosomal instability[108,187]. To assure that each gene contributes equally to a signature score, single expression values were divided by the mean expression of the corresponding gene in all samples. For each patient, the calculated values were added. Balanced scores were statistically associated using the Spearman's rank correlation coefficient.

3.6.3 Detection of lncRNAs in serum samples

Total RNA was isolated from serum samples using the miRNeasy Serum/Plasma Advanced Kit according to the manufacturer's protocol. For this, 100-200 µl serum were transferred into a 2 ml reaction tube. Afterwards, 60 µl of the lysis buffer RPL were added, vortexed for 5 s and incubated at RT for 3 min to ensure a complete lysis and denaturation of protein complexes. To account for variances introduced in the RNA isolation process, 3 µl of a custom spike-in control (10 nM) was added to the lysate. Subsequently, 20 µl of buffer RPP was added to samples, which were then vigorously vortexed for 20 s, incubated at RT for 3 min, and centrifuged at 12,000 g at RT for 3 min to precipitate inhibitors and highly concentrated proteins. The supernatant was transferred into a new tube and 1 volume of isopropanol was added to provide appropriate binding conditions for RNA molecules. The samples were then loaded onto RNeasy UCP MinElute spin columns and centrifuged at 8,000 g for 15 s to bind total RNA to the membrane. After a series of washing steps to efficiently remove all

contaminants (700 µl buffer RWT, 8,000 g for 15 s; 500 µl buffer RPE, 8,000 g for 15s; 500 µl 80% ethanol, 8,000 g for 2 min) columns were dried and the RNA was eluted with 20 µl RNase-free H_2O. RNA was stored at -80°C.

Reverse transcription was performed with 7 µl total RNA using PrimeScript RT Master Mix according to the manufacturer's instructions. Patient-derived cDNA was stored at -80°C. After cDNA synthesis, the lncRNAs of interest were pre-amplified using the Prelude PreAmp Master Mix. For this, equal volumes of each specific primer pair for candidate lncRNAs, negative control lncRNAs and spike-in control were added to each sample (final concentration: 500 nM). The pre-amplification reaction was performed with the following cycling conditions: 95°C for 2 min, followed by 14 cycles of 95°C for 10 s and 60°C for 4 min. qPCR was used as previously described to quantify lncRNA serum expression levels. The results were normalized to the spike-in control to account for any technical variances that occurred during the isolation process. The use of a spike-in control was required as, no reliable endogenous serum-derived house-keeping genes has been described for serum sample normalization.

3.6.4 Correlation of lncRNA serum score with nuclear YAP abundance

To investigate YAP activity in tissue samples, nuclear YAP expression was assessed by immunohistochemistry. A score was derived by the following scoring system: 1, not detected; 2, low; 3, moderate; and 4, high. lncRNA signature scores for serum samples were calculated according to 3.6.2. Balanced lncRNA serum scores and the corresponding nuclear YAP IHC scores were statistically associated using the Spearman's rank correlation coefficient.

3.6.5 TMA analysis

To visually analyze the TMA staining, a score was derived for each tissue sample from the following scoring system: quantity (1, ≤1% positive; 2, 1%–5% positive; 3, 6%–20%; and 4, ≥20% positive cells) and intensity (1, low/not detected; 2, moderate; and 3, high). The product of quantity and intensity was calculated (range: 1-12). For YAP, the nuclear and cytoplasmic staining scores were evaluated separately. For Ki-67 stains, only quantity scores were determined (range 1-4). Regarding in situ hybridization analysis of TMAs, a scoring system consisting of quantitative parameters was applied (1, not detected; 2, very low; 3, low; 4, moderate; and 5, high). Visual evaluation was performed by two experienced investigators.

3.7 Statistical analysis

Data is presented as mean ± standard deviation. Suitable statistical tests were performed using GraphPad Prism 9 software and R version 4.1.0. For each experiment, statistical details can be found in the figure legends. Statistical comparison of two groups relied on the nonparametric Mann-Whitney U test. The association between data series was calculated using the Spearman correlation coefficient. For multiple testing, Dunnett's test was employed. Overall patient survival was assessed by the Kaplan-Meier method and statistically compared using the log-rank (Mantel-Cox) test or Gehan-Breslow-Wilcoxon test. Receiver operating characteristics (ROC) curve analysis was performed using the R package pROC[174]. Significance levels were defined as follows: *p≤0.05, **p≤0.01, ***p≤0.001.

4 Results

4.1 Identification of YAP/TAZ-regulated lncRNAs in cancer cells

The role of the Hippo pathway and its downstream effectors YAP and TAZ in carcinogenesis has been described and protein-coding gene signatures exist that serve as proxy for YAP/TAZ activity (YAP signature[108,187], YAP/TAZ target gene signature[111]). To identify lncRNAs that may serve as cancer-spanning biomarkers for YAP/TAZ, I established an *in vitro* screening approach integrating RNA-seq data from siRNA screens and publicly available ChIP-seq data. For this, the HCC cell line HLF and the LUAD cell line A549 were selected due to their high intrinsic YAP/TAZ activity as illustrated by high protein levels of YAP and TAZ, increased expression of Hippo pathway-associated genes and target gene signatures, as well as nuclear abundance of both effector proteins (Figure 4A-C). To ensure that the screening approach predominantly captured lncRNAs that were directly regulated by YAP/TAZ and not indirectly through secondary regulatory mechanisms, siRNA-mediated silencing of YAP/TAZ was optimized to identify the earliest possible knockdown for both proteins. In this process, HLF cells were transfected with two different combinations of siRNAs targeting YAP and TAZ and total protein was isolated to identify the earliest time when YAP/TAZ protein levels are reduced by at least 75%. As shown by Western blot analysis YAP and TAZ abundance was decreased 24 h post-transfection (Figure 4D). Real-time PCR confirmed the efficient inhibition of YAP/TAZ transcripts in HLF and A549 cells (Figure 4E).

The integrative analysis workflow for the identification of pan-cancer YAP/TAZ-dependent lncRNAs is illustrated in Figure 5A. After combined YAP/TAZ inhibition and subsequent NGS analysis, 5,476 (HCC) and 6,447 (LUAD) significantly regulated genes were identified (FDR ≤ 0.5), 258 (HCC) and 322 (LUAD) of which were pseudo- and long non-coding RNAs (lncRNAs; Figure 5B). To identify lncRNAs that may serve as markers for increased YAP/TAZ activity, the data was filtered for downregulated lncRNAs (fold change ≤ 0.75), which resulted in 45 (HCC) and 48 (LUAD) potential candidates that were directly regulated by YAP and/or TAZ (Figure 5C). Importantly, the expression of protein-coding gene signatures that define YAP/TAZ activation was downregulated upon YAP/TAZ silencing, thereby confirming the validity of the siRNA screens (Figure Appendix 1A and Figure Appendix 2A).
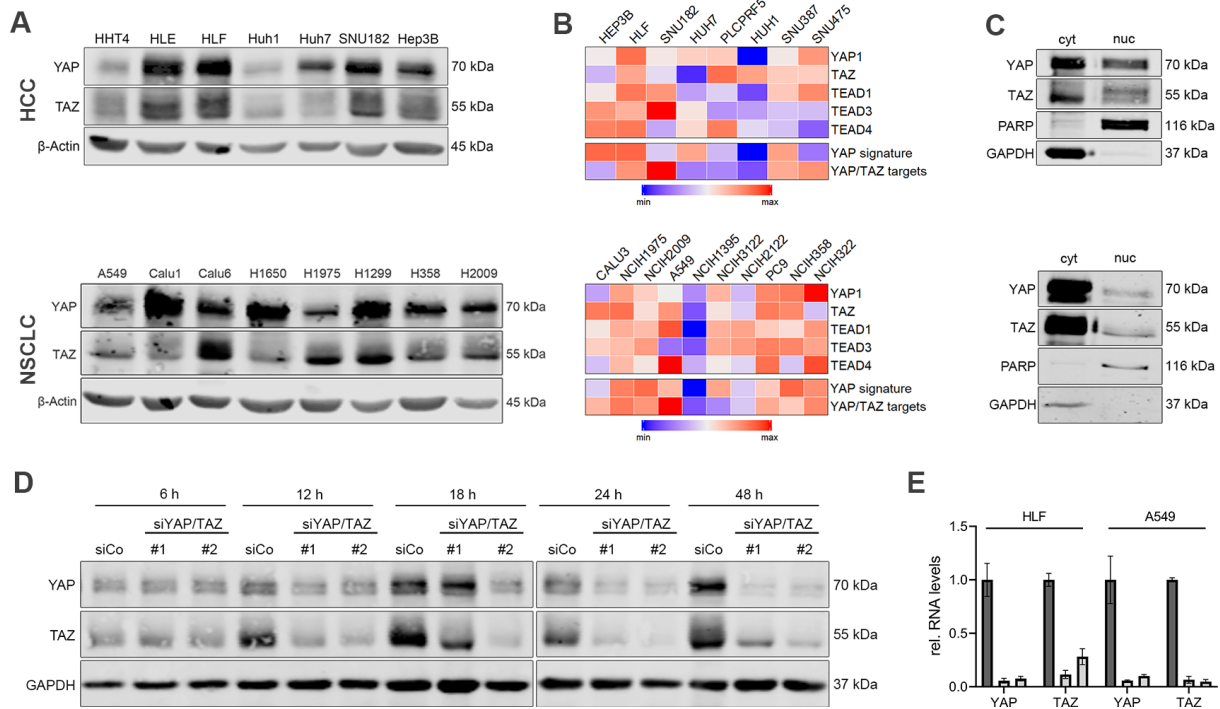
Figure 4 | Parameter optimization prior to RNA-sequencing. (A) Western immunoblot illustrating YAP/TAZ protein abundance in different HCC (upper panel) and NSCLC cell lines (lower panel). HHT4 was used as proxy for normal hepatocytes. β-Actin served as loading control. **(B)** Heatmap summarizing CCLE gene expression data of HCC (top) and NSCLC cell lines (bottom), including Hippo-pathway relevant genes and known YAP/TAZ target gene signatures. **(C)** Western immunoblot of YAP/TAZ after subcellular fractionation in HLF (upper panel) and A549 (lower panel) cells. PARP and GAPDH served as fractionation control for nuclear (nuc) and cytoplasmic (cyt) protein fractions, respectively. **(D)** Western immunoblot illustrating protein reduction of YAP/TAZ in HLF cells after transfection of different combinations of YAP/TAZ-specific siRNAs at indicated time points. GAPDH served as loading control. **(E)** qPCR analysis of YAP/TAZ after combined YAP/TAZ silencing in HLF and A549 cells for 24 h.

As YAP and TAZ are transcriptional co-activators, which interact with TEAD transcription factors to control target gene expression, I used publicly available ChIP-Seq data sets of TEAD1/3/4 derived from liver cancer cells (HepG2 and HuCCT1) and TEAD4 derived from LUAD cells (A549) to further narrow down the number of potential YAP/TAZ-dependent lncRNA candidates[109,178-180]. The liver cancer datasets were filtered for lncRNAs with predicted bindings sites of at least two TEAD family members (n = 1,728) (Figure 5D). For LUAD, 1,294 lncRNAs with TEAD4 binding sites in their promotor region were identified. Combining the results from both experimental and bioinformatic analyses for each tumor entity led to 23 and 17 lncRNA candidates that were probably directly regulated by YAP/TAZ/TEAD in HCC and LUAD, respectively (Figure 5E, Figure Appendix 1B, and Figure Appendix 2B).
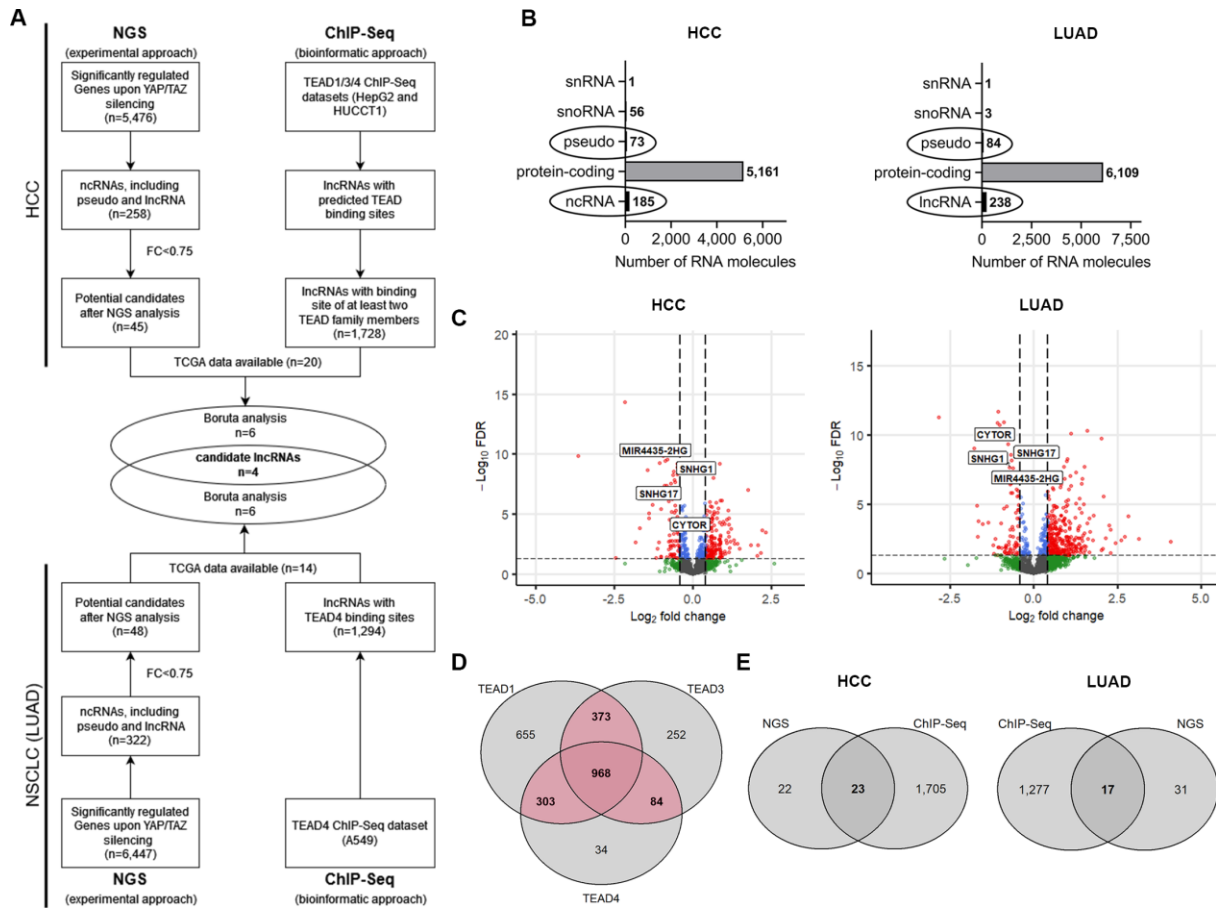
Figure 5 | Identification of YAP/TAZ regulated lncRNAs in HCC and LUAD cells. (A) Schematic overview of analysis workflow integrating NGS data after combined YAP/TAZ inhibition in HLF (HCC) and A549 (LUAD) cells and publicly available ChIP-Seq data (for TEADs). For the siRNA screens, two different siRNA combinations targeting YAP and TAZ were used (siYAP/TAZ #1 and #2). ChIP-Seq data were derived from the GEO database (TEAD1/3/4 for HCC; TEAD4 for LUAD). **(B)** Bar graph summarizing RNA species significantly regulated by YAP/TAZ in HLF (left) and A549 (right) cells. Pseudo and ncRNA were used for further selection steps (n = 258 for HCC; n = 322 for LUAD). **(C)** Exemplary volcano plots of differentially expressed lncRNAs after YAP/TAZ siRNA#1 inhibition in HLF (left) and A549 (right) cells. The final four candidate lncRNAs are highlighted. Horizontal dashed line represents FDR = 0.05; vertical dashed lines represent fold change = 0.75. **(D)** Venn diagram illustrating the presence of TEAD family member binding sites (TEAD1/3/4) in the promotor region of lncRNAs in liver cancer cells. lncRNAs with at least two TEAD binding sites were used for further analysis (highlighted in red; n = 1,728) **(E)** Venn diagram showing the comparison of NGS and ChIP-Seq data analysis in HCC (left) and LUAD (right). In total, 23 and 17 lncRNA candidates were selected for subsequent analysis.

In a next step, the relevance of each lncRNA for cancer patient classification was analyzed by random forest-based Boruta ranking using HCC and LUAD TCGA data. TCGA expression data was not available for 3 of the candidate lncRNAs in both cohorts, which let me include 20

(HCC) and 14 (LUAD) potential lncRNAs in the subsequent analyses[12,168]. This method showed that a panel of 13/20 (HCC) and 10/14 (LUAD) lncRNAs was able to divide patients into two groups (high and low expression of lncRNAs) as their importance was valued higher than the best randomized feature (shadowMax) (Figure 6A). However, the results also illustrate that 6 lncRNAs were visually more important for the classification of HCC and LUAD patients than the remaining lncRNAs (red line). Thus, integrating both screening approaches allowed me to define a small lncRNA panel consisting of cytoskeleton regulator RNA (CYTOR), MIR4435-2 host gene (MIR4435-2HG), small nucleolar RNA host gene 1 (SNHG1), and small nucleolar RNA host gene 17 (SNHG17), which was commonly regulated by YAP/TAZ in HCC and LUAD cells (see intersection area in Figure 5A).

This 4-lncRNA signature was able to divide HCC and LUAD patients into low and high-expressing groups using k-mean clustering (Figure 6B). In order to investigate if the panel of lncRNAs was indicative for YAP activity in both cohorts, a balanced lncRNA signature score was calculated and correlated with a YAP-dependent protein-coding gene panel[108,187]. The results illustrated a significant positive correlation between lncRNA and YAP signature abundance in HCC (r = 0.286) and LUAD (r = 0.523) (Figure 6C). Furthermore, the general expression of the lncRNA signature in tumor tissues compared to tissue samples from healthy individuals was analyzed, which showed significant overexpression of lncRNA expression levels in HCC and LUAD tissues (Figure 6D). To test, if the lncRNA signature was predictive for patient prognosis, survival data were analyzed and revealed that lncRNA signature abundance significantly correlated with poor patient survival, which classified the lncRNA signature as a negative prognostic marker (Figure 6E). However, lncRNA signature overexpression did not statistically associate with any relevant clinicopathological features in HCC and LUAD cohorts (data not shown).

Taken together, the integrative screening approach combining experimental data and bioinformatic methods led to the identification of a 4-lncRNA signature that are controlled by YAP/TAZ activity in different tumor cell types and whose overexpression is indicative for poor clinical outcome in HCC and LUAD patients.
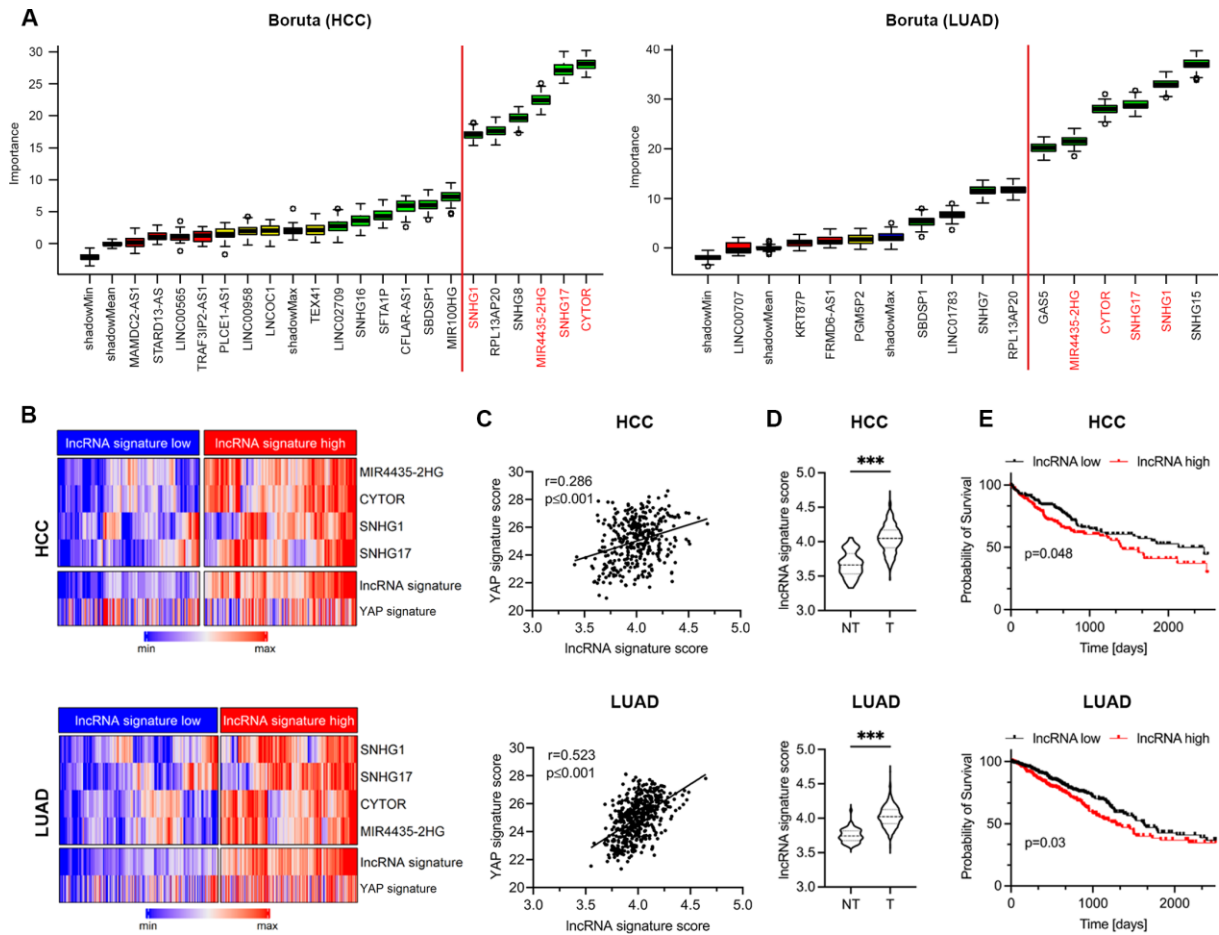
Figure 6 | Definition of a 4-lncRNA signature. (A) Feature selecting Boruta algorithm was applied to identify the most important lncRNAs needed for the classification of HCC (left) and LUAD (right) patients into two groups. 6/20 and 6/14 lncRNAs for HCC and LUAD, respectively, are visually more important than the remaining lncRNAs, indicated by the red line. Those lncRNAs that are present in both tumor cell types were considered as signature constituents The final 4-lncRNA signature consists of CYTOR, MIR4435-2HG, SNHG17 and SNHG1 (highlighted in red). Patient data was obtained from the TCGA database. **(B)** Heatmaps summarizing the expression of the identified 4 lncRNAs, the balanced lncRNA signature score, and YAP target gene signature score in HCC (top, n = 369) and LUAD patients (bottom, n = 510). Patients were stratified into two groups based on k-mean clustering. For HCC: lncRNA low, n = 178; lncRNA high, n = 191. For LUAD: lncRNA low, n = 270; lncRNA high, n = 240. **(C)** Spearman correlations of lncRNA signature score and YAP signature score in HCC (top) and LUAD (bottom). Statistical test: Spearman's rank coefficient. p-values are indicated. **(D)** Violin plots comparing the lncRNA signature expression in tumor (T) and non-tumorous tissue (NT). For HCC (top), 369 tumor and 50 non-tumor specimens were analyzed. For LUAD (bottom), 510 tumor and 58 non-tumor samples were included. Statistical test: Mann–Whitney U test, ***P ≤ 0.001. **(E)** Kaplan-Meier survival curves for HCC and LUAD patients with low and high lncRNA signature expression. p-values are indicated (log-rank test and Gehan-Breslow-Wilcoxon test, respectively).

4.2 Pan-cancer relevance of YAP/TAZ-dependent lncRNA signature

As previously reported, lncRNA abundance and expression levels are considered to be highly cell type and tissue-specific[50]. By including two cancer entities in the identification process, I aimed to define a lncRNA signature whose expression is conserved among different cancer cell lines and thereby could function as a surrogate for YAP/TAZ activity in different tumor entities. To pursue the idea of a cancer-spanning lncRNA signature, I performed a comprehensive analysis of the TCGA mRNA/lncRNA data derived from 32 tumor types[12].

Table 24 | Correlation of balanced lncRNA signature score with YAP-dependent target gene signature in 32 tumor entities (TCGA data)

Tumor entity	r (YAP targets)	p (YAP targets)	n (patients)	
LUAD	0.5225	0.001	510	*strong correlation*
ACC	0.4958	0.001	79	
STAD	0.4682	0.001	373	
LGG	0.3675	0.001	500	
MESO	0.364	0.001	81	
TGCT	0.3245	0.001	149	
READ	0.3189	0.001	163	
KIRC	0.3021	0.001	526	
KIRP	0.2955	0.001	287	
BRCA	0.2894	0.001	1072	
LIHC (HCC)	0.2863	0.001	369	
COAD	0.2825	0.001	453	*moderate correlation*
UVM	0.2674	0.02	77	
GBM	0.2479	0.003	144	
THYM	0.2459	0.007	119	
BLCA	0.2395	0.001	405	
PRAD	0.2206	0.001	481	
HNSC	0.2171	0.001	495	
LUSC	0.2157	0.001	496	
SKCM	0.2122	0.03	103	
THCA	0.21	0.001	497	
CHOL	0.183	0.29	36	*no/weak correlation*
UCEC	0.1783	0.001	537	
PAAD	0.171	0.02	177	
ESCA	0.1593	0.05	152	
OV	0.1562	0.003	354	
SARC	0.1457	0.02	258	
UCS	0.1412	0.47	56	
CESC	0.1151	0.05	296	
DLBC	0.1014	0.5	47	
PCPG	0.0893	0.11	175	
KICH	0.043	0.73	65	

Results

To investigate if the lncRNA signature could be used as a proxy for YAP/TAZ activity in different cancer entities, I analyzed the statistical association of lncRNA signature abundance with the presence of a YAP-dependent mRNA signature. The results illustrated a wide spectrum of correlation between both signature scores, ranging from no/weak to moderate or strong statistical association (Table 24). Interestingly, high discrepancies concerning tumor entities from the same organ could be observed (LUAD, $r = 0.5225$; lung squamous cell carcinoma, $r = 0.2157$), which underlines the cell type-specific character of lncRNA expression and/or the existence of distinct molecular mechanisms that control lncRNA abundance in groups of cancer types.

In addition to HCC and LUAD, renal clear cell carcinoma (KIRC) and colon adenocarcinoma (COAD) represented examples of moderate/strong statistical association between the lncRNA signature score and the YAP target gene signature ($r = 0.3021$, $r = 0.2825$, respectively). K-mean clustering of the expression data sufficiently divided both patient cohorts into two groups and the lncRNA signature was significantly overexpressed in tumors in comparison to non-tumorous tissue. Furthermore, upregulated signature expression statistically correlated with worse overall survival (Figure 7). For some tumor types with strong statistical association between the lncRNA signature score and the YAP target gene signature, no 'normal' tissue was available for comparison with tumor tissue such as adrenocortical carcinoma (ACC, $r = 0.496$) and low-grade glioma (LGG, $r = 0.368$). Nevertheless, increased lncRNA signature expression significantly correlated with poor patient survival in both cohorts (Figure Appendix 3). In contrast, some cancer entities showed much weaker or no association of the lncRNA signature score and the YAP target gene signature, e.g. uterine endometrial carcinoma (UCEC, $r = 0.178$) and esophageal carcinoma (ESCA, $r = 0.159$). Despite their increased signature levels in tumors in comparison to non-tumorous tissue, no statistical association with overall survival could be observed (Figure 7).

Taken together, TCGA data analysis demonstrated that the YAP-dependent lncRNA signature is detectable in several tumor types and could serve as entity-spanning, robust biomarker to identify patients with YAP/TAZ activity.
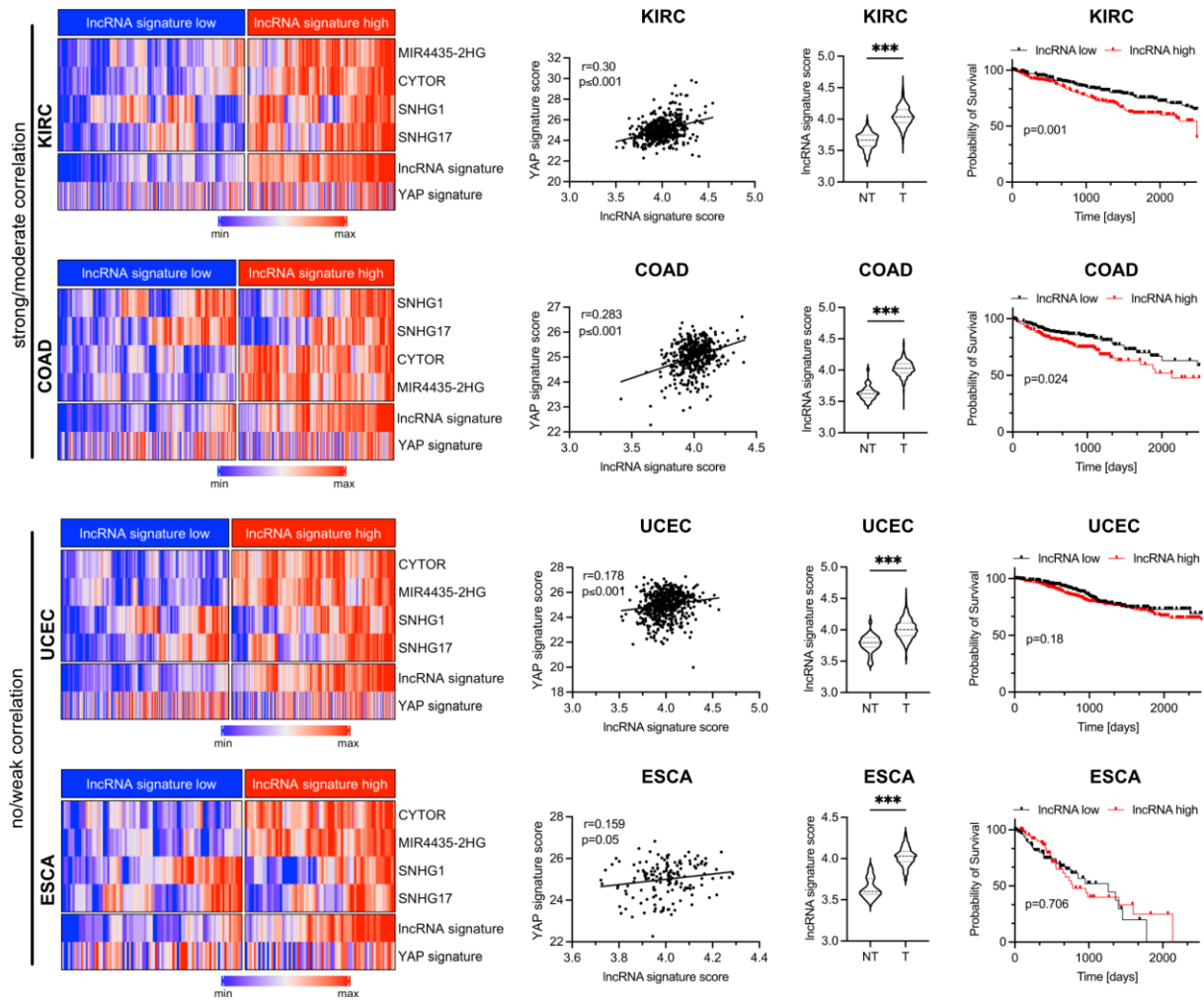
Figure 7 | Analysis of the YAP/TAZ-dependent lncRNA signature in different cancer entities. TCGA mRNA/lncRNA data derived from 32 tumor types was used to investigate 4-lncRNA signature abundance. For instance, renal clear cell carcinoma (KIRC) and colon adenocarcinoma (COAD) show a moderate/strong correlation between the lncRNA signature score and the YAP target gene signature. In contrast, uterine corpus endometrial carcinoma (UCEC) and esophageal carcinoma (ESCA) are examples for a weak association between both lncRNA and YAP signatures. For the exemplary tumor types, the respective heatmap after K-mean clustering, lncRNA/YAP signature correlation, expression of the lncRNA signature in normal and tumor specimen, as well as patient survival are shown (Kaplan-Meier analysis with low and high lncRNA signature expression, log-rank test).

4.3 YAP/TAZ transcriptionally control lncRNA signature expression in HCC cells

To confirm the findings of the screening approach and to investigate YAP/TAZ-dependency of the predicted lncRNA candidates mechanistically, I performed several experiments in HCC cells focusing on relevant features of the Hippo signaling pathway. For all experiments, the known YAP/TAZ target genes CTGF, ANKRD1, and CYR61 served as positive controls. Moreover, RNA-seq data after YAP/TAZ inhibition in HLF cells was screened for suitable YAP/TAZ-independent lncRNAs resulting in the identification of deleted in lymphocytic leukemia 1 (DLEU1) and FTX transcript XIST regulator (FTX), which were further used as negative controls (Figure 8A).

First, I confirmed the results for all 4 lncRNA candidates by independent siRNA-knockdown experiments in HLF cells. The results illustrated a reduction of lncRNA expression upon YAP/TAZ silencing (Figure 8B). Similar results were observed in another HCC cell line (Huh7, Figure 8C/D). Next, cell density-dependent expression was investigated as the Hippo pathway is a critical mediator of cell-cell contact[114]. Indeed, high cell density culture conditions led to the nuclear exclusion of YAP as shown by immunofluorescent staining (Figure 8E). I further investigated if increasing cell density had an impact on lncRNA expression levels. For this, I seeded HLF cells under different cell density conditions ranging from low (100,000 in 6-well plates) to high density (1,000,0000 in 6-well plates) and detected a significant reduction of lncRNA expression with increasing cell numbers (Figure 8F). As expected, the YAP/TAZ target genes CTGF, ANKRD1, and CYR61 were equally regulated while the negative control lncRNAs DLEU1 and FTX did not significantly respond. Next, I examined the YAP/TAZ dependency of the lncRNAs candidates by individually silencing both effectors in HLF cells. The results illustrate that YAP and TAZ knockdown resulted in an equal decrease of CYTOR and SNHG17 levels (Figure 8G). In contrast, YAP silencing led to a stronger reduction of MIR4435-2HG and SNHG1 expression than TAZ knockdown, pointing towards a subordinate role of TAZ in regulating lncRNA expression.
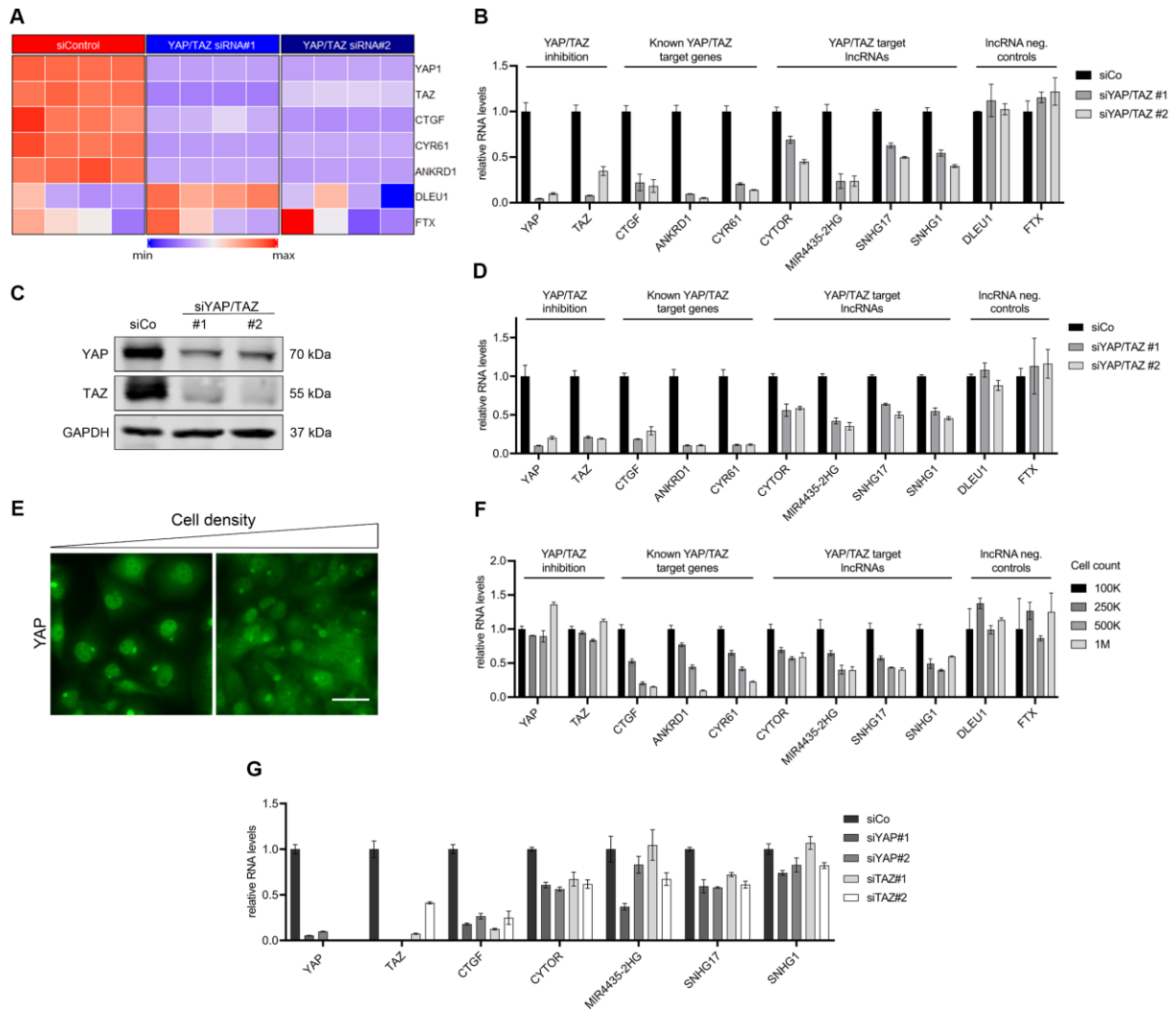
Figure 8 | YAP/TAZ directly control lncRNA signature expression. (A) Heatmap summarizing RNA-seq data for YAP/TAZ, positive controls (CTGF, CYR61, ANKRD1), and lncRNAs DLEU1 and FTX in HLF cells after YAP/TAZ silencing. DLEU1 and FTX were selected as negative controls for further experiments since no significant effect upon YAP/TAZ silencing was observed. Two different siRNA combinations for YAP/TAZ were employed (#1, #2); 4 biological replicates for control and inhibitions were analyzed. **(B), (D)** qPCR analysis of YAP/TAZ, known YAP/TAZ target genes (CTGF, ANKRD1, CYR61), lncRNA candidates (CYTOR, MIR4425-2HG, SNHG17, SNHG1), and negative control lncRNAs (DLEU1, FTX) after combined YAP/TAZ inhibition in HLF and Huh7 cells, respectively. **(C)** Exemplary Western immunoblot of YAP/TAZ after transfection of two different siRNA combinations targeting YAP/TAZ in Huh7 cells. Silencing efficiency for HLF cells was previously tested (Figure 4D). **(E)** Immunofluorescent staining of YAP in HLF cells at different cell density concentrations (100,000 and 500,000 cells/well, respectively). Scale bar: 20 μm **(F)** qPCR analysis of YAP/TAZ, known YAP/TAZ target genes (CTGF, ANKRD1, CYR61), lncRNA candidates (CYTOR, MIR4425-2HG, SNHG17, SNHG1), and negative control lncRNAs (DLEU1, FTX) at different cell density conditions in HLF cells. **(G)** qPCR analysis of YAP/TAZ, CTGF, and lncRNA candidates (CYTOR, MIR4435-2HG, SNHG17, SNHG1) after individual knockdown of YAP and TAZ using two different siRNAs each.

Results

ChIP-Seq data analysis suggested that lncRNA candidates are transcriptionally controlled by TEAD family members (Figure 5A). To functionally confirm this TEAD-dependence, I simultaneously inhibited TEAD1/3/4 by RNA*interference* (RNAi) in HLF cells. For this, the siRNAs were designed to specifically target only TEAD1/3/4 family members. TEAD2 was not included due to variations in sequence identity and structural differences in the binding sites of TEAD family members. The results illustrated that all lncRNAs were regulated by combined TEAD silencing, while the negative control lncRNA DLEU1 did not significantly change (Figure 9A). Interestingly, FTX was affected by TEAD silencing. This was probably due to TEAD binding sites in the FTX gene promoter as predicted by ChIP-seq analysis. Next, we treated HLF cells with increasing concentrations of Verteporfin, a pharmacological inhibitor that disrupts the YAP/TAZ/TEAD interaction in a concentration-dependent manner[188]. Again, the treatment led to a concentration-dependent decrease of lncRNA and positive control gene expression while the negative controls did not respond (Figure 9B).
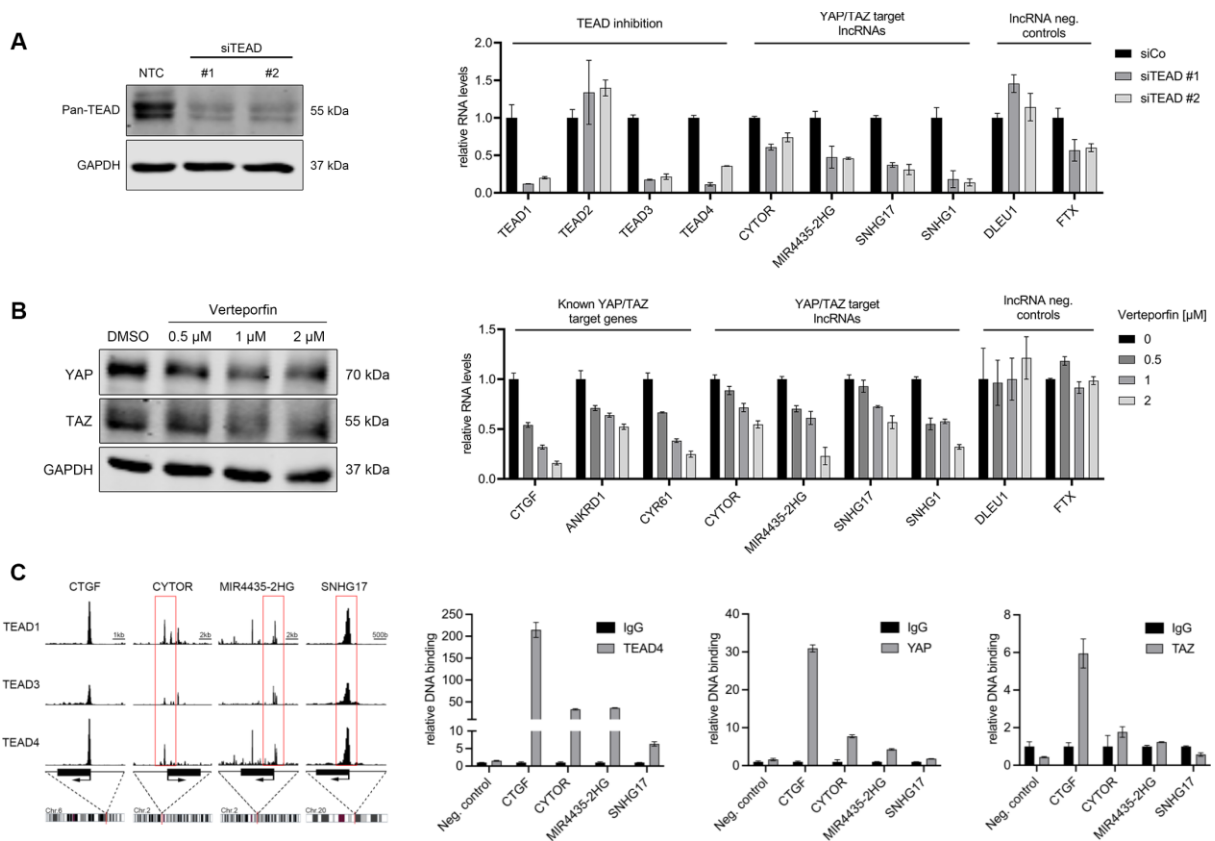

Figure 9 | TEAD-dependency of lncRNA signature. (A) Western immunoblot of all TEAD family members after siRNA-mediated knockdown of TEAD1/3/4 isoforms in HLF cells (TEAD2 is structurally different). qPCR analysis of TEAD1-4, YAP/TAZ target lncRNAs (CYTOR, MIR4435-2HG, SNHG17, SNHG1) and negative control lncRNAs (DLEU1, FTX) after combined silencing of TEAD1/3/4 in HLF cells after 24 h. **(B)** Western immunoblot of YAP/TAZ after treatment with Verteporfin (0.5 - 2 µM). qPCR analysis of YAP/TAZ target genes (CTGF, ANKRD1, CYR61), YAP/TAZ target lncRNAs (CYTOR, MIR4435-2HG, SNHG17, SNHG1), and negative control lncRNAs (DLEU1, FTX) after Verteporfin

treatment in HLF cells for 24 h. DMSO served as control. **(C)** Scheme depicting predicted TEAD1/3/4 binding sites in the promoter region of selected lncRNA candidates (CYTOR, MIR4435-2HG, and SNHG17) and the positive control CTGF. Red box highlights the genomic location used for ChIP primer design. Exemplary ChIP experiments were performed with TEAD4, YAP and TAZ in HLF cells. Primers located in the upstream region of the CTGF promoter served as negative control. IgG was used as antibody control. Results were normalized to the respective IgG controls.

Furthermore, I investigated the physical binding of YAP/TAZ and TEAD4 at three selected lncRNA promotors (SNHG17, CYTOR, and MIR4435-2HG). For this, TEAD4 binding sites were identified through ChIP-Seq data analysis in combination with the JASPAR database[167]. Subsequent ChIP experiments with YAP and TEAD4 immunoprecipitation revealed that both YAP and TEAD4 bound to the predicted target site in all three lncRNA genes (Figure 9C). Commercially available primers covering the human CTGF promoter and primers covering the CTGF upstream region were employed as positive and negative controls, respectively. Interestingly, weaker promoter binding was detectable for TAZ, pointing towards a minor role of this effector in the regulation of Hippo pathway-dependent lncRNAs.

Together, these results demonstrated that YAP and to a minor extent TAZ transcriptionally drive the expression of a distinct set of lncRNAs in HCC cells *in vitro*.

4.4 Increased lncRNA expression in YAP-transgenic mice

In the previous part, I demonstrated a central role of the YAP/TAZ/TEAD complex in regulating lncRNA expression in human cells *in vitro*. Next, I investigated if this relationship could be transferred to an *in vivo* context. For this, I focused on the lncRNAs SNHG1, SNHG17, and MIR4435-2HG for which mouse orthologues exist (murine Snhg1, Snhg17, and Morrbid, respectively). The expression of murine lncRNAs was analyzed in transgenic mice with inducible and liver-specific overexpression of constitutively active YAP (YAP^{S127A})[108,152].

To determine whether YAP transgenic mice showed increased expression of lncRNA signature genes, liver tissue samples from wildtype (WT) (n = 7) and YAP^{S127A} expressing mice (6 weeks after transgene induction; n = 7) were analyzed. Indeed, increased levels of Morrbid and Snhg1 were detectable in YAP transgenic mice in comparison to WT animals, while no change was observed for Snhg17 (Figure 10A). To substantiate cell-type specificity, *in situ* hybridization for Morrbid and immunohistochemical stains for YAP and the proliferation marker Ki67 were performed. YAP and Ki67 stains were visually analyzed, while *in situ* hybridization signals of Morrbid were detected using quantitative image analysis. For this, a random-forest model was trained to recognize Morrbid *in situ* signals, which were subsequently thresholded and quantified using Ilastik and ImageJ, respectively (see methods 3.5.2). The results illustrated

that Morrbid levels were elevated in YAP^{S127A} mice and associated with YAP^{S127A} abundance (r = 0.872, p = 0.067, n = 5; Figure 10B). Furthermore, Morrbid and YAP positivity correlated with the presence of Ki67 (r = 0.9487, p = 0.067, n = 5; r = 0.9733, p ≤ 0.033, n = 5).
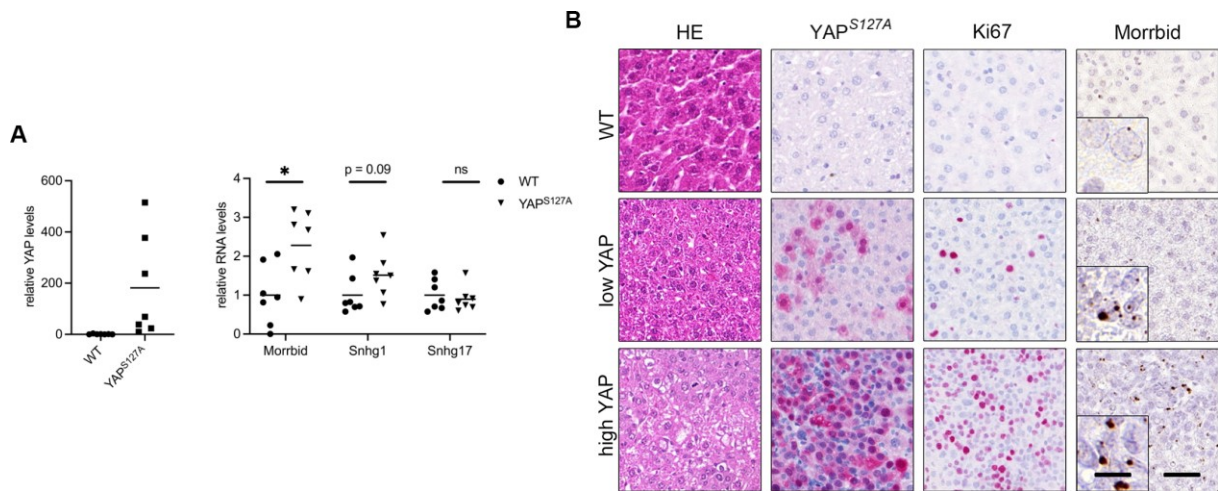

Figure 10 | YAP-dependent expression of lncRNAs *in vivo*. **(A)** qPCR analysis of YAP and lncRNAs for which mouse orthologues exist (Morrbid, Snhg1, Snhg17). Mouse liver tissues from WT (n = 7) and YAP^{S127A}-transgenic (n = 7) animals 6 weeks after transgene induction with no tumor formation were analyzed. Statistical test: Mann–Whitney U test, *P ≤ 0.05; ns: not significant. **(B)** Exemplary hematoxylin and eosin (HE) stains, immunohistochemical stains for YAP^{S127A} and Ki67, as well as *in situ* hybridization of Morrbid are depicted. Specimens with low and high YAP^{S127A} positivity in hepatocytes were selected. Scale bar: lower magnification: 100 µm; higher magnification: 20 µm.

Together, these results illustrated that some signature lncRNAs are transcriptionally controlled by YAP *in vivo*, highlighting their potential as conserved markers for YAP activity.

4.5 YAP/TAZ-dependent lncRNAs facilitate pro-tumorigenic functions of Hippo pathway effectors

YAP/TAZ activation positively correlated with proliferation and HCC cell survival[108] and Morrbid statistically associated with proliferation of YAP-positive hepatocytes (Figure 10B). Because lncRNAs may actively support tumor cell biology[93], I examined if selected lncRNAs do not only serve as potential biomarkers but also contribute to the tumor-supporting phenotype of YAP and TAZ.
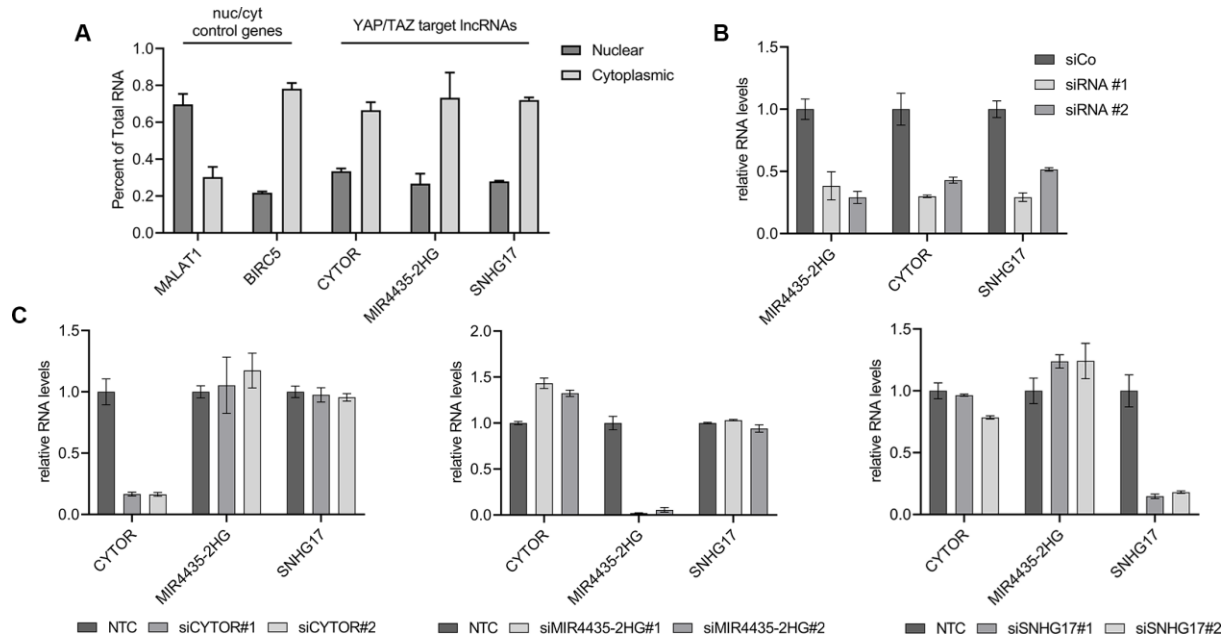
Figure 11 | Silencing of selected lncRNA candidates. (A) qPCR analysis illustrating the subcellular localization of selected lncRNA signature constituents. MALAT1 and BIRC5 served as nuclear and cytoplasmic fractionation controls, respectively. Results are shown as percent of total RNA. **(B), (C)** Exemplary qPCR analysis of lncRNA candidates MIR4435-2HG, CYTOR, or SNHG17 after specific siRNA-mediated knockdown in HLF cells for 72 h.

For this, I first determined their subcellular distribution, since lncRNA knockdown strategies vary in efficacy depending on the cellular localization of lncRNAs[189]. The results illustrated that MIR4425-2HG, CYTOR, and SNHG17 were predominantly localized in the cytoplasm, which pointed to RNAi as the method of choice for lncRNA silencing experiments (Figure 11A). Indeed, lncRNA expression levels were reduced up to 50% upon transfection with two different gene-specific siRNAs (Figure 11B). Importantly, siRNA-mediated silencing exclusively affected the predetermined target lncRNA and not the other tested lncRNAs, which suggested that only lncRNA-specific phenotypes were observed (Figure 11C).
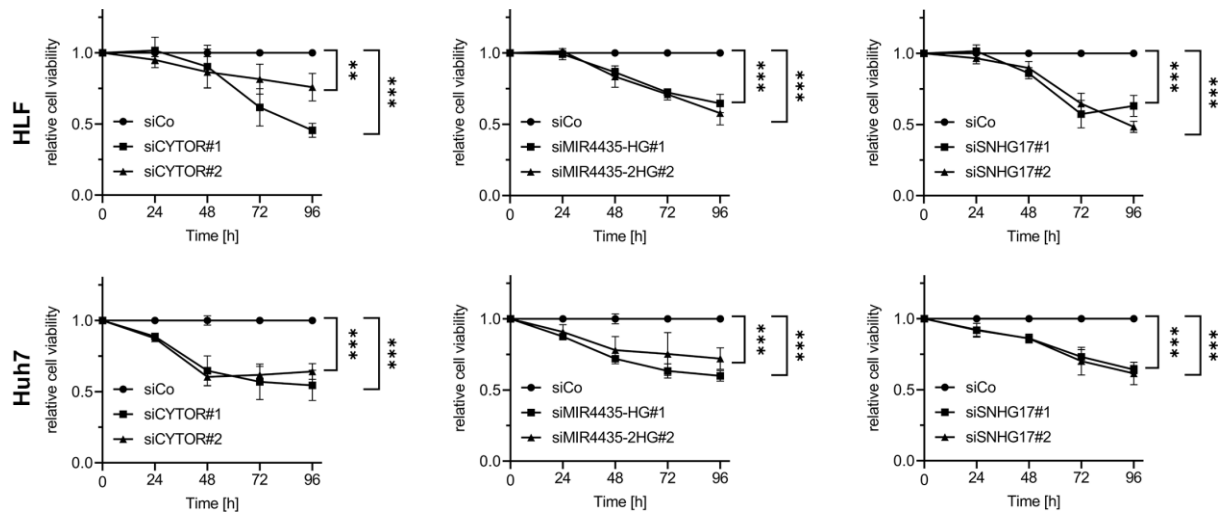
Figure 12 | Silencing of lncRNA candidates reduces cell viability. Resazurin-based cell viability assay in HLF cells (top) and Huh7 cells (bottom) after siRNA-mediated inhibition of CYTOR, MIR4435-2HG, SNHG17 at different time points. The graph summarizes the results of 3 independent experiments. For all experiments, siCo-transfected cells served as controls. All results are normalized to respective controls. Each experiment was performed with 2 independent siRNAs (#1, #2). Statistical test: Dunnett's multiple comparison test, *P≤0.05, **P≤0.01, ***P≤0.001.

To investigate if selected lncRNAs contribute to the pro-tumorigenic phenotype of YAP/TAZ, I performed RNAi-mediated knockdown experiments of MIR4435-2HG, CYTOR, or SNHG17 in two HCC cell lines (HLF, Huh7) and measured cell viability. The results illustrated a significant reduction in cell viability for all three selected lncRNAs in both cell lines starting at 48/72 h post transfection (Figure 12). This relatively late effect on cell viability suggested that knockdown of these lncRNAs affected cellular mechanisms concerning cell proliferation rather than apoptosis. To confirm this, I performed colony formation and BrdU proliferation assays for all three selected lncRNAs, which demonstrated reduced cell proliferation and colony formation properties upon lncRNA inhibition (Figure 13 and Figure 14, respectively). SNHG1 was not functionally investigated since previous studies have already shown its tumor-supporting properties in HCC cells[190].
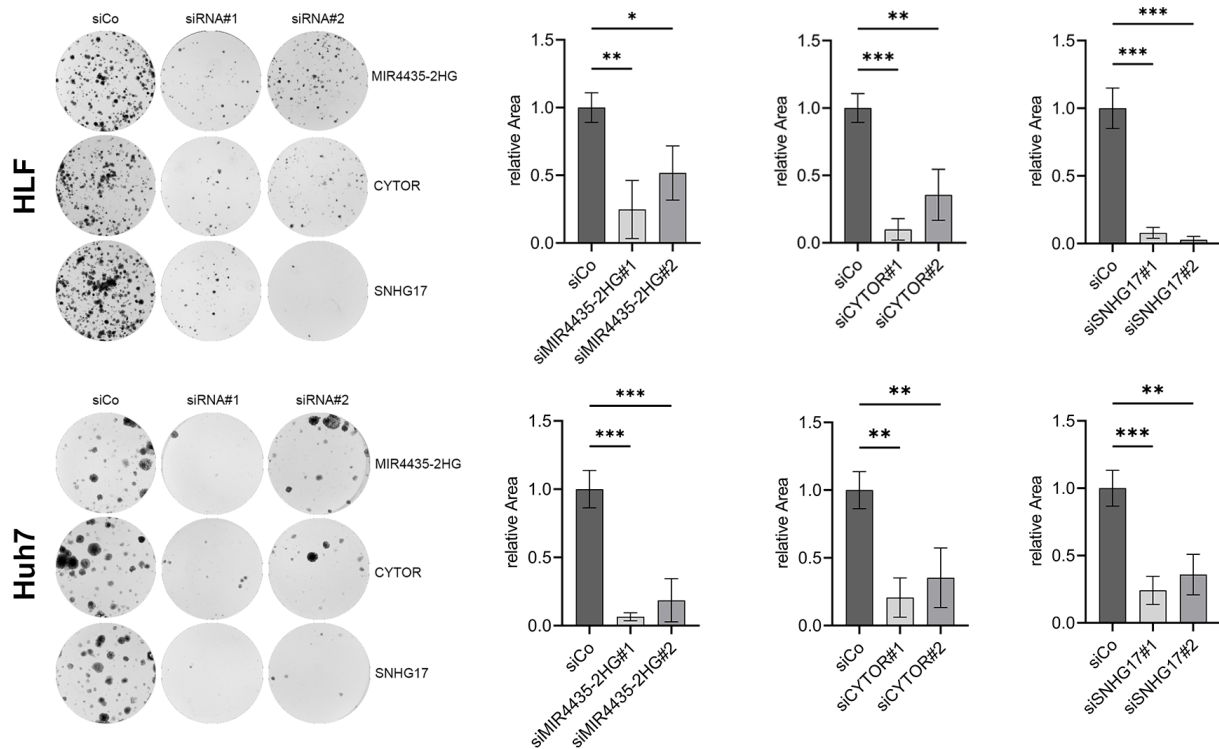
Figure 13 | Silencing of lncRNAs reduces colony formation. Colony formation assay of HLF cells (top) and Huh7 cells (bottom) after siRNA-mediated silencing of the lncRNAs MIR4435-2HG, CYTOR, or SNHG17. Quantification includes 3 independent biological replicates. For all experiments, siCo-transfected cells served as controls. All results are normalized to respective controls. Each experiment was performed with 2 independent siRNAs (#1, #2). Statistical test: Dunnett's multiple comparison test, *P ≤ 0.05, **P ≤ 0.01, ***P ≤ 0.001.

To further substantiate that the observed biological effects were indeed YAP/TAZ-dependent, an epistasis/rescue experiment was exemplarily performed for CYTOR. For this, I stably overexpressed CYTOR in HLF cells (Figure 15A), simultaneous performed RNAi-mediated knockdown of YAP and TAZ, and measured colony formation. The results revealed that overexpression of CYTOR indeed partially rescued the negative effect of YAP/TAZ silencing on cell viability (Figure 15B). Interestingly, overexpression of CYTOR alone did not show an effect on colony formation, indicating that endogenous expression already saturated the pro-proliferative properties of CYTOR in HLF cells.
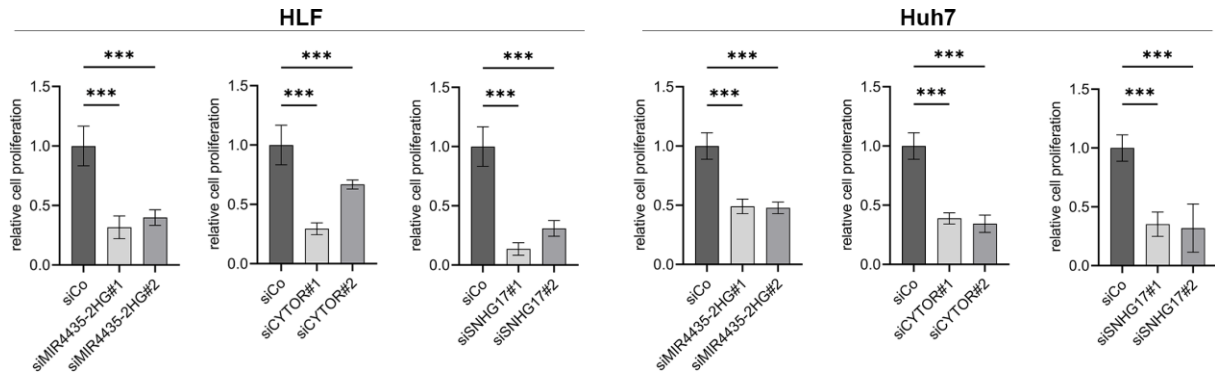
Figure 14 | Silencing of lncRNAs reduces cell proliferation. BrdU ELISA cell proliferation assay of HLF cells (left) and Huh7 cells (right) after siRNA-mediated knockdown of lncRNAs MIR4435-2HG, CYTOR, or SNHG17 after 72 h. The bar graphs summarize the results of 3 independent experiments. For all experiments, siCo-transfected cells served as controls. All results are normalized to respective controls. Each experiment was performed with 2 independent siRNAs (#1, #2). Statistical test: Dunnett's multiple comparison test, *P ≤ 0.05, **P ≤ 0.01, ***P ≤ 0.001.

These findings demonstrated that next to their potential role as biomarkers, YAP/TAZ-regulated lncRNAs actively contribute to the tumor-supporting properties of the Hippo/YAP/TAZ signaling pathway.
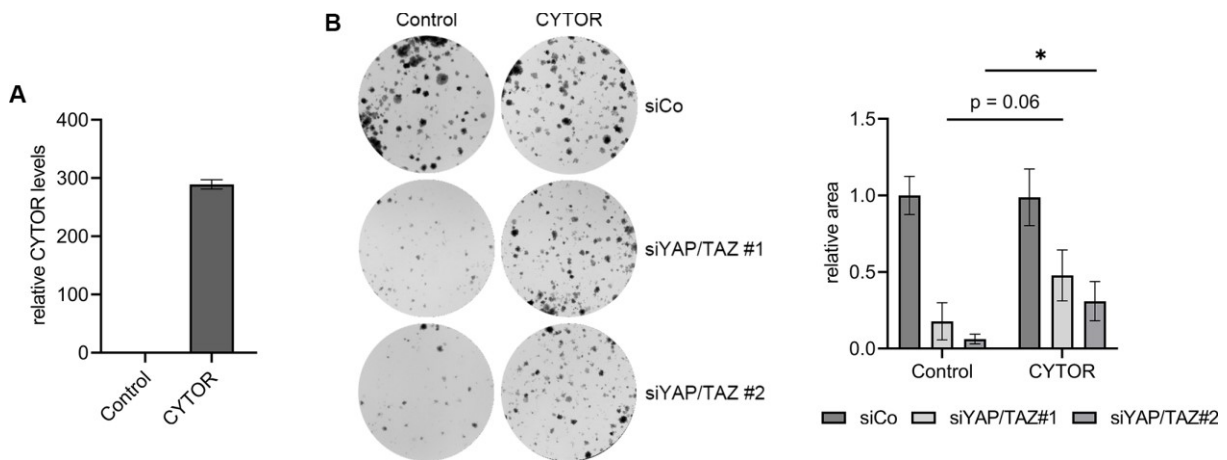

Figure 15 | CYTOR overexpression partially abolishes negative effect of YAP/TAZ silencing on colony formation. (A) qPCR analysis of HLF cells with and without stable CYTOR overexpression. **(B)** Colony formation assay of HLF cells stably overexpressing CYTOR after siRNA-mediated knockdown of YAP/TAZ. HLF cells stably transfected with an empty vector served as control. Quantification includes 3 biological replicates. For all experiments, siCo-transfected cells served as controls. All results are normalized to respective controls. Each experiment was performed with 2 independent siRNA combinations (#1, #2). Statistical test: Dunnett's multiple comparison test, *P ≤ 0.05.

4.6 The presence of the lncRNA signature defines HCC patients with YAP activation

So far, the data showed that overexpression of the lncRNA signature correlated with poor prognosis in HCC patients and that YAP/TAZ transcriptionally controlled the expression of the lncRNA signature constituents *in vitro* and partially *in vivo*.
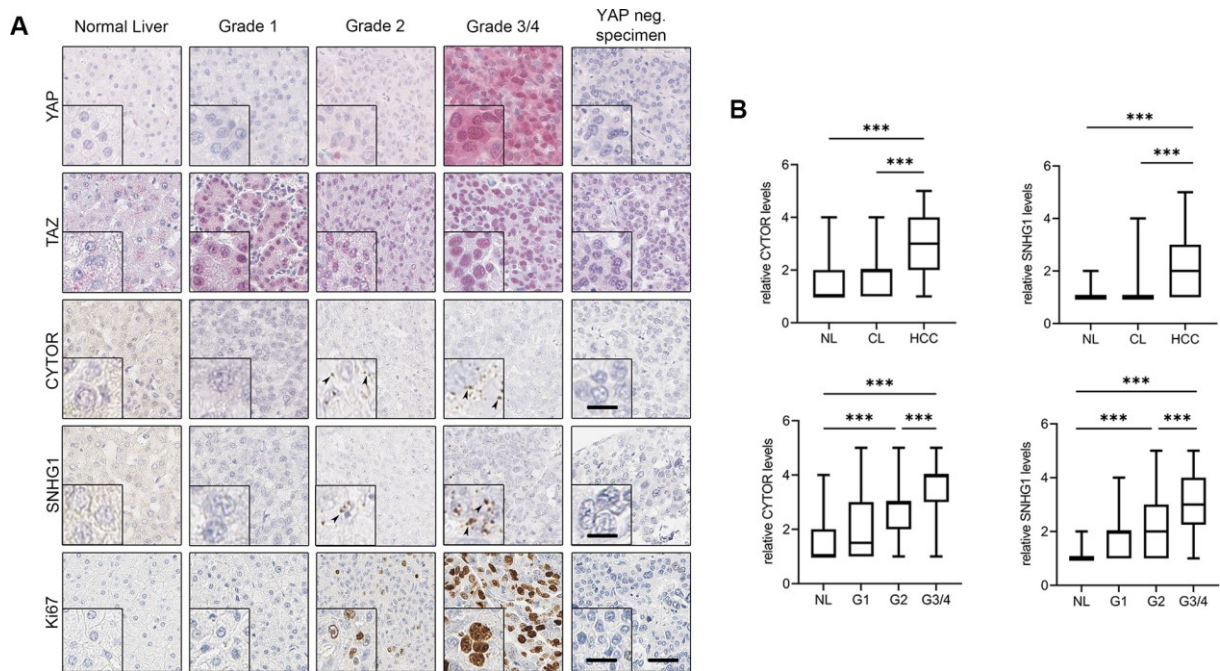

Figure 16 | lncRNA expression correlates with nuclear YAP positivity in HCC patients. (A) IHC stains (YAP, TAZ, Ki67) and *in situ* hybridization (CYTOR, SNHG1) of human HCC tissue microarray consisting of 40 non-tumorous liver tissues, 174 cirrhotic liver tissues, and 476 HCCs (grading: G1 = 87, G2 = 311, G3/4 = 78). Exemplary liver tissues and HCCs with good (G1/G2) and poorly differentiated tumors (G3/G4), as well as one YAP-negative specimen are shown. Scale bar: lower magnification: 100 μm; moderate magnification: 20 μm, highest magnification (*in situ* inserts): 5 μm. **(B)** Upper boxplots illustrate *in situ* hybridization signal distribution in normal livers (NL), cirrhotic livers (CL), and HCC samples for CYTOR (left) and SNHG1 (right). Lower boxplots show *in situ* hybridization signal distribution in NLs and HCCs with different dedifferentiation (NL, G1, G2, and G3/4).

To investigate, whether lncRNA signature expression was also associated with increased YAP/TAZ activity in human HCC patients, TMA analysis was performed. The TMA contained 40 non-tumorous liver tissues, 174 cirrhotic liver tissues, and 476 HCCs (grading: G1 = 87, G2 = 311, G3/4 = 78), which were stained by IHC for YAP and TAZ, as well as Ki67 and *in situ* hybridization was performed for the lncRNAs CYTOR and SNHG1. Visual evaluation revealed that both CYTOR and SNHG1 positivity correlated with nuclear YAP expression in HCC cells (Figure 16A; r = 0.702, p ≤ 0.001; r = 0.67, p ≤ 0.001, respectively). Interestingly, both lncRNAs

showed a weaker correlation with nuclear TAZ levels in HCC cells (r = 0.390, p ≤ 0.001; r = 0.450, p ≤ 0.001, respectively), which strengthens the idea of YAP as the predominant regulator of lncRNA signature expression. In addition, lncRNA abundance statistically associated with the proliferation marker Ki67 (r = 0.497, p ≤ 0.001; r = 0.601, p ≤ 0.001, respectively), thereby confirming the results from the functional assays. Furthermore, both analyzed lncRNAs were elevated in HCC specimens in comparison to normal liver or cirrhotic liver samples, and a positive correlation between lncRNA expression levels and tumor grading was observed (Figure 16B).

Taken together, these results showed that lncRNA signature positivity is indicative for nuclear YAP expression in HCC patients.

4.7 YAP-dependent lncRNA signature levels in serum of HCC patients correlate with YAP activation in tumor tissue

After the identification and verification of a YAP-dependent lncRNA signature, I wanted to examine whether this lncRNA signature was detectable in serum samples of HCC patients and whether it could serve as a proxy for YAP activity in HCC tissues. Thus, I established a novel multistep protocol for the sensitive and reliable detection of lncRNAs in human serum samples (see methods 3.6.3). In collaboration with the Medizinische Hochschule Hannover and the Department of Gastroenterology in Heidelberg, I collected a retrospective cohort, including serum derived from healthy persons (n = 20) and HCC patients (n = 29, cohort 1). Measuring the signature lncRNA constituents in this cohort revealed that all individual lncRNAs could be consistently detected in serum samples with elevated levels in a subgroup of HCC patients compared to healthy controls (Figure 17A). Furthermore, the balanced lncRNA signature score was upregulated in 76% of HCC patients in comparison to the mean lncRNA signature score of healthy donors, indicating expected variable YAP activity in HCCs (Figure 17B).

Next, I focused on those HCC patients for which FFPE material with viable tumor cell content was available (Figure 17B, highlighted in red) and performed immunohistochemical staining for YAP (n = 17, Figure 17C). Subsequently, YAP stains were rated based on a whole slide scoring system (see methods 3.6.4) and correlated with the relative abundance of the lncRNA signature in the corresponding serum. The results showed a clear positive and significant statistical association between lncRNA signature serum levels and nuclear YAP positivity in the tissues (r = 0.75, p ≤ 0.001, Figure 17D). Importantly, the negative control lncRNA signature consisting of DLEU1 and FTX failed to correlate with nuclear YAP expression (r = 0.006, p ≤ 0.982, Figure 17E), confirming the validity of the results.
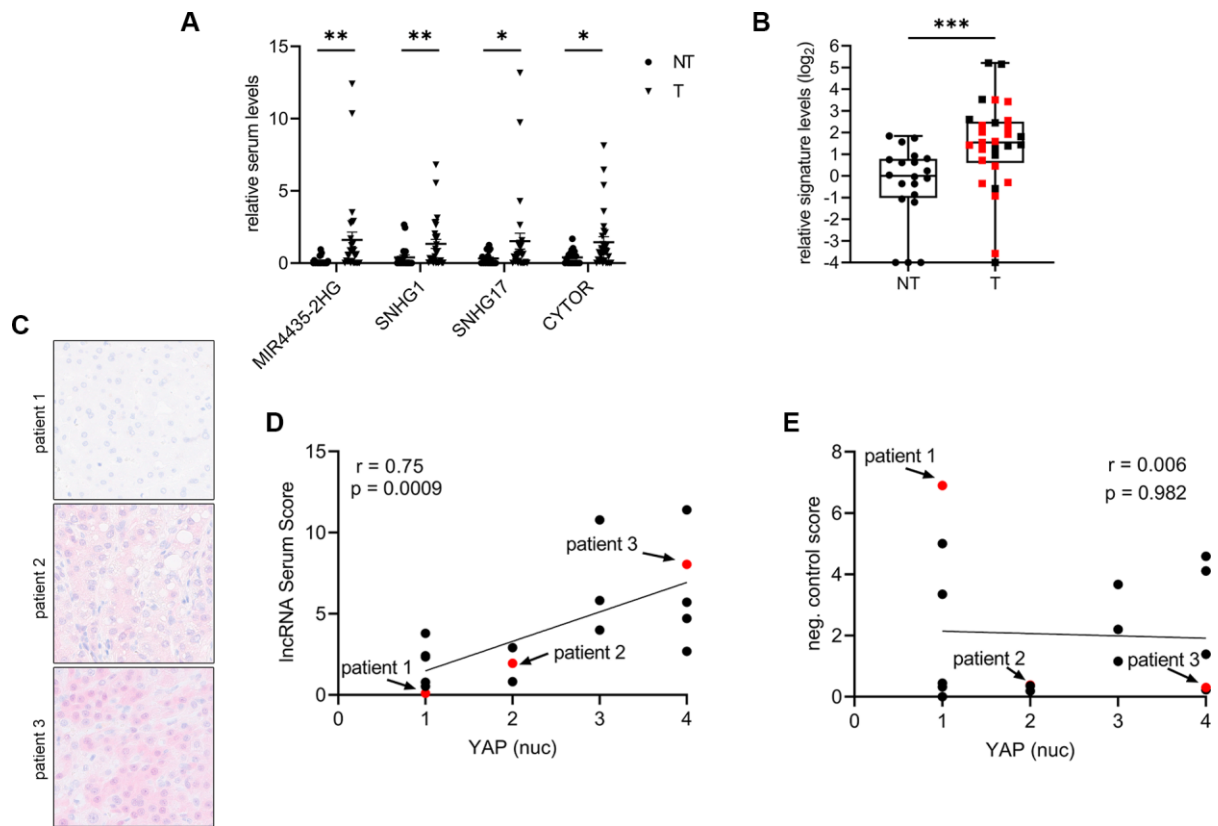
Figure 17 | lncRNA signature levels in serum correlate with nuclear YAP positivity in HCC tissues (cohort 1). (A) qPCR analysis illustrating expression of individual lncRNA signature constituents in serum derived from healthy persons (NT, n = 20) and HCC patients (T, n = 29). Statistical test: Mann–Whitney U test, *P ≤ 0.05, **P ≤ 0.01. **(B)** Boxplot illustrating lncRNA signature score levels (log2) in serum derived from healthy persons (NT, n = 20) and HCC patients (T, n = 29). Serum samples with available FFPE tissue specimens are highlighted in red. Statistical test: Mann–Whitney U test, ***P ≤ 0.001. **(C)** Exemplary YAP IHC stains of liver sections with low (patient 1), moderate (patient 2) and high nuclear YAP expression (patient 3). **(D)** Linear regression analysis of lncRNA signature levels and nuclear YAP abundance in corresponding serum/tissue samples. Exemplary patients from **(C)** are highlighted in red and marked by arrows. Statistical test: Spearman correlation. p-value is indicated. **(E)** Linear regression analysis of negative control lncRNAs (DLEU1, FTX) and nuclear YAP abundance in corresponding serum/tissue samples. Exemplary patients from **(C)** are highlighted in red. Statistical test: Spearman correlation. p-value is indicated.

Despite this strong positive correlation between lncRNA signature levels in the serum and YAP activation in HCC tissues, a moderate scattering of the data points could be observed (Figure 17D), which may be explained by the partially long-time lag between serum and tissue sampling in this cohort (up to 136 months). Thus, I initiated a prospective study in collaboration with the Newgiza University in Cairo, in which serum and tissue from HCC patients were collected simultaneously (n = 8, cohort 2). Similarly to cohort 1, individual lncRNAs could be detected in serum samples and were upregulated in a subgroup of HCC patients in comparison

to healthy donors (Figure 18A). In addition, the respective signature scores were elevated in 75% of the cases, which confirmed the results from the first cohort (Figure 18B). Importantly, correlation between lncRNA signature abundance in the serum and nuclear YAP positivity in corresponding tissues was even stronger, despite the smaller cohort (r = 0.8, p ≤ 0.001, Figure 18C/D). The latter finding shows that serum constituents reflect the status quo in the respective tumors.
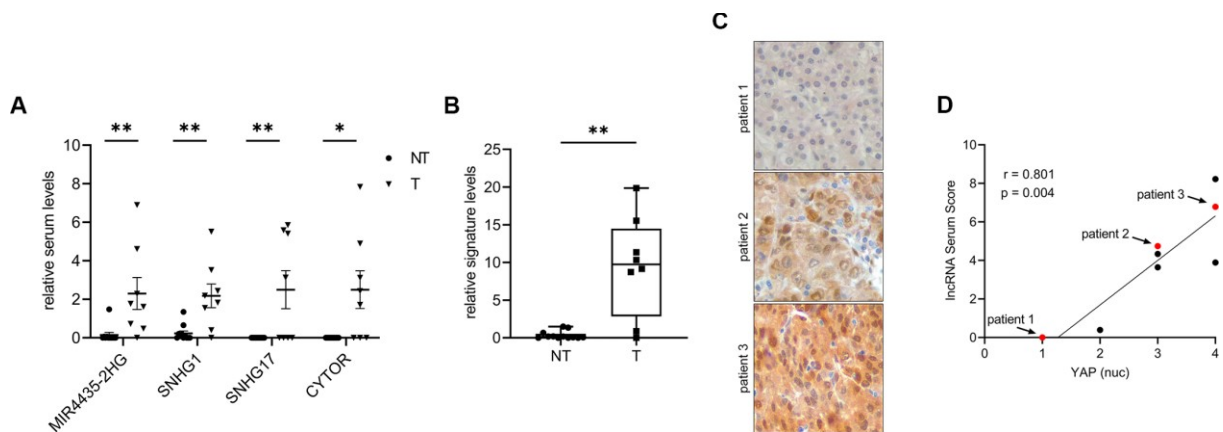

Figure 18 | lncRNA signature levels in serum correlate with nuclear YAP positivity in HCC tissues (cohort 2). (A) qPCR analysis illustrating expression of individual lncRNA signature constituents in serum derived from healthy persons (NT, n = 11) and HCC patients (T, n = 8). Statistical test: Mann–Whitney U test, *P ≤ 0.05, **P ≤ 0.01. **(B)** Boxplot illustrating lncRNA signature score levels (log2) in serum derived from healthy persons (NT, n = 11) and HCC patients (T, n = 8). Statistical test: Mann–Whitney U test, **P ≤ 0.01. **(C)** Exemplary YAP IHC stains of liver sections with low (patient 1), moderate (patient 2) and high nuclear YAP expression (patient 3). **(D)** Linear regression analysis of lncRNA signature levels and nuclear YAP abundance in corresponding serum/tissue samples. Exemplary patients from **(C)** are highlighted in red and marked by arrows. Statistical test: Spearman correlation. p-value is indicated.

Next, to define the predictive power of the lncRNA signature and to evaluate how it performed in comparison to its individual lncRNAs, cohort 1 and 2 were combined and subjected to ROC curve analysis. The results illustrated that the lncRNA signature in serum can predict the presence of nuclear YAP with high precision (AUC = 98.05). Furthermore, the combination of all four lncRNA performed better compared to individual lncRNAs, reaching statistical significance for SNHG1 (AUC = 80.52, p = 0.036) and SNHG17 (AUC = 73.38, p = 0.027). For CYTOR (AUC = 80.84, p = 0.091) and MIR4435-2HG alone (AUC = 84.52, p = 0.132) (Figure 19A), no statistical significance was observed, which can be attributed to the low case numbers. As expected, the discrepancy in performance was even more pronounced

comparing the lncRNA signature with the negative controls DLEU1 and FTX in cohort 1 (Figure 19B).

Together, these findings demonstrated that serum lncRNA signatures could serve as liquid biopsy biomarkers and predict tumor-endogenous oncogene activation with high sensitivity and specificity.
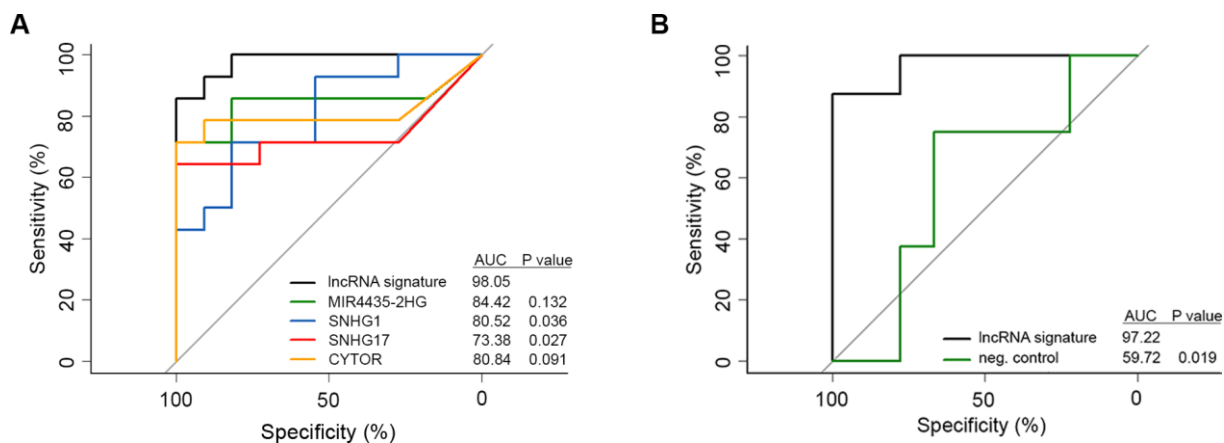

Figure 19 | lncRNA signature levels in serum define YAP positivity with high predictive power. **(A)** ROC curve analysis comparing the performance of lncRNA signature and individual lncRNA serum levels in predicting nuclear YAP abundance in tissues of corresponding HCC patients (n = 25, combination of cohort 1 and 2). p-values are indicated (Two-sided DeLong's test). **(B)** ROC curve analysis comparing the performance of lncRNA signature and negative control lncRNA signature in HCC patients (n = 17, cohort 1). p-values are indicated (Two-sided DeLong's test).

4.8 lncRNA signature expression predicts susceptibility of HCC cells towards Hippo pathway-directed therapy

The aim of this project was to identify YAP/TAZ-dependent lncRNAs that could be used as a proxy for YAP/TAZ activation in tumors in order to identify patient that would be suitable for Hippo pathway-directed therapy. Thus, to investigate the potential of my lncRNA signature as a predictor for therapeutic success, I screened CCLE expression data for HCC cell lines with relatively high (HLF, HEP3B) and low (SNU475, SNU449) lncRNA signature scores (Figure 20A, upper panel). Subsequently, I examined their susceptibility to treatment with the specific YAP/TEAD inhibitor TED-347[191]. According to the dose-response curves and respective IC50 values, HLF and HEP3B cells with higher expression of the lncRNA signature were more sensitive to TED-347 than SNU475 and SNU449 cells with low lncRNA signature abundance (Figure 20A, lower panel). Similarly to treatment with Verteporfin (Figure 9B), exposure to TED-347 led to a concentration-dependent decrease of lncRNA and positive control gene

expression in YAP/TAZ inhibition sensitive cell lines (Figure 20B/C), emphasizing the potential of the lncRNA signature for monitoring treatment response. In contrast, no such effect on lncRNA signature levels was observed in YAP/TAZ inhibition resistant cells (Figure 20B/D).
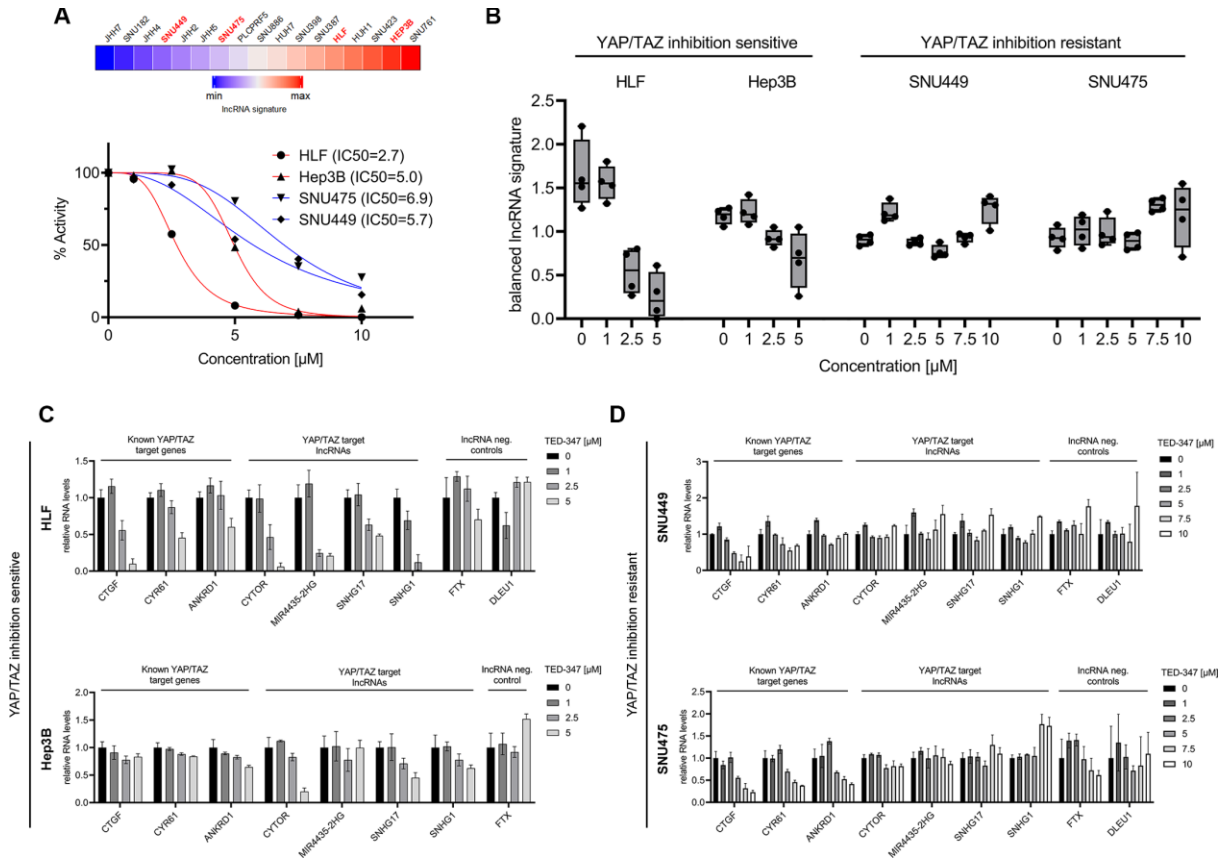

Figure 20 | lncRNA signature defines responsiveness of HCC cells to Hippo pathway-directed pharmacological inhibition. (A) Heatmap summarizing balanced lncRNA signature scores of 17 HCC cell lines (CCLE expression data). Exemplary cell lines with low (SNU449, SNU475) and high (Hep3B, HLF) signature scores were selected (highlighted in red, upper panel). Graph shows dose-response curves in selected HCC cells after treatment with different concentrations of TED-347 for 48 h. One exemplary experiment is shown. IC50 values are indicated. **(B)** Boxplots illustrate balanced lncRNA signature scores in YAP/TAZ inhibition sensitive and resistant HCC cell lines after TED-347 treatment for 48 h. For YAP/TAZ inhibition sensitive cells, no measurement of 7.5 and 10 µM TED-347 was possible due to low cell viability. **(C) (D)** qPCR analysis of YAP/TAZ target genes (CTGF, ANKRD1, CYR61), YAP/TAZ target lncRNAs (CYTOR, MIR4435-2HG, SNHG17, SNHG1), and negative control lncRNAs (DLEU1, FTX) after TED-347 treatment in YAP/TAZ inhibition sensitive **(C)** and YAP/TAZ inhibition resistant **(D)** HCC cells for 48 h. DLEU1 is not highly expressed in Hep3B cells and was thereby excluded from the analysis. DMSO served as control.

In summary, lncRNA signatures represent a valuable tool to identify patients eligible for specific oncogene-targeted therapies and to monitor treatment response.

5 Discussion

Tumor-derived constituents in body fluids are informative concerning conditions in tumor cells. This study illustrates the applicability of blood serum lncRNA signatures as prognostic biomarkers for aberrant oncogene activity in tumors. Using the Hippo pathway as a showcase, I defined a tumor entity-spanning lncRNA signature consisting of CYTOR, SNHG1, SNHG17, and MIR4435-2HG, which is transcriptionally controlled by the YAP/TAZ/TEAD complex. This 4-lncRNA signature represents a robust predictor of YAP activity in cancer patients and its overexpression is associated with poor overall survival in different cancer types. Furthermore, selected signature constituents contribute to pro-tumorigenic functions of the Hippo pathway through tumor cell-intrinsic mechanisms. Importantly, lncRNA signature abundance in blood serum specimens statistically correlates with YAP activity in respective tumor tissues. Lastly, lncRNA signature expression levels define cancer cell lines, which are sensitive to YAP/TAZ-directed therapy. These data highlight that lncRNA-based markers represent valuable tools for diagnostics, therapy design, and monitoring treatment response.

5.1 Evolution of liquid biopsy concepts

Over the last decade, different liquid biopsy concepts have been developed to overcome the drawbacks associated with conventional tissue biopsy[39]. Here, most successful liquid biopsy approaches focused on detecting cfDNA and CTCs in patient material.

Tumor-derived cfDNA, also known as circulating tumor DNA (ctDNA), is informative regarding many cancer-specific molecular characteristics, including single nucleotide variants, epigenetic changes, chromosomal rearrangements, amplifications, microsatellite instability, and loss of heterozygosity[192-194]. These genetic alterations have been studied in several tumor types. For instance, the mutational status of genes, for which FDA-approved drugs exist, e.g., EGFR, ALK, ROS1, BRAF, was identified in patient serum with high tissue concordance in a clinical trial comprising therapy-naive metastatic NSCLC patients[195]. Due to the informative nature of cfDNAs as well as the simple isolation from patient blood, and analysis procedures, first cfDNA-based approaches have reached the stage of clinical applicability. For example, the Cobas EGFR Mutation Test v2, which was approved by the FDA and introduced to the clinics in 2015, is a qPCR test for the qualitative detection of exon 19 and exon 21 deletions in the EGFR gene utilizing plasma samples of NSCLC patients[196] Another FDA-approved test represents Epi proColon, which reports the methylation status of the SEPT9 promoter in the plasma of colorectal cancer patients[197]. Consequently, cfDNA-based approaches could provide clinicians with useful information to design patient-tailored therapies. However, one

major drawback of the analysis of cfDNA in blood samples of cancer patients is the low number of DNA-related abnormalities. Thus, genomic alterations can be recognized, but tumor-specific aberrations on transcriptomic, proteomic, and metabolomic levels remain undiscovered. Accordingly, cfDNA analysis cannot result in a complete reflection of the tumor-intrinsic conditions. Another challenge includes the need for highly sensitive technologies to discriminate between low-abundant mutant and high numbers of WT alleles. In this context, a detected biological mutation in blood samples may be challenging because WT material can conceal tumor-derived information.

In contrast to cfDNA, CTCs represent a population of migrating and intact tumor cells that are released in the bloodstream from primary tumor sites and could be responsible for the development of metastasis[198,199]. Indeed, CTCs are considered to provide a more complete picture regarding the conditions in the tumors in comparison to cfDNAs as these cells contain DNA with high structural integrity, RNAs, as well as proteins[200]. Already in 2004, the FDA approved the CellSearch system as a validated method for CTC detection and analysis[201]. Since then, studies have demonstrated the potential of CTCs as independent prognostic markers for different tumor entities, such as prostate cancer and breast cancer[202,203]. However, one major disadvantage of CTCs as liquid biopsy markers is that the CTC concentration in the blood is usually very low (1-10 cells/ml blood)[204]. Thus, difficulties in isolating this rare population of cells, which requires specialized equipment and extensive analyses, have hindered the introduction of CTC-based liquid biopsy techniques to the clinics so far. In addition, CTCs provide information of metastatic cancer cells but neglect information on non-metastatic cells in the primary tumor mass, which also contribute to the clinical outcome. Consequently, CTCs only partially provide insights about tumor heterogeneity and therefore the presence of other genetic alterations.

In this work, I therefore focused on circulating lncRNAs as potential biomarkers, which on the one hand are easy to detect and analyze from solid and liquid patient material, but on the other hand provide information regarding tumor-intrinsic conditions independent from their underlying regulatory mechanism. In addition, the high stability and relatively high levels of circulating lncRNAs qualify them as robust and reliable liquid biopsy markers. Indeed, previous studies have already shown that lncRNA levels in the blood correlate with the presence of different cancer types. For instance, the blood of patients with NSCLC has shown to contain elevated levels of the lncRNA MALAT1[72]. Another example is the lncRNA HULC, whose plasma levels could reflect the presence of HCC[205]. Thus, individual lncRNA in serum may serve as proxy for the presence of specific cancers in patients.

My study now broadens previous concepts of liquid biopsy applicability at different stages: First, to my knowledge, all previous lncRNA-based approaches only focus on the correlation of lncRNA abundance in the blood with the presence of a specific cancer type. Here, I showed

that circulating lncRNAs can also provide information about potential druggable oncogene activity in the tumor itself, which can guide clinicians in designing patient-tailored therapies (e.g., by combining inhibitors according to the abundance of oncogene-specific lncRNA signatures). Second, most studies indicate that the expression of lncRNAs is considered to be highly cell type and organ-specific. However, independent studies have demonstrated that individual lncRNA can be associated with multiple types of cancer. For example, elevated levels of circulating UCA1 correlate with the presence of gastric and liver cancer[89,206]. Based on this, I integrated experimental HCC and LUAD, and patient data to define a lncRNA signature that can identify patients with aberrant YAP/TAZ activity in different cancer types. Lastly, to my knowledge, all liquid biopsy studies focus on the direct comparison of body fluids derived from cancer patients and healthy individuals to identify meaningful biomarkers[93]. However, analyses solely based on patient-derived material have limitations, including "interfering noise" from non-tumorous cells, the lack of knowledge regarding the underlying molecular mechanism of lncRNA expression, and the inability to measure lncRNA expression dynamics (e.g., to monitor therapy success). To overcome these limitations, I used *in vitro* cell culture experiments to identify tumor cell-specific and functionally relevant lncRNAs that were transcriptionally regulated by the YAP/TAZ/TEAD complex. Subsequently, I demonstrated their capability to classify patients with Hippo pathway dysregulation according to serum expression levels. In summary, my data suggests that stringently selected lncRNA signatures specific for transcriptional regulators/oncogenes may serve as robust cancer entity-spanning biomarkers.

5.2 Applicability of lncRNA-based liquid biopsy markers in clinics

In this study, I defined a lncRNA signature that was transcriptionally regulated by the transcriptional YAP/TAZ/TEAD complex and whose serum abundance statistically associate with YAP activity in tumor cells of human HCC specimens. In addition, *in vitro* experiments showed that lncRNA expression levels correlate with the sensitivity of HCC cell lines to Hippo pathway-directed therapeutics. Integrating these findings suggest that elevated lncRNA signatures in serum samples may identify patients who could benefit from specific treatments and thus guide clinicians in therapy design. Although lncRNA-based biomarker approaches have not reached the stage of clinical applicability, this conclusion is supported by other, already established FDA-approved liquid biopsy techniques. For instance, cfDNA-based detection of EGFR mutations, such as exon 19 deletions and point mutations in exon 21, is associated with the sensitivity of NSCLC patients to tyrosine kinase inhibitors (TKI), including erlotinib, gefitinib, and afatinib[207]. Furthermore, the presence of ALK and ROS1 rearrangements as well as KRAS mutations are a predictive factor of TKI resistance and could

also be detected by cfDNA-based liquid biopsy approaches[208]. Thus, oncologists can make treatment decisions based on the presence/absence of specific sensitizing and resistance mutations in blood samples of NSCLC patients, respectively[209].

Next, I also showed that treatment of YAP/TAZ inhibition-sensitive HCC cells with Verteporfin or TED-347 led to a concentration-dependent decrease of lncRNA signature levels. It is therefore tempting to speculate that frequent longitudinal serum sampling and the subsequent analysis of lncRNA expression levels in patients allow the monitoring of treatment response and therapeutic success. The applicability of liquid biopsy-based data for patient monitoring in response to therapy has been demonstrated in a clinical trial comprising 125 colorectal cancer patients. Here, the authors showed that ctDNA with specific mutational profiles was detected in 88.5% of preoperative plasma samples. After surgery, only 10.6% of these patients were positive for ctDNA, which emphasizes the decrease of tumor cells and disease-specific liquid biopsy markers in response to therapy[5]. Interestingly, the presence of ctDNA in postoperative plasma samples was associated with a significantly higher recurrence rate, illustrating that this approach is highly sensitive and can detect even the smallest numbers of floating tumor-derived ctDNA. This has been confirmed by additional, independent clinical studies comprising patients with gastroesophageal adenocarcinoma and non-Hodgkin lymphoma[210,211]. Consequently, due to easy sampling before and after treatment (e.g., after surgical tumor resection or administration of drugs), lncRNA signatures could serve as informative and rapid read-out/biomarkers for therapeutic success or relapse.

In this case study, I identified a universal lncRNA signature that is regulated by the Hippo pathway and whose presence in serum samples is indicative for increased YAP activity in HCC tissues. Thus, it may seem obvious that other transcriptional regulators equally control the expression of distinct panel of lncRNAs that could serve as liquid biopsy markers for aberrant oncogene/tumor suppressor gene activity in tumor cells. Indeed, genome-wide studies have already defined specific lncRNA signatures, which are transcriptionally regulated by the oncogene c-MYC or the tumor suppressor gene p53, respectively[70,72]. However, their applicability as blood-derived biomarkers for aberrant transcription factor activity has not been tested yet. The presence of transcription factor-specific serum lncRNA signatures could guide treatment decisions and enable the design of patient-tailored therapies (e.g., combining drugs targeting pathways/transcriptional modules, whose specific lncRNA signatures are upregulated in serum samples). Especially in tumors with high heterogeneity, this might represent a valuable tool to target tumor cells with genetically different backgrounds.

Furthermore, considering that some cancer patients acquire resistance to a specific therapy, frequent longitudinal serum sampling and subsequent genetic characterization of tumor cells based on lncRNA signature expression could detect resistance mechanisms or alternative

therapeutic target structures. Thus, clinicians could adjust therapy strategies accordingly to prevent tumor progression (e.g., by using drugs targeting relapse-specific cellular pathways). In summary, serum lncRNA signatures may represent valuable tools for the characterization of tumor cells in patients. However, so far there is only little evidence about the applicability of lncRNA signatures as biomarkers in clinics and thus more research is required in order to further elucidate the usefulness of lncRNA-based blood markers.

5.3 Pro-tumorigenic functions of lncRNA signature constituents

In this work, I have shown that the lncRNA signature constituents are not only transcriptionally controlled by the YAP/TAZ/TEAD complex but also contribute to the pro-proliferative characteristics of the Hippo pathway in HCC cells. In the following part, I discuss the previous findings on how these signature lncRNAs exert their pro-tumorigenic functions. For this, I divided the lncRNA signature into 2 groups: the small nucleolar host genes SNHG1/SNHG17 and the lncRNAs CYTOR/MIR4435-2HG, which evolutionary originate from the same locus[212]. In general, the family of SNHGs appear to be highly relevant YAP/TAZ target genes. The screening results revealed that besides SNHG1 and SNHG17, several additional SNHGs were regulated by YAP/TAZ (e.g. SNHG8, SNHG16 for HCC; SNHG15, SNHG7 for LUAD; Figure Appendix 1B and Figure Appendix 2B). Because of their cell type-specific regulation, many SNHG isoforms were not included in the YAP/TAZ-dependent lncRNA signature. SNHGs represent a versatile group of lncRNAs with 32 family members. On the one hand, they can act as host genes containing the information for specific snoRNAs in their intronic sequences[213]. On the other hand, they can function as lncRNAs by keeping the full-length transcript through alternative splicing[213,214]. Although their name might suggest otherwise, the accumulation of snoRNA is independent of the host RNA levels[215,216]. In fact, many host genes are subjected to degradation upon splicing and it remains unclear how the transcriptional system decides the fate of intronic snoRNAs and SNHGs[216]. Thus, I will focus in this discussion on the functions of SNHGs, in particular SNHG1 as well as SNHG17, and their role in cancer development and progression.

Previous studies have mainly investigated SNHG1/17 functions as competing endogenous RNAs that bind miRNAs and eventually promote tumor progression[217,218]. However, SNHGs have additional mode-of-actions and exert their functions depending on their intracellular localization[213]. In the nucleus, SNHGs can directly influence gene expression by binding to transcription factors or indirectly by mediating the introduction of epigenetic modifications. For example, SNHG1 binds to the Mediator complex, which facilitates enhancer-promoter interaction and promotes the transcription of the oncogene SLC3A2[219]. Furthermore, SNHG17 is part of a positive feedback loop that controls the Hippo pathway by epigenetic silencing of

Discussion

LATS expression through guiding the methyltransferase EZH2 to the LATS promoter[220]. In the cytoplasm, besides miRNA sponging, SNHGs can also directly interact with mRNAs or proteins to prevent ubiquitination[214]. For instance, SNHG1 directly binds to p53 mRNA molecules, thereby affecting p53 protein levels as well as p53 target gene expression in colorectal cancer[221]. The fact that changes in SNHG abundance can have a significant impact on gene expression has been demonstrated in a siRNA screen targeting SNHG17. The results revealed that 637 genes were upregulated while 581 were downregulated upon silencing of SNHG17 with direct impact on tumor cell proliferation and migration[222]. Regarding the role in cancer progression and development, the presence of SNHG1 and SNHG17 is associated with increased proliferation, cell viability, and invasion/migration. Moreover, both SNHGs are upregulated and represent adverse prognostic markers in multiple cancer types[223,224]. Together, these findings demonstrate that SNHG1/17 may play a central role in cellular and pathogenic processes.

CYTOR and MIR4435-2HG represent an interesting group of lncRNAs since CYTOR evolutionary arises from duplication of the MIR4435-2HG locus on chromosome 2[212]. Thus, the genomic regions of both paralogs potentially contain the same regulatory elements, which would explain their equal regulation by YAP and TAZ as well as the tight correlation of their expression levels as observed in the TCGA data analyses (Figure 6/7). This chromosomal duplication is exclusive to the human genome and both paralogs contain high sequence similarities[212]. However, several isoforms of both transcripts with distinguishable exon/intron structures exist that allow the separate analysis of the lncRNAs[225]. Similar to SNHGs, previous research has mainly focused on their role as miRNA sponges to promote tumor growth and progression[226,227]. Additional mode-of-actions are based on the direct interaction with proteins. For instance, nuclear-localized CYTOR binds to HNRNPC, which inhibits protein ubiquitination leading to the stabilization of ZEB1 mRNA. This HNRNPC-CYTOR-ZEB1 axis promotes metastasis in oral squamous cell carcinoma[228]. Another example represents the heterotrimeric complex formation of CYTOR, NCL, and Sam68 resulting in the activation of NF-κB signaling, which contributes to the progression of colorectal cancer[229]. Expression profiling after CYTOR inhibition resulted in 1,294 dysregulated genes among other things involved in oxidative phosphorylation and alternative splicing, which again highlights the high impact of CYTOR and lncRNAs in general on gene expression[228]. In contrast, the functions of MIR4435-2HG are barely described mechanistically besides its miRNA sponging capabilities[212,226]. Regarding their role in cancer development and progression, both paralogs are associated with increased proliferation, cell viability, and invasion/migration and their upregulation significantly correlates with poor overall survival in multiple tumor types[226,230].

Altogether, results from this study and other reports highlight the oncogenic potential of the lncRNA signature constituents. In addition, first studies have vaguely drawn a connection

between the individual lncRNAs and the Hippo pathway[220,231-235]. Here, it was demonstrated that each lncRNA to some extent can increase YAP and/or TAZ activity. Integrating these findings with my results suggests that the lncRNA signature constituents are on the one hand transcriptionally controlled by the YAP/TAZ/TEAD complex but also are a part of a positive feedback loop controlling Hippo pathway signaling. Thus, the lncRNAs may support tumorigenesis in a multi-modal manner by sponging miRNAs, introducing protein modifications, or recruiting multi-protein complexes.

5.4 Targeting Hippo pathway activity

For this pilot study, I chose the Hippo pathway as a showcase since its transcriptional regulators YAP and TAZ have been demonstrated to be involved in liver and lung cancer development[236]. Thus, the Hippo pathway represents an appealing target for therapy and current research results elucidate that novel YAP/TAZ-directed drugs will be available in the future[144,145,237]. Indeed, I could illustrate the negative effects of Hippo pathway-directed drugs on HCC cell viability, which underlines the potential of targeting this pathway.

The first evidence for the druggability of the Hippo pathway was demonstrated in a drug screen comprising a library of FDA-approved compounds. In this process, Verteporfin was identified as a substance that disrupts YAP/TEAD interaction and suppresses tumor growth in mice[188]. However, subsequent reports have demonstrated that in addition to its poor pharmacokinetics, Verteporfin causes many off-target effects, which hindered the translation of this compound as cancer therapeutic to the clinic[238,239]. Nevertheless, the discovery of Verteporfin as a potent inhibitor of YAP/TEAD activity has initiated a plethora of screening efforts to identify novel compounds targeting the YAP/TAZ/TEAD transcriptional module[240]. Here, studies have mainly focused on small molecule inhibitors, which are able to bind the TEAD lipid pocket to block TEAD palmitoylation. As a result, the interaction between YAP/TAZ and TEAD is blocked, which silences YAP/TAZ/TEAD-dependent gene expression[144,145,237]. For example, the small molecule inhibitor TED-347 covalently binds the TEAD palmitoylation site leading to irreversible inhibition of YAP/TEAD binding[191]. In this study, I used Verteporfin and TED-347 as two exemplary drugs targeting the interaction between YAP/TAZ and TEAD. Both substances were potent in inhibiting YAP/TAZ activity as shown by the reduction of YAP/TAZ target genes and lncRNA signature gene expression, which highlights the effectiveness of targeting this transcriptional module.

Furthermore, additional strategies show promise in modulating Hippo pathway activity, including altering the localization and stability of YAP/TAZ, as well as inhibiting YAP/TAZ-regulated proteins[236]. Indeed, the intracellular localization of YAP/TAZ is crucial for their activity[241]. This was also illustrated in the cell density-dependent experiment, in which the

nuclear exclusion of YAP led to a decrease in target gene expression (Figure 8F). Thus, targeting the nuclear-cytoplasmic shuttling of YAP/TAZ represents a valid approach to regulate Hippo pathway activity. Indeed, pharmacological inhibition of SCD1, an enzyme involved in monounsaturated fatty synthesis, blocks the nuclear translocation of YAP/TAZ, thereby reducing their activity[242]. Moreover, the inhibition of proteins encoded by YAP/TAZ-regulated genes represents an option to partly suppress the pro-tumorigenic characteristics of the Hippo pathway. For instance, administration of a CTGF-specific monoclonal antibody decreased tumor growth and metastasis in a pancreatic cancer nude mouse model[243]. Another example represents NUAK2, a YAP/TAZ target gene, which is part of a positive feedback mechanism, that enhances YAP/TAZ activity by silencing LATS-mediated phosphorylation of YAP/TAZ. Pharmacological inhibition of NUAK2 reduces cell viability *in vitro* and tumor growth in mice[244]. Partial inhibition of YAP/TAZ effects might be advantageous in comparison to complete silencing of the transcriptional module. Cancer therapy is often systemic, thereby affecting cells all over the body. Thus, silencing of YAP/TAZ activity might cause severe side effects in regions, where both effectors are endogenously active, e.g., in intestinal self-renewal and regeneration[245].

Taken together, these findings demonstrate that targeting the interaction of YAP/TAZ/TEAD has shown the most promise for therapy so far. Indeed, several clinical trials with focus on Hippo pathway constituents (e.g., with NF2 mutation, NF2-deficiency) or the presence of YAP/TAZ fusion proteins in mesothelioma have been initiated[246-248]. With potential YAP/TAZ-directed therapies on the horizon, this underlines the necessity for robust and sensitive biomarkers to identify patients eligible for such treatments, monitor treatment response, and prematurely detect acquired resistance.

5.5 Different roles of YAP/TAZ in controlling lncRNA expression

YAP and TAZ are considered to be highly redundant regarding their functions to the point that they are functionally identical and therefore often referred to as YAP/TAZ. Consequently, in the initial selection process, I simultaneously silenced both proteins to avoid one effector compensating for the loss of function of the other and *vice versa*. As a result, I defined a lncRNA signature, whose constituents are transcriptionally controlled by YAP and TAZ. Confirmatory *in vitro* experiments demonstrated that both effectors to some extent equally control the expression of the signature lncRNAs. Interestingly, ChIP experiments showed no/weaker lncRNA promoter binding of TAZ, pointing towards a minor role of this effector in the regulation of Hippo pathway-dependent lncRNAs in HCC. This finding was further supported by analyzing human HCC patient data. First, nuclear TAZ expression showed a weaker correlation with CYTOR and SNHG1 abundance than nuclear YAP levels in the TMA.

Second, lncRNA serum levels did not correlate with nuclear TAZ expression in the respective HCC tissues (data not shown). This might be due to both effectors possibly engaging in negative feedback regulation. For example, it has been shown that YAP unidirectional promotes the proteasomal degradation of TAZ in both mice and humans[249]. However, this is controversial since TAZ knockdown led to increased YAP levels in corneal fibroblasts[250]. These contradictory results hint towards a context-dependent, cell type-specific, and mutual regulation of both Hippo pathway effectors. It has been shown that TAZ functions as an oncogenic driver in breast cancer[132]. Therefore, it is tempting to speculate that in other cancer entities than HCC, TAZ plays the leading role in regulating lncRNA signature expression.

Another explanation for why the *in vitro* results do not translate to the patient data may be the lower stability of TAZ in comparison to YAP. Due to an additional N-terminal phosphodegron, the half-life of TAZ amounts to 2 h, whereas YAP protein levels remain stable for 6 h[251]. Thus, TAZ protein levels are rapidly fluctuating in response to sudden changes in the cellular environment, while YAP abundance remains relatively stable. Under the assumption that some cancer cells show constitutive activation of the YAP/TAZ-dependent transcriptional program, this may indicate that nuclear YAP expression is a better predictor for Hippo pathway dysregulation in cancer cells and thus better correlates with lncRNA abundance in tissue and serum. However, this is contradicted by the fact that YAP and TAZ have exclusive binding partners leading to some unique transcriptional targets. For instance, the integrin ITGAV is an exclusive target of TAZ, which is upregulated in HCC and statistically associates with poor overall survival of patients[157]. Furthermore, ANGPTL4 is a direct target of TAZ, which promotes ferroptosis in ovarian cancer[252]. These findings demonstrate that TAZ indeed contributes to oncogenesis and tumor progression and drugs should be designed to account for the pro-tumorigenic functions of both Hippo pathway effectors.

Nevertheless, it remains unclear to what extent YAP and TAZ contribute to the transcriptional regulation of the lncRNA signature constituents in different cancer types. Further experiments are required to assess the role of TAZ as a predictor of Hippo pathway dysregulation in different cancer entities.

5.6 Outlook

In this work, I was able to define a lncRNA signature, which is transcriptionally controlled by YAP and TAZ in different tumor types (HCC, LUAD). Subsequent analysis of lncRNA expression data derived from the TCGA database indicated similar molecular relationships in different cancer entities (e.g., COAD, ACC). Thus, it is tempting to hypothesize that "core lncRNA signatures" exist, which are controlled by transcriptional regulators independent of the cellular background. However, further work is required to verify this concept: First, I only

demonstrated a significant correlation between lncRNA signature levels in serum and YAP activation in respective HCC tissue specimens. To confirm the idea of a pan-cancerous biomarker for aberrant Hippo pathway activity, this observed statistical association has to be validated in a different cancer cohort (e.g., LUAD, COAD). Second, it would be of high importance to understand why some tumors (e.g., UCEC, ESCA) do not show the same association of the lncRNA signature with YAP target gene levels. For these cancer entities, Hippo pathway-independent mechanisms could be of higher therapeutic relevance. Third, I chose the Hippo pathway as a showcase since its linearity and relative simplicity in comparison to other oncogenic pathways. Further work is required to define relevant and unique signatures that define aberrant activity of different oncogenes. Here, a potential strategy may be to not only focus on the transcriptional modules but also target upstream signaling components to identify pathway-specific lncRNAs. Moreover, I selected the YAP/TAZ-dependent lncRNA signature constituents based on the genetic manipulation of both key effectors. It may be of interest to include clinically relevant drugs in the selection process in order to define lncRNA signatures, whose abundance in the serum of patients directly correlates with therapeutic response to a certain medication.

As proof of principle, my data suggest that serum lncRNA signatures are predictive for the activity of transcriptional regulators in human cells. Considering that aberrant lncRNA expression is not only associated with cancer but also with other diseases and pre-malignancies[60], it is tempting to speculate that similar lncRNA signature read-outs exist that define specific disease characteristics. One potential example represents the formation of steatosis/fat accumulation/steatohepatitis in hepatocytes as well as fibrosis mediated by hepatic stellate cells. During the events of the pathogenesis of the liver, different lipogenesis-relevant transcription factors, such as USF1 and SREBP1[253], and pro-fibrotic transcription factors, including ATF3 and STAT3[254,255], are activated in hepatocytes and hepatic stellate cells, respectively. Thus, transcription factor-specific lncRNA signatures could serve as a proxy for the degree and severity level of steatosis, non-alcoholic steatohepatitis, and fibrosis in patients. Consequently, lncRNA signatures could represent valuable diagnostic tools for monitoring phases of precancerous liver damage.

Altogether, this work demonstrates the utility of lncRNA signatures as a surrogate for aberrant oncogenic activity. I developed a multi-step protocol for the reliable detection of lncRNAs in the serum of cancer patients. However, this method is not feasible for rapid high-throughput analyses in clinical routine. Thus, further research is required to develop suitable detection assays and to establish lncRNA-based liquid biopsy techniques as robust and sensitive tools in diagnostics.

6 Literature

1. National Research Council (US) Committee on A Framework for Developing a New Taxonomy of Disease. (2011). In Toward Precision Medicine: Building a Knowledge Network for Biomedical Research and a New Taxonomy of Disease.

2. Ashley, E.A. (2016). Towards precision medicine. Nat Rev Genet *17*, 507-522.

3. Adams, S.A., and Petersen, C. (2016). Precision medicine: opportunities, possibilities, and challenges for patients and providers. J Am Med Inform Assoc *23*, 787-790.

4. Hanahan, D., and Weinberg, R.A. (2011). Hallmarks of cancer: the next generation. Cell *144*, 646-674.

5. Reinert, T., Henriksen, T.V., Christensen, E., et al. (2019). Analysis of Plasma Cell-Free DNA by Ultradeep Sequencing in Patients With Stages I to III Colorectal Cancer. JAMA Oncol *5*, 1124-1131.

6. Kumar-Sinha, C., and Chinnaiyan, A.M. (2018). Precision oncology in the age of integrative genomics. Nat Biotechnol *36*, 46-60.

7. Riely, G.J., Neal, J.W., Camidge, D.R., et al. (2021). Activity and Safety of Mobocertinib (TAK-788) in Previously Treated Non-Small Cell Lung Cancer with EGFR Exon 20 Insertion Mutations from a Phase I/II Trial. Cancer Discov *11*, 1688-1699.

8. Wainwright, C.E., Elborn, J.S., Ramsey, B.W., et al. (2015). Lumacaftor-Ivacaftor in Patients with Cystic Fibrosis Homozygous for Phe508del CFTR. N Engl J Med *373*, 220-231.

9. Tutt, A.N.J., Garber, J.E., Kaufman, B., et al. (2021). Adjuvant Olaparib for Patients with BRCA1- or BRCA2-Mutated Breast Cancer. N Engl J Med *384*, 2394-2405.

10. FDA-NIH Biomarker Working Group. (2016). In BEST (Biomarkers, EndpointS, and other Tools) Resource.

11. Edgar, R., Domrachev, M., and Lash, A.E. (2002). Gene Expression Omnibus: NCBI gene expression and hybridization array data repository. Nucleic acids research *30*, 207-210.

12. The Cancer Genome Atlas Research Network, Weinstein, J.N., Collisson, E.A., et al. (2013). The Cancer Genome Atlas Pan-Cancer analysis project. Nature genetics *45*, 1113-1120.

13. Ilie, M., and Hofman, P. (2016). Pros: Can tissue biopsy be replaced by liquid biopsy? Transl Lung Cancer Res *5*, 420-423.

14. Gerlinger, M., Rowan, A.J., Horswell, S., et al. (2012). Intratumor heterogeneity and branched evolution revealed by multiregion sequencing. N Engl J Med *366*, 883-892.

15. Sholl, L.M., Aisner, D.L., Allen, T.C., et al. (2016). Liquid Biopsy in Lung Cancer: A Perspective From Members of the Pulmonary Pathology Society. Arch Pathol Lab Med *140*, 825-829.

16. Trujillo, B., Wu, A., Wetterskog, D., et al. (2022). Blood-based liquid biopsies for prostate cancer: clinical opportunities and challenges. Br J Cancer *127*, 1394-1402.

17. Siravegna, G., Marsoni, S., Siena, S., et al. (2017). Integrating liquid biopsies into the management of cancer. Nat Rev Clin Oncol *14*, 531-548.

18. Ignatiadis, M., Sledge, G.W., and Jeffrey, S.S. (2021). Liquid biopsy enters the clinic - implementation issues and future challenges. Nat Rev Clin Oncol *18*, 297-312.

19. Ko, J.M.Y., Ng, H.Y., Lam, K.O., et al. (2020). Liquid Biopsy Serial Monitoring of Treatment Responses and Relapse in Advanced Esophageal Squamous Cell Carcinoma. Cancers (Basel) *12*.

20. Lim, M., Kim, C.J., Sunkara, V., et al. (2018). Liquid Biopsy in Lung Cancer: Clinical Applications of Circulating Biomarkers (CTCs and ctDNA). Micromachines (Basel) *9*.

21. Maltoni, R., Casadio, V., Ravaioli, S., et al. (2017). Cell-free DNA detected by "liquid biopsy" as a potential prognostic biomarker in early breast cancer. Oncotarget *8*, 16642-16649.

22. Toden, S., and Goel, A. (2022). Non-coding RNAs as liquid biopsy biomarkers in cancer. Br J Cancer.

23. Thakur, B.K., Zhang, H., Becker, A., et al. (2014). Double-stranded DNA in exosomes: a novel biomarker in cancer detection. Cell Res *24*, 766-769.

24. Bardelli, A., and Pantel, K. (2017). Liquid Biopsies, What We Do Not Know (Yet). Cancer cell *31*, 172-179.

25. Siravegna, G., Mussolin, B., Venesio, T., et al. (2019). How liquid biopsies can change clinical practice in oncology. Ann Oncol *30*, 1580-1590.

26. Reckamp, K.L., Melnikova, V.O., Karlovich, C., et al. (2016). A Highly Sensitive and Quantitative Test Platform for Detection of NSCLC EGFR Mutations in Urine and Plasma. J Thorac Oncol *11*, 1690-1700.

27. Carethers, J.M. (2020). Fecal DNA Testing for Colorectal Cancer Screening. Annu Rev Med *71*, 59-69.

28. Wang, Y., Springer, S., Mulvey, C.L., et al. (2015). Detection of somatic mutations and HPV in the saliva and plasma of patients with head and neck squamous cell carcinomas. Sci Transl Med *7*, 293ra104.

29. Bobillo, S., Crespo, M., Escudero, L., et al. (2021). Cell free circulating tumor DNA in cerebrospinal fluid detects and monitors central nervous system involvement of B-cell lymphomas. Haematologica *106*, 513-521.

30. Ryder, S.D., and British Society of, G. (2003). Guidelines for the diagnosis and treatment of hepatocellular carcinoma (HCC) in adults. Gut *52 Suppl 3*, iii1-8.

31. Gosselaar, C., Roobol, M.J., Roemeling, S., et al. (2006). Screening for prostate cancer without digital rectal examination and transrectal ultrasound: results after four years in the European Randomized Study of Screening for Prostate Cancer (ERSPC), Rotterdam. Prostate *66*, 625-631.

32. Mocan, T., Simao, A.L., Castro, R.E., et al. (2020). Liquid Biopsies in Hepatocellular Carcinoma: Are We Winning? J Clin Med *9*.

33. Thompson, I.M., Pauler, D.K., Goodman, P.J., et al. (2004). Prevalence of prostate cancer among men with a prostate-specific antigen level < or =4.0 ng per milliliter. N Engl J Med *350*, 2239-2246.

34. Sartore-Bianchi, A., Pietrantonio, F., Lonardi, S., et al. (2022). Circulating tumor DNA to guide rechallenge with panitumumab in metastatic colorectal cancer: the phase 2 CHRONOS trial. Nat Med *28*, 1612-1618.

35. Warren, J.D., Xiong, W., Bunker, A.M., et al. (2011). Septin 9 methylated DNA is a sensitive and specific blood test for colorectal cancer. BMC Med *9*, 133.

36. Sacher, A.G., Paweletz, C., Dahlberg, S.E., et al. (2016). Prospective Validation of Rapid Plasma Genotyping for the Detection of EGFR and KRAS Mutations in Advanced Lung Cancer. JAMA Oncol *2*, 1014-1022.

37. Laufer-Geva, S., Rozenblum, A.B., Twito, T., et al. (2018). The Clinical Impact of Comprehensive Genomic Testing of Circulating Cell-Free DNA in Advanced Lung Cancer. J Thorac Oncol *13*, 1705-1716.

38. Riethdorf, S., O'Flaherty, L., Hille, C., et al. (2018). Clinical applications of the CellSearch platform in cancer patients. Adv Drug Deliv Rev *125*, 102-121.

39. De Rubis, G., Rajeev Krishnan, S., and Bebawy, M. (2019). Liquid Biopsies in Cancer Diagnosis, Monitoring, and Prognosis. Trends Pharmacol Sci *40*, 172-186.

40. Bertone, P., Stolc, V., Royce, T.E., et al. (2004). Global identification of human transcribed sequences with genome tiling arrays. Science *306*, 2242-2246.

41. Kapranov, P., Cheng, J., Dike, S., et al. (2007). RNA maps reveal new RNA classes and a possible function for pervasive transcription. Science *316*, 1484-1488.

42. Carninci, P., Kasukawa, T., Katayama, S., et al. (2005). The transcriptional landscape of the mammalian genome. Science *309*, 1559-1563.

43. Gutschner, T., and Diederichs, S. (2012). The hallmarks of cancer: a long non-coding RNA point of view. RNA biology *9*, 703-719.

44. Carthew, R.W., and Sontheimer, E.J. (2009). Origins and Mechanisms of miRNAs and siRNAs. Cell *136*, 642-655.

45. Malone, C.D., Brennecke, J., Dus, M., et al. (2009). Specialized piRNA pathways act in germline and somatic tissues of the Drosophila ovary. Cell *137*, 522-535.

46. Bartel, D.P. (2004). MicroRNAs: genomics, biogenesis, mechanism, and function. Cell *116*, 281-297.

47. Calin, G.A., and Croce, C.M. (2006). MicroRNA signatures in human cancers. Nat Rev Cancer *6*, 857-866.

48. Mattick, J.S., and Makunin, I.V. (2006). Non-coding RNA. Hum Mol Genet *15 Spec No 1*, R17-29.

49. Wu, Q., Kim, Y.C., Lu, J., et al. (2008). Poly A- transcripts expressed in HeLa cells. PLoS One *3*, e2803.

50. Cabili, M.N., Trapnell, C., Goff, L., et al. (2011). Integrative annotation of human large intergenic noncoding RNAs reveals global properties and specific subclasses. Genes Dev *25*, 1915-1927.

51. Washietl, S., Kellis, M., and Garber, M. (2014). Evolutionary dynamics and tissue specificity of human long noncoding RNAs in six mammals. Genome Res *24*, 616-628.

52. Zhao, X.Y., and Lin, J.D. (2015). Long Noncoding RNAs: A New Regulatory Code in Metabolic Control. Trends in biochemical sciences *40*, 586-596.

53. Balas, M.M., and Johnson, A.M. (2018). Exploring the mechanisms behind long noncoding RNAs and cancer. Noncoding RNA Res *3*, 108-117.

54. Huarte, M., Guttman, M., Feldser, D., et al. (2010). A large intergenic noncoding RNA induced by p53 mediates global gene repression in the p53 response. Cell *142*, 409-419.

55. Spitale, R.C., Tsai, M.C., and Chang, H.Y. (2011). RNA templating the epigenome: long noncoding RNAs as molecular scaffolds. Epigenetics *6*, 539-543.

56. Bousard, A., Raposo, A.C., Zylicz, J.J., et al. (2019). The role of Xist-mediated Polycomb recruitment in the initiation of X-chromosome inactivation. EMBO Rep *20*, e48019.

57. Zhu, H., Liu, Q., Yang, X., et al. (2022). LncRNA LINC00649 recruits TAF15 and enhances MAPK6 expression to promote the development of lung squamous cell carcinoma via activating MAPK signaling pathway. Cancer Gene Ther *29*, 1285-1295.

58. Hung, T., Wang, Y., Lin, M.F., et al. (2011). Extensive and coordinated transcription of noncoding RNAs within cell-cycle promoters. Nature genetics *43*, 621-629.

59. Poliseno, L., Salmena, L., Zhang, J., et al. (2010). A coding-independent function of gene and pseudogene mRNAs regulates tumour biology. Nature *465*, 1033-1038.

60. Bao, Z., Yang, Z., Huang, Z., et al. (2019). LncRNADisease 2.0: an updated database of long non-coding RNA-associated diseases. Nucleic acids research *47*, D1034-D1037.

61. Faghihi, M.A., Modarresi, F., Khalil, A.M., et al. (2008). Expression of a noncoding RNA is elevated in Alzheimer's disease and drives rapid feed-forward regulation of beta-secretase. Nat Med *14*, 723-730.

62. Moran, I., Akerman, I., van de Bunt, M., et al. (2012). Human beta cell transcriptome analysis uncovers lncRNAs that are tissue-specific, dynamically regulated, and abnormally expressed in type 2 diabetes. Cell metabolism *16*, 435-448.

Acknowledgments

63. Huarte, M. (2015). The emerging role of lncRNAs in cancer. Nat Med *21*, 1253-1261.

64. Yap, K.L., Li, S., Munoz-Cabello, A.M., et al. (2010). Molecular interplay of the noncoding RNA ANRIL and methylated histone H3 lysine 27 by polycomb CBX7 in transcriptional silencing of INK4a. Mol Cell *38*, 662-674.

65. Kotake, Y., Nakagawa, T., Kitagawa, K., et al. (2011). Long non-coding RNA ANRIL is required for the PRC2 recruitment to and silencing of p15(INK4B) tumor suppressor gene. Oncogene *30*, 1956-1962.

66. Cunnington, M.S., Santibanez Koref, M., Mayosi, B.M., et al. (2010). Chromosome 9p21 SNPs Associated with Multiple Disease Phenotypes Correlate with ANRIL Expression. PLoS Genet *6*, e1000899.

67. Tsai, M.C., Manor, O., Wan, Y., et al. (2010). Long noncoding RNA as modular scaffold of histone modification complexes. Science *329*, 689-693.

68. Zhang, J., Zhang, P., Wang, L., et al. (2014). Long non-coding RNA HOTAIR in carcinogenesis and metastasis. Acta Biochim Biophys Sin (Shanghai) *46*, 1-5.

69. Gupta, R.A., Shah, N., Wang, K.C., et al. (2010). Long non-coding RNA HOTAIR reprograms chromatin state to promote cancer metastasis. Nature *464*, 1071-1076.

70. Sanchez, Y., Segura, V., Marin-Bejar, O., et al. (2014). Genome-wide analysis of the human p53 transcriptional network unveils a lncRNA tumour suppressor signature. Nat Commun *5*, 5812.

71. Kim, T., Cui, R., Jeon, Y.J., et al. (2014). Long-range interaction and correlation between MYC enhancer and oncogenic long noncoding RNA CARLo-5. Proc Natl Acad Sci U S A *111*, 4173-4178.

72. Kim, T., Jeon, Y.J., Cui, R., et al. (2015). Role of MYC-regulated long noncoding RNAs in cell cycle regulation and tumorigenesis. J Natl Cancer Inst *107*.

73. Yoon, J.H., Abdelmohsen, K., Srikantan, S., et al. (2012). LincRNA-p21 suppresses target mRNA translation. Mol Cell *47*, 648-655.

74. Beltran, M., Puig, I., Pena, C., et al. (2008). A natural antisense transcript regulates Zeb2/Sip1 gene expression during Snail1-induced epithelial-mesenchymal transition. Genes Dev *22*, 756-769.

75. Poliseno, L., Haimovic, A., Christos, P.J., et al. (2011). Deletion of PTENP1 pseudogene in human melanoma. J Invest Dermatol *131*, 2497-2500.

76. Prensner, J.R., Iyer, M.K., Balbin, O.A., et al. (2011). Transcriptome sequencing across a prostate cancer cohort identifies PCAT-1, an unannotated lincRNA implicated in disease progression. Nat Biotechnol *29*, 742-749.

77. Li, Q., Shao, Y., Zhang, X., et al. (2015). Plasma long noncoding RNA protected by exosomes as a potential stable biomarker for gastric cancer. Tumour biology : the journal of the International Society for Oncodevelopmental Biology and Medicine *36*, 2007-2012.

78. Arita, T., Ichikawa, D., Konishi, H., et al. (2013). Circulating long non-coding RNAs in plasma of patients with gastric cancer. Anticancer Res *33*, 3185-3193.

79. Reis, E.M., and Verjovski-Almeida, S. (2012). Perspectives of Long Non-Coding RNAs in Cancer Diagnostics. Front Genet *3*, 32.

80. Ji, P., Diederichs, S., Wang, W., et al. (2003). MALAT-1, a novel noncoding RNA, and thymosin beta4 predict metastasis and survival in early-stage non-small cell lung cancer. Oncogene *22*, 8031-8041.

81. Ren, S., Peng, Z., Mao, J.H., et al. (2012). RNA-seq analysis of prostate cancer in the Chinese population identifies recurrent gene fusions, cancer-associated long noncoding RNAs and aberrant alternative splicings. Cell Res *22*, 806-821.

82. Weber, D.G., Johnen, G., Casjens, S., et al. (2013). Evaluation of long noncoding RNA MALAT1 as a candidate blood-based biomarker for the diagnosis of non-small cell lung cancer. BMC Res Notes *6*, 518.

Acknowledgments

83. Ren, S., Wang, F., Shen, J., et al. (2013). Long non-coding RNA metastasis associated in lung adenocarcinoma transcript 1 derived miniRNA as a novel plasma-based biomarker for diagnosing prostate cancer. Eur J Cancer *49*, 2949-2959.

84. Yu, W., Hurley, J., Roberts, D., et al. (2021). Exosome-based liquid biopsies in cancer: opportunities and challenges. Ann Oncol *32*, 466-477.

85. Svoboda, M., Slyskova, J., Schneiderova, M., et al. (2014). HOTAIR long non-coding RNA is a negative prognostic factor not only in primary tumors, but also in the blood of colorectal cancer patients. Carcinogenesis *35*, 1510-1515.

86. He, Z.H., Qin, X.H., Zhang, X.L., et al. (2018). Long noncoding RNA GIHCG is a potential diagnostic and prognostic biomarker and therapeutic target for renal cell carcinoma. European review for medical and pharmacological sciences *22*, 46-54.

87. El-Tawdi, A.H., Matboli, M., Shehata, H.H., et al. (2016). Evaluation of Circulatory RNA-Based Biomarker Panel in Hepatocellular Carcinoma. Mol Diagn Ther *20*, 265-277.

88. Hashad, D., Elbanna, A., Ibrahim, A., et al. (2016). Evaluation of the Role of Circulating Long Non-Coding RNA H19 as a Promising Novel Biomarker in Plasma of Patients with Gastric Cancer. J Clin Lab Anal *30*, 1100-1105.

89. Xian, H.P., Zhuo, Z.L., Sun, Y.J., et al. (2018). Circulating long non-coding RNAs HULC and ZNFX1-AS1 are potential biomarkers in patients with gastric cancer. Oncology letters *16*, 4689-4698.

90. Tan, L., Yang, Y., Shao, Y., et al. (2016). Plasma lncRNA-GACAT2 is a valuable marker for the screening of gastric cancer. Oncology letters *12*, 4845-4849.

91. Hu, X., Bao, J., Wang, Z., et al. (2016). The plasma lncRNA acting as fingerprint in non-small-cell lung cancer. Tumour biology : the journal of the International Society for Oncodevelopmental Biology and Medicine *37*, 3497-3504.

92. Yan, S., Du, L., Jiang, X., et al. (2020). Evaluation of Serum Exosomal lncRNAs as Diagnostic and Prognostic Biomarkers for Esophageal Squamous Cell Carcinoma. Cancer management and research *12*, 9753-9763.

93. Badowski, C., He, B., and Garmire, L.X. (2022). Blood-derived lncRNAs as biomarkers for cancer diagnosis: the Good, the Bad and the Beauty. NPJ Precis Oncol *6*, 40.

94. Zhao, B., Lei, Q.Y., and Guan, K.L. (2008). The Hippo-YAP pathway: new connections between regulation of organ size and cancer. Curr Opin Cell Biol *20*, 638-646.

95. Xu, T., Wang, W., Zhang, S., et al. (1995). Identifying tumor suppressors in genetic mosaics: the Drosophila lats gene encodes a putative protein kinase. Development *121*, 1053-1063.

96. Huang, J., Wu, S., Barrera, J., et al. (2005). The Hippo signaling pathway coordinately regulates cell proliferation and apoptosis by inactivating Yorkie, the Drosophila Homolog of YAP. Cell *122*, 421-434.

97. Meng, Z., Moroishi, T., and Guan, K.L. (2016). Mechanisms of Hippo pathway regulation. Genes Dev *30*, 1-17.

98. Callus, B.A., Verhagen, A.M., and Vaux, D.L. (2006). Association of mammalian sterile twenty kinases, Mst1 and Mst2, with hSalvador via C-terminal coiled-coil domains, leads to its stabilization and phosphorylation. FEBS J *273*, 4264-4276.

99. Praskova, M., Xia, F., and Avruch, J. (2008). MOBKL1A/MOBKL1B phosphorylation by MST1 and MST2 inhibits cell proliferation. Curr Biol *18*, 311-321.

100. Chan, E.H., Nousiainen, M., Chalamalasetty, R.B., et al. (2005). The Ste20-like kinase Mst2 activates the human large tumor suppressor kinase Lats1. Oncogene *24*, 2076-2086.

101. Dong, J., Feldmann, G., Huang, J., et al. (2007). Elucidation of a universal size-control mechanism in Drosophila and mammals. Cell *130*, 1120-1133.

102. Lei, Q.Y., Zhang, H., Zhao, B., et al. (2008). TAZ promotes cell proliferation and epithelial-mesenchymal transition and is inhibited by the hippo pathway. Mol Cell Biol *28*, 2426-2436.

103. Zhao, B., Li, L., Tumaneng, K., et al. (2010). A coordinated phosphorylation by Lats and CK1 regulates YAP stability through SCF(beta-TRCP). Genes Dev *24*, 72-85.

104. Liu, C.Y., Zha, Z.Y., Zhou, X., et al. (2010). The hippo tumor pathway promotes TAZ degradation by phosphorylating a phosphodegron and recruiting the SCF{beta}-TrCP E3 ligase. J Biol Chem *285*, 37159-37169.

105. Sugihara, T., Werneburg, N.W., Hernandez, M.C., et al. (2018). YAP Tyrosine Phosphorylation and Nuclear Localization in Cholangiocarcinoma Cells Are Regulated by LCK and Independent of LATS Activity. Mol Cancer Res *16*, 1556-1567.

106. Varelas, X., Samavarchi-Tehrani, P., Narimatsu, M., et al. (2010). The Crumbs complex couples cell density sensing to Hippo-dependent control of the TGF-beta-SMAD pathway. Dev Cell *19*, 831-844.

107. Strano, S., Munarriz, E., Rossi, M., et al. (2001). Physical interaction with Yes-associated protein enhances p73 transcriptional activity. J Biol Chem *276*, 15164-15173.

108. Weiler, S.M.E., Pinna, F., Wolf, T., et al. (2017). Induction of Chromosome Instability by Activation of Yes-Associated Protein and Forkhead Box M1 in Liver Cancer. Gastroenterology *152*, 2037-2051.e2022.

109. Zhao, B., Ye, X., Yu, J., et al. (2008). TEAD mediates YAP-dependent gene induction and growth control. Genes & development *22*, 1962-1971.

110. Kaneko, K.J., and DePamphilis, M.L. (1998). Regulation of gene expression at the beginning of mammalian development and the TEAD family of transcription factors. Dev Genet *22*, 43-55.

111. Wang, Y., Xu, X., Maglic, D., et al. (2018). Comprehensive Molecular Characterization of the Hippo Signaling Pathway in Cancer. Cell Rep *25*, 1304-1317 e1305.

112. Piccolo, S., Dupont, S., and Cordenonsi, M. (2014). The biology of YAP/TAZ: hippo signaling and beyond. Physiol Rev *94*, 1287-1312.

113. Ota, M., and Sasaki, H. (2008). Mammalian Tead proteins regulate cell proliferation and contact inhibition as transcriptional mediators of Hippo signaling. Development *135*, 4059-4069.

114. Zhao, B., Wei, X., Li, W., et al. (2007). Inactivation of YAP oncoprotein by the Hippo pathway is involved in cell contact inhibition and tissue growth control. Genes Dev *21*, 2747-2761.

115. Low, B.C., Pan, C.Q., Shivashankar, G.V., et al. (2014). YAP/TAZ as mechanosensors and mechanotransducers in regulating organ size and tumor growth. FEBS Lett *588*, 2663-2670.

116. Dupont, S., Morsut, L., Aragona, M., et al. (2011). Role of YAP/TAZ in mechanotransduction. Nature *474*, 179-183.

117. Aragona, M., Panciera, T., Manfrin, A., et al. (2013). A mechanical checkpoint controls multicellular growth through YAP/TAZ regulation by actin-processing factors. Cell *154*, 1047-1059.

118. Yu, F.X., Zhao, B., Panupinthu, N., et al. (2012). Regulation of the Hippo-YAP pathway by G-protein-coupled receptor signaling. Cell *150*, 780-791.

119. DeRan, M., Yang, J., Shen, C.H., et al. (2014). Energy stress regulates hippo-YAP signaling involving AMPK-mediated regulation of angiomotin-like 1 protein. Cell Rep *9*, 495-503.

120. Lehtinen, M.K., Yuan, Z., Boag, P.R., et al. (2006). A conserved MST-FOXO signaling pathway mediates oxidative-stress responses and extends life span. Cell *125*, 987-1001.

121. Ma, B., Chen, Y., Chen, L., et al. (2015). Hypoxia regulates Hippo signalling through the SIAH2 ubiquitin E3 ligase. Nat Cell Biol *17*, 95-103.

122. Cunningham, R., and Hansen, C.G. (2022). The Hippo pathway in cancer: YAP/TAZ and TEAD as therapeutic targets in cancer. Clin Sci (Lond) *136*, 197-222.

123. Wang, L., Shi, S., Guo, Z., et al. (2013). Overexpression of YAP and TAZ is an independent predictor of prognosis in colorectal cancer and related to the proliferation and metastasis of colon cancer cells. PLoS One *8*, e65539.

124. Diep, C.H., Zucker, K.M., Hostetter, G., et al. (2012). Down-regulation of Yes Associated Protein 1 expression reduces cell proliferation and clonogenicity of pancreatic cancer cells. PLoS One *7*, e32783.

125. Zanconato, F., Cordenonsi, M., and Piccolo, S. (2016). YAP/TAZ at the Roots of Cancer. Cancer cell *29*, 783-803.

126. Koo, J.H., Plouffe, S.W., Meng, Z., et al. (2020). Induction of AP-1 by YAP/TAZ contributes to cell proliferation and organ growth. Genes Dev *34*, 72-86.

127. Mizuno, T., Murakami, H., Fujii, M., et al. (2012). YAP induces malignant mesothelioma cell proliferation by upregulating transcription of cell cycle-promoting genes. Oncogene *31*, 5117-5122.

128. Liu, X., Li, H., Rajurkar, M., et al. (2016). Tead and AP1 Coordinate Transcription and Motility. Cell Rep *14*, 1169-1180.

129. Rosenbluh, J., Nijhawan, D., Cox, A.G., et al. (2012). beta-Catenin-driven cancers require a YAP1 transcriptional complex for survival and tumorigenesis. Cell *151*, 1457-1473.

130. Song, Q., Mao, B., Cheng, J., et al. (2015). YAP enhances autophagic flux to promote breast cancer cell survival in response to nutrient deprivation. PLoS One *10*, e0120790.

131. Bartucci, M., Dattilo, R., Moriconi, C., et al. (2015). TAZ is required for metastatic activity and chemoresistance of breast cancer stem cells. Oncogene *34*, 681-690.

132. Cordenonsi, M., Zanconato, F., Azzolin, L., et al. (2011). The Hippo transducer TAZ confers cancer stem cell-related traits on breast cancer cells. Cell *147*, 759-772.

133. Hayashi, H., Higashi, T., Yokoyama, N., et al. (2015). An Imbalance in TAZ and YAP Expression in Hepatocellular Carcinoma Confers Cancer Stem Cell-like Behaviors Contributing to Disease Progression. Cancer Res *75*, 4985-4997.

134. Yimlamai, D., Christodoulou, C., Galli, G.G., et al. (2014). Hippo pathway activity influences liver cell fate. Cell *157*, 1324-1338.

135. Evans, D.G. (2009). Neurofibromatosis 2 [Bilateral acoustic neurofibromatosis, central neurofibromatosis, NF2, neurofibromatosis type II]. Genet Med *11*, 599-610.

136. Zhang, N., Zhao, Z., Long, J., et al. (2017). Molecular alterations of the NF2 gene in hepatocellular carcinoma and intrahepatic cholangiocarcinoma. Oncology reports *38*, 3650-3658.

137. Johnson, R., and Halder, G. (2014). The two faces of Hippo: targeting the Hippo pathway for regenerative medicine and cancer treatment. Nat Rev Drug Discov *13*, 63-79.

138. Tanas, M.R., Sboner, A., Oliveira, A.M., et al. (2011). Identification of a disease-defining gene fusion in epithelioid hemangioendothelioma. Sci Transl Med *3*, 98ra82.

139. Antonescu, C.R., Le Loarer, F., Mosquera, J.M., et al. (2013). Novel YAP1-TFE3 fusion defines a distinct subset of epithelioid hemangioendothelioma. Genes Chromosomes Cancer *52*, 775-784.

140. Andreiuolo, F., Varlet, P., Tauziede-Espariat, A., et al. (2019). Childhood supratentorial ependymomas with YAP1-MAMLD1 fusion: an entity with characteristic clinical, radiological, cytogenetic and histopathological features. Brain Pathol *29*, 205-216.

Acknowledgments

141. Overholtzer, M., Zhang, J., Smolen, G.A., et al. (2006). Transforming properties of YAP, a candidate oncogene on the chromosome 11q22 amplicon. Proc Natl Acad Sci U S A *103*, 12405-12410.

142. Zender, L., Spector, M.S., Xue, W., et al. (2006). Identification and validation of oncogenes in liver cancer using an integrative oncogenomic approach. Cell *125*, 1253-1267.

143. Plouffe, S.W., Hong, A.W., and Guan, K.L. (2015). Disease implications of the Hippo/YAP pathway. Trends Mol Med *21*, 212-222.

144. Heinrich, T., Peterson, C., Schneider, R., et al. (2022). Optimization of TEAD P-Site Binding Fragment Hit into In Vivo Active Lead MSC-4106. J Med Chem *65*, 9206-9229.

145. Holden, J.K., Crawford, J.J., Noland, C.L., et al. (2020). Small Molecule Dysregulation of TEAD Lipidation Induces a Dominant-Negative Inhibition of Hippo Pathway Signaling. Cell Rep *31*, 107809.

146. Tscharganeh, D.F., Chen, X., Latzko, P., et al. (2013). Yes-associated protein up-regulates Jagged-1 and activates the Notch pathway in human hepatocellular carcinoma. Gastroenterology *144*, 1530-1542 e1512.

147. Xu, M.Z., Yao, T.J., Lee, N.P., et al. (2009). Yes-associated protein is an independent prognostic marker in hepatocellular carcinoma. Cancer *115*, 4576-4585.

148. Guo, Y., Pan, Q., Zhang, J., et al. (2015). Functional and clinical evidence that TAZ is a candidate oncogene in hepatocellular carcinoma. J Cell Biochem *116*, 2465-2475.

149. Lin, C., Hu, Z., Lei, B., et al. (2017). Overexpression of Yes-associated protein and its association with clinicopathological features of hepatocellular carcinoma: A meta-analysis. Liver international : official journal of the International Association for the Study of the Liver *37*, 1675-1681.

150. Cai, W.Y., Lin, L.Y., Hao, H., et al. (2017). Yes-associated protein/TEA domain family member and hepatocyte nuclear factor 4-alpha (HNF4alpha) repress reciprocally to regulate hepatocarcinogenesis in rats and mice. Hepatology *65*, 1206-1221.

151. Perra, A., Kowalik, M.A., Ghiso, E., et al. (2014). YAP activation is an early event and a potential therapeutic target in liver cancer development. J Hepatol *61*, 1088-1096.

152. Camargo, F.D., Gokhale, S., Johnnidis, J.B., et al. (2007). YAP1 increases organ size and expands undifferentiated progenitor cells. Curr Biol *17*, 2054-2060.

153. Shen, S., Guo, X., Yan, H., et al. (2015). A miR-130a-YAP positive feedback loop promotes organ size and tumorigenesis. Cell Res *25*, 997-1012.

154. Zhang, N., Bai, H., David, K.K., et al. (2010). The Merlin/NF2 tumor suppressor functions through the YAP oncoprotein to regulate tissue homeostasis in mammals. Dev Cell *19*, 27-38.

155. Xiao, H., Jiang, N., Zhou, B., et al. (2015). TAZ regulates cell proliferation and epithelial-mesenchymal transition of human hepatocellular carcinoma. Cancer Sci *106*, 151-159.

156. Xiao, W., Wang, J., Ou, C., et al. (2013). Mutual interaction between YAP and c-Myc is critical for carcinogenesis in liver cancer. Biochem Biophys Res Commun *439*, 167-172.

157. Weiler, S.M.E., Lutz, T., Bissinger, M., et al. (2020). TAZ target gene ITGAV regulates invasion and feeds back positively on YAP and TAZ in liver cancer cells. Cancer Lett *473*, 164-175.

158. Moon, H., Park, H., Chae, M.J., et al. (2022). Activated TAZ induces liver cancer in collaboration with EGFR/HER2 signaling pathways. BMC Cancer 22, 423.

159. Wang, H., Zhang, S., Zhang, Y., et al. (2022). TAZ is indispensable for c-MYC-induced hepatocarcinogenesis. J Hepatol *76*, 123-134.

160. Zhou, D., Conrad, C., Xia, F., et al. (2009). Mst1 and Mst2 maintain hepatocyte quiescence and suppress hepatocellular carcinoma development through inactivation of the Yap1 oncogene. Cancer cell *16*, 425-438.

161. Kim, J.M., Kang, D.W., Long, L.Z., et al. (2011). Differential expression of Yes-associated protein is correlated with expression of cell cycle markers and pathologic TNM staging in non-small-cell lung carcinoma. Human pathology *42*, 315-323.

162. Cui, Z.L., Han, F.F., Peng, X.H., et al. (2012). YES-associated protein 1 promotes adenocarcinoma growth and metastasis through activation of the receptor tyrosine kinase Axl. Int J Immunopathol Pharmacol *25*, 989-1001.

163. Luo, S.Y., Sit, K.Y., Sihoe, A.D., et al. (2014). Aberrant large tumor suppressor 2 (LATS2) gene expression correlates with EGFR mutation and survival in lung adenocarcinomas. Lung Cancer *85*, 282-292.

164. Lau, A.N., Curtis, S.J., Fillmore, C.M., et al. (2014). Tumor-propagating cells and Yap/Taz activity contribute to lung tumor progression and metastasis. The EMBO journal *33*, 468-481.

165. Noguchi, S., Saito, A., Horie, M., et al. (2014). An integrative analysis of the tumorigenic role of TAZ in human non-small cell lung cancer. Clin Cancer Res *20*, 4660-4672.

166. Zhang, W., Gao, Y., Li, F., et al. (2015). YAP promotes malignant progression of Lkb1-deficient lung adenocarcinoma through downstream regulation of survivin. Cancer Res *75*, 4450-4457.

167. Fornes, O., Castro-Mondragon, J.A., Khan, A., et al. (2020). JASPAR 2020: update of the open-access database of transcription factor binding profiles. Nucleic acids research *48*, D87-D92.

168. Kursa, M.B., and Rudnicki, W.R. (2010). Feature Selection with the Boruta Package. Journal of Statistical Software *36*, 1 - 13.

169. Yu, G., Wang, L.G., and He, Q.Y. (2015). ChIPseeker: an R/Bioconductor package for ChIP peak annotation, comparison and visualization. Bioinformatics *31*, 2382-2383.

170. Guzman, C., Bagga, M., Kaur, A., et al. (2014). ColonyArea: an ImageJ plugin to automatically quantify colony formation in clonogenic assays. PLoS One *9*, e92444.

171. Gu, Z., Eils, R., and Schlesner, M. (2016). Complex heatmaps reveal patterns and correlations in multidimensional genomic data. Bioinformatics *32*, 2847-2849.

172. Bray, N.L., Pimentel, H., Melsted, P., et al. (2016). Near-optimal probabilistic RNA-seq quantification. Nat Biotechnol *34*, 525-527.

173. Ritchie, M.E., Phipson, B., Wu, D., et al. (2015). limma powers differential expression analyses for RNA-sequencing and microarray studies. Nucleic acids research *43*, e47.

174. Robin, X., Turck, N., Hainard, A., et al. (2011). pROC: an open-source package for R and S+ to analyze and compare ROC curves. BMC Bioinformatics *12*, 77.

175. TW, H.B., and Girke, T. (2016). systemPipeR: NGS workflow and report generation environment. BMC Bioinformatics *17*, 388.

176. Pohl, A., and Beato, M. (2014). bwtool: a tool for bigWig files. Bioinformatics *30*, 1618-1619.

177. Chen, H., and Boutros, P.C. (2011). VennDiagram: a package for the generation of highly-customizable Venn and Euler diagrams in R. BMC Bioinformatics *12*, 35.

178. Galli, G.G., Carrara, M., Yuan, W.-C., et al. (2015). YAP Drives Growth by Controlling Transcriptional Pause Release from Dynamic Enhancers. Mol Cell *60*, 328-337.

179. Consortium, E.P. (2012). An integrated encyclopedia of DNA elements in the human genome. Nature *489*, 57-74.

180. Gertz, J., Savic, D., Varley, K.E., et al. (2013). Distinct properties of cell-type-specific and shared transcription factor binding sites. Mol Cell *52*, 25-36.

181. Pellegrino, R., Castoldi, M., Ticconi, F., et al. (2022). LINC00152 Drives a Competing Endogenous RNA Network in Human Hepatocellular Carcinoma. Cells *11*.

Acknowledgments

182. Barretina, J., Caponigro, G., Stransky, N., et al. (2012). The Cancer Cell Line Encyclopedia enables predictive modelling of anticancer drug sensitivity. Nature *483*, 603-607.

183. Rueden, C.T., Schindelin, J., Hiner, M.C., et al. (2017). ImageJ2: ImageJ for the next generation of scientific image data. BMC Bioinformatics *18*, 529.

184. Berg, S., Kutra, D., Kroeger, T., et al. (2019). ilastik: interactive machine learning for (bio)image analysis. Nat Methods *16*, 1226-1232.

185. Schindelin, J., Arganda-Carreras, I., Frise, E., et al. (2012). Fiji: an open-source platform for biological-image analysis. Nat Methods *9*, 676-682.

186. Goldman, M.J., Craft, B., Hastie, M., et al. (2020). Visualizing and interpreting cancer genomics data via the Xena platform. Nat Biotechnol *38*, 675-678.

187. Carter, S.L., Eklund, A.C., Kohane, I.S., et al. (2006). A signature of chromosomal instability inferred from gene expression profiles predicts clinical outcome in multiple human cancers. Nature genetics *38*, 1043-1048.

188. Liu-Chittenden, Y., Huang, B., Shim, J.S., et al. (2012). Genetic and pharmacological disruption of the TEAD-YAP complex suppresses the oncogenic activity of YAP. Genes Dev *26*, 1300-1305.

189. Lennox, K.A., and Behlke, M.A. (2016). Cellular localization of long non-coding RNAs affects silencing by RNAi more than by antisense oligonucleotides. Nucleic acids research *44*, 863-877.

190. Li, B., Li, A., You, Z., et al. (2020). Epigenetic silencing of CDKN1A and CDKN2B by SNHG1 promotes the cell cycle, migration and epithelial-mesenchymal transition progression of hepatocellular carcinoma. Cell Death Dis *11*, 823.

191. Bum-Erdene, K., Zhou, D., Gonzalez-Gutierrez, G., et al. (2019). Small-Molecule Covalent Modification of Conserved Cysteine Leads to Allosteric Inhibition of the TEADYap Protein-Protein Interaction. Cell Chem Biol *26*, 378-389 e313.

192. Chan, K.C., Jiang, P., Zheng, Y.W., et al. (2013). Cancer genome scanning in plasma: detection of tumor-associated copy number aberrations, single-nucleotide variants, and tumoral heterogeneity by massively parallel sequencing. Clin Chem *59*, 211-224.

193. Balgkouranidou, I., Chimonidou, M., Milaki, G., et al. (2014). Breast cancer metastasis suppressor-1 promoter methylation in cell-free DNA provides prognostic information in non-small cell lung cancer. Br J Cancer *110*, 2054-2062.

194. Elshimali, Y.I., Khaddour, H., Sarkissyan, M., et al. (2013). The clinical utilization of circulating cell free DNA (CCFDNA) in blood of cancer patients. Int J Mol Sci *14*, 18925-18958.

195. Leighl, N.B., Page, R.D., Raymond, V.M., et al. (2019). Clinical Utility of Comprehensive Cell-free DNA Analysis to Identify Genomic Biomarkers in Patients with Newly Diagnosed Metastatic Non-small Cell Lung Cancer. Clin Cancer Res *25*, 4691-4700.

196. Brown, P. (2016). The Cobas(R) EGFR Mutation Test v2 assay. Future Oncol *12*, 451-452.

197. Hitchins, M.P., Vogelaar, I.P., Brennan, K., et al. (2019). Methylated SEPTIN9 plasma test for colorectal cancer detection may be applicable to Lynch syndrome. BMJ Open Gastroenterol *6*, e000299.

198. Lianidou, E.S., Strati, A., and Markou, A. (2014). Circulating tumor cells as promising novel biomarkers in solid cancers. Crit Rev Clin Lab Sci *51*, 160-171.

199. Masuda, T., Hayashi, N., Iguchi, T., et al. (2016). Clinical and biological significance of circulating tumor cells in cancer. Molecular oncology *10*, 408-417.

200. Micalizzi, D.S., Maheswaran, S., and Haber, D.A. (2017). A conduit to metastasis: circulating tumor cell biology. Genes Dev *31*, 1827-1840.

Acknowledgments

201. Allard, W.J., Matera, J., Miller, M.C., et al. (2004). Tumor cells circulate in the peripheral blood of all major carcinomas but not in healthy subjects or patients with nonmalignant diseases. Clin Cancer Res *10*, 6897-6904.

202. Lack, J., Gillard, M., Cam, M., et al. (2017). Circulating tumor cells capture disease evolution in advanced prostate cancer. J Transl Med *15*, 44.

203. Bidard, F.C., Michiels, S., Riethdorf, S., et al. (2018). Circulating Tumor Cells in Breast Cancer Patients Treated by Neoadjuvant Chemotherapy: A Meta-analysis. J Natl Cancer Inst *110*, 560-567.

204. Hardingham, J.E., Grover, P., Winter, M., et al. (2015). Detection and Clinical Significance of Circulating Tumor Cells in Colorectal Cancer--20 Years of Progress. Mol Med *21 Suppl 1*, S25-31.

205. Xie, H., Ma, H., and Zhou, D. (2013). Plasma HULC as a promising novel biomarker for the detection of hepatocellular carcinoma. Biomed Res Int *2013*, 136106.

206. Kamel, M.M., Matboli, M., Sallam, M., et al. (2016). Investigation of long noncoding RNAs expression profile as potential serum biomarkers in patients with hepatocellular carcinoma. Translational research : the journal of laboratory and clinical medicine *168*, 134-145.

207. Rosell, R., Moran, T., Queralt, C., et al. (2009). Screening for epidermal growth factor receptor mutations in lung cancer. N Engl J Med *361*, 958-967.

208. Chong, C.R., and Janne, P.A. (2013). The quest to overcome resistance to EGFR-targeted therapies in cancer. Nat Med *19*, 1389-1400.

209. Mayo-de-Las-Casas, C., Jordana-Ariza, N., Garzon-Ibanez, M., et al. (2017). Large scale, prospective screening of EGFR mutations in the blood of advanced NSCLC patients to guide treatment decisions. Ann Oncol *28*, 2248-2255.

210. Openshaw, M.R., Mohamed, A.A., Ottolini, B., et al. (2020). Longitudinal monitoring of circulating tumour DNA improves prognostication and relapse detection in gastroesophageal adenocarcinoma. Br J Cancer *123*, 1271-1279.

211. Ji, H., Long, X., Gu, J., et al. (2021). Longitudinal Monitoring of Plasma Circulating Tumour DNA Enables the Prediction of Early Relapse in Patients with Non-Hodgkin Lymphoma: A Case Series. Diagnostics (Basel) *11*.

212. Binder, S., Zipfel, I., Friedrich, M., et al. (2020). Master and servant: LINC00152 - a STAT3-induced long noncoding RNA regulates STAT3 in a positive feedback in human multiple myeloma. BMC medical genomics *13*, 22.

213. Williams, G.T., and Farzaneh, F. (2012). Are snoRNAs and snoRNA host genes new players in cancer? Nat Rev Cancer *12*, 84-88.

214. Zimta, A.A., Tigu, A.B., Braicu, C., et al. (2020). An Emerging Class of Long Non-coding RNA With Oncogenic Role Arises From the snoRNA Host Genes. Frontiers in oncology *10*, 389.

215. Lykke-Andersen, S., Chen, Y., Ardal, B.R., et al. (2014). Human nonsense-mediated RNA decay initiates widely by endonucleolysis and targets snoRNA host genes. Genes Dev *28*, 2498-2517.

216. Kufel, J., and Grzechnik, P. (2019). Small Nucleolar RNAs Tell a Different Tale. Trends Genet *35*, 104-117.

217. Liu, L., Shi, Y., Shi, J., et al. (2019). The long non-coding RNA SNHG1 promotes glioma progression by competitively binding to miR-194 to regulate PHLDA1 expression. Cell Death Dis *10*, 463.

218. Chen, W., Wang, L., Li, X., et al. (2021). LncRNA SNHG17 regulates cell proliferation and invasion by targeting miR-338-3p/SOX4 axis in esophageal squamous cell carcinoma. Cell Death Dis *12*, 806.

Acknowledgments

219. Sun, Y., Wei, G., Luo, H., et al. (2017). The long noncoding RNA SNHG1 promotes tumor growth through regulating transcription of both local and distal genes. Oncogene *36*, 6774-6783.

220. Zhang, H., Wang, S.Q., Wang, L., et al. (2022). m6A methyltransferase METTL3-induced lncRNA SNHG17 promotes lung adenocarcinoma gefitinib resistance by epigenetically repressing LATS2 expression. Cell Death Dis *13*, 657.

221. Zhao, Y., Qin, Z.S., Feng, Y., et al. (2018). Long non-coding RNA (lncRNA) small nucleolar RNA host gene 1 (SNHG1) promote cell proliferation in colorectal cancer by affecting P53. European review for medical and pharmacological sciences *22*, 976-984.

222. Xu, T., Yan, S., Jiang, L., et al. (2019). Gene Amplification-Driven Long Noncoding RNA SNHG17 Regulates Cell Proliferation and Migration in Human Non-Small-Cell Lung Cancer. Mol Ther Nucleic Acids *17*, 405-413.

223. Huang, L., Jiang, X., Wang, Z., et al. (2018). Small nucleolar RNA host gene 1: A new biomarker and therapeutic target for cancers. Pathol Res Pract *214*, 1247-1252.

224. Ma, L., Gao, J., Zhang, N., et al. (2022). Long noncoding RNA SNHG17: a novel molecule in human cancers. Cancer cell international *22*, 104.

225. Nötzold, L., Frank, L., Gandhi, M., et al. (2017). The long non-coding RNA LINC00152 is essential for cell cycle progression through mitosis in HeLa cells. Scientific reports *7*, 2265.

226. Zhong, C., Xie, Z., Zeng, L.H., et al. (2022). MIR4435-2HG Is a Potential Pan-Cancer Biomarker for Diagnosis and Prognosis. Front Immunol *13*, 855078.

227. Wu, T., Zhang, D.L., Wang, J.M., et al. (2020). TRIM29 inhibits miR-873-5P biogenesis via CYTOR to upregulate fibronectin 1 and promotes invasion of papillary thyroid cancer cells. Cell Death Dis *11*, 813.

228. Zhu, W., Wang, J., Liu, X., et al. (2022). lncRNA CYTOR promotes aberrant glycolysis and mitochondrial respiration via HNRNPC-mediated ZEB1 stabilization in oral squamous cell carcinoma. Cell Death Dis *13*, 703.

229. Wang, X., Yu, H., Sun, W., et al. (2018). The long non-coding RNA CYTOR drives colorectal cancer progression by interacting with NCL and Sam68. Molecular cancer *17*, 110.

230. Yu, Y., Yang, J., Li, Q., et al. (2017). LINC00152: A pivotal oncogenic long non-coding RNA in human cancers. Cell proliferation *50*.

231. Liu, Y., Li, M., Yu, H., et al. (2020). lncRNA CYTOR promotes tamoxifen resistance in breast cancer cells via sponging miR-125a-5p. International journal of molecular medicine *45*, 497-509.

232. Liu, C.Y., Chan, S.W., Guo, F., et al. (2016). MRTF/SRF dependent transcriptional regulation of TAZ in breast cancer cells. Oncotarget *7*, 13706-13716.

233. Dong, X., Yang, Z., Yang, H., et al. (2020). Long Non-coding RNA MIR4435-2HG Promotes Colorectal Cancer Proliferation and Metastasis Through miR-206/YAP1 Axis. Frontiers in oncology *10*, 160.

234. Shen, W., Zhang, J., Pan, Y., et al. (2021). LncRNA MIR4435-2HG functions as a ceRNA against miR-125a-5p and promotes neuroglioma development by upregulating TAZ. J Clin Lab Anal *35*, e24066.

235. Cheng, F., Wang, L., Yi, S., et al. (2022). Long non-coding RNA SNHG1/microRNA-195-5p/Yes-associated protein axis affects the proliferation and metastasis of gastric cancer via the Hippo signaling pathway. Funct Integr Genomics *22*, 1043-1055.

236. Dey, A., Varelas, X., and Guan, K.L. (2020). Targeting the Hippo pathway in cancer, fibrosis, wound healing and regenerative medicine. Nat Rev Drug Discov *19*, 480-494.

237. Tang, T.T., Konradi, A.W., Feng, Y., et al. (2021). Small Molecule Inhibitors of TEAD Auto-palmitoylation Selectively Inhibit Proliferation and Tumor Growth of NF2-deficient Mesothelioma. Mol Cancer Ther *20*, 986-998.

238. Dasari, V.R., Mazack, V., Feng, W., et al. (2017). Verteporfin exhibits YAP-independent anti-proliferative and cytotoxic effects in endometrial cancer cells. Oncotarget *8*, 28628-28640.

239. Zhang, H., Ramakrishnan, S.K., Triner, D., et al. (2015). Tumor-selective proteotoxicity of verteporfin inhibits colon cancer progression independently of YAP1. Sci Signal *8*, ra98.

240. Santucci, M., Vignudelli, T., Ferrari, S., et al. (2015). The Hippo Pathway and YAP/TAZ-TEAD Protein-Protein Interaction as Targets for Regenerative Medicine and Cancer Treatment. J Med Chem *58*, 4857-4873.

241. Wehling, L., Keegan, L., Fernandez-Palanca, P., et al. (2022). Spatial modeling reveals nuclear phosphorylation and subcellular shuttling of YAP upon drug-induced liver injury. Elife *11*.

242. Noto, A., De Vitis, C., Pisanu, M.E., et al. (2017). Stearoyl-CoA-desaturase 1 regulates lung cancer stemness via stabilization and nuclear localization of YAP/TAZ. Oncogene *36*, 4573-4584.

243. Aikawa, T., Gunn, J., Spong, S.M., et al. (2006). Connective tissue growth factor-specific antibody attenuates tumor growth, metastasis, and angiogenesis in an orthotopic mouse model of pancreatic cancer. Mol Cancer Ther *5*, 1108-1116.

244. Gill, M.K., Christova, T., Zhang, Y.Y., et al. (2018). A feed forward loop enforces YAP/TAZ signaling during tumorigenesis. Nat Commun *9*, 3510.

245. Yui, S., Azzolin, L., Maimets, M., et al. (2018). YAP/TAZ-Dependent Reprogramming of Colonic Epithelium Links ECM Remodeling to Tissue Regeneration. Cell Stem Cell *22*, 35-49 e37.

246. ClinicalTrial (2021). A Phase I Study of IAG933 in Patients With Advanced Mesothelioma and Other Solid Tumors. https://ClinicalTrials.gov/show/NCT04857372.

247. ClinicalTrial (2021). Study to Evaluate VT3989 in Patients With Metastatic Solid Tumors Enriched for Tumors With NF2 Gene Mutations. https://ClinicalTrials.gov/show/NCT04665206.

248. ClinicalTrial (2022). Oral TEAD Inhibitor Targeting the Hippo Pathway in Subjects With Advanced Solid Tumors. https://ClinicalTrials.gov/show/NCT05228015.

249. Finch-Edmondson, M.L., Strauss, R.P., Passman, A.M., et al. (2015). TAZ Protein Accumulation Is Negatively Regulated by YAP Abundance in Mammalian Cells. J Biol Chem *290*, 27928-27938.

250. Muppala, S., Raghunathan, V.K., Jalilian, I., et al. (2019). YAP and TAZ are distinct effectors of corneal myofibroblast transformation. Exp Eye Res *180*, 102-109.

251. Miranda, M.Z., Bialik, J.F., Speight, P., et al. (2017). TGF-beta1 regulates the expression and transcriptional activity of TAZ protein via a Smad3-independent, myocardin-related transcription factor-mediated mechanism. J Biol Chem *292*, 14902-14920.

252. Yang, W.H., Huang, Z., Wu, J., et al. (2020). A TAZ-ANGPTL4-NOX2 Axis Regulates Ferroptotic Cell Death and Chemoresistance in Epithelial Ovarian Cancer. Mol Cancer Res *18*, 79-90.

253. Wang, Y., Viscarra, J., Kim, S.J., et al. (2015). Transcriptional regulation of hepatic lipogenesis. Nat Rev Mol Cell Biol *16*, 678-689.

254. Shi, Z., Zhang, K., Chen, T., et al. (2020). Transcriptional factor ATF3 promotes liver fibrosis via activating hepatic stellate cells. Cell Death Dis *11*, 1066.

255. Xiang, D.M., Sun, W., Ning, B.F., et al. (2018). The HLF/IL-6/STAT3 feedforward circuit drives hepatic stellate cell activation to promote liver fibrosis. Gut *67*, 1704-1715.

7 Acknowledgments

Mein Dank gilt zunächst Prof. Dr. Peter Schirmacher und PD Dr. Kai Breuhahn für die Möglichkeit, meine Doktorarbeit am Pathologischen Institut des Universitätsklinikums Heidelberg zu verfassen und für Ihre Unterstützung in den letzten Jahren.

Ganz besonders möchte ich mich bei Dr. Kai Breuhahn bedanken, der mir dieses spannende Projekt anvertraut hat und mir immer mit Rat und Tat zur Seite stand. Kai, vielen Dank für die jederzeit offene Tür, deine Unterstützung sowie dein in mich gesetztes Vertrauen bei der Umsetzung dieses auf dem Papier nicht ganz risikoarmen Projekts. Ich glaube, wir haben einen ganz guten Job gemacht. Durch deine Ideen und dein Mitwirken konnte ich mich in vielen Bereichen weiterentwickeln. Außerdem vielen Dank für die tolle und produktive Arbeitsatmosphäre sowie die Begutachtung dieser Arbeit.

Ich möchte mich auch herzlich bei Prof. Dr. Peter Angel für die Bereitschaft bedanken, diese Arbeit zu betreuen und zu begutachten.

Prof. Dr. Stefan Wölfl möchte ich für seine Bereitschaft danken, als Prüfer in meiner Disputation zu fungieren und diese Dissertation vor der Biowissenschaftlichen Fakultät der Universität Heidelberg zu vertreten.

Mein weiterer Dank gilt auch Prof. Dr. Ursula Klingmüller für ihre Bereitschaft, als Prüferin an meiner Disputation teilzunehmen.

Zudem möchte ich mich bei allen Kollaborationspartnern bedanken, die einen wesentlichen Beitrag zum Gelingen dieser Arbeit geleistet haben:

- Prof. Dr. Ahmed Ihab Abdelaziz Fahmy und den Mitgliedern seiner Arbeitsgruppe für die gelungene Kollaboration und die hilfreichen Diskussionen während unser regelmäßigen Telefonkonferenzen
- Prof. Dr. Norbert Gretz, Dr. Carsten Sticht und Dr. Carolina de la Torre für die Unterstützung bei der Analyse der RNA-Sequenzierungsdaten
- Prof. Dr. Arndt Vogel, Prof. Dr. Heike Bantel, Prof. Dr. Thomas Illig, Dr. Anna Saborowksi und PD Dr. Bruno C. Köhler für die Bereitstellung von HCC-Patientenmaterial (Serum und Gewebe)

Acknowledgments
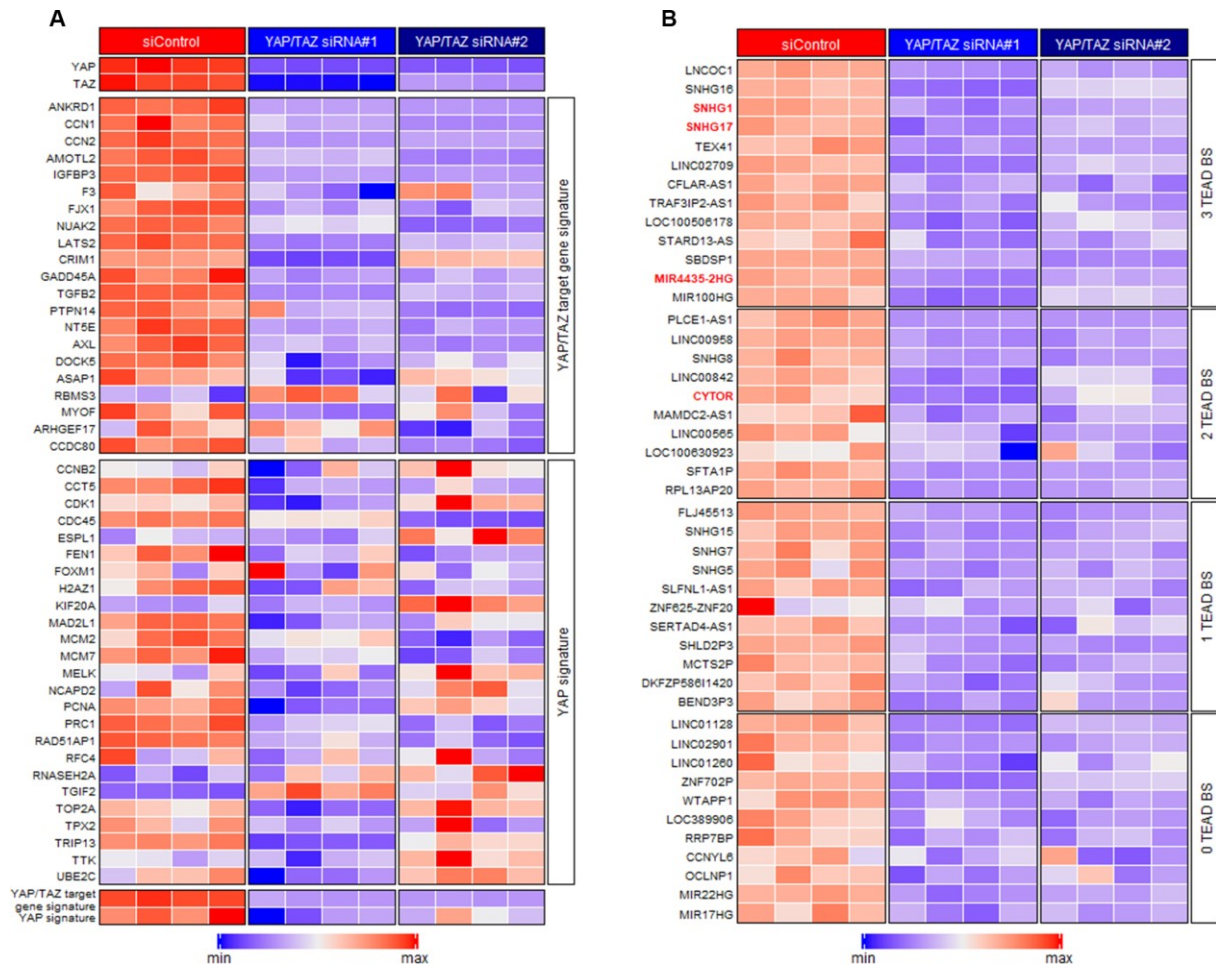
APPENDIX

Figure Appendix 1

Figure Appendix 1 | Identification of YAP/TAZ-regulated lncRNAs in HCC cells. (A) Heatmap summarizing NGS data for YAP/TAZ and YAP/TAZ-known target genes in HLF cells after combined inhibition of YAP/TAZ for 24 h. Genes were retrieved from a previously published Hippo pathway signature (21/22 genes)[111] and a YAP target gene signature associated with chromosomal instability (CIN25; 25/25 genes)[108,187]. Two different combinations of different siRNAs for YAP and TAZ were employed (#1, #2); 4 biologically independent samples for each inhibition and control were analyzed. **(B)** Heatmap summarizing NGS data for differentially expressed lncRNAs in HLF cells after YAP/TAZ inhibition for 24 h. lncRNAs (n = 45) were clustered according to the number of predicted TEAD BS (0-3 TEAD BS) and only lncRNAs with at least 2 TEAD BS were considered for further analysis (n = 23). Constituents of the final lncRNA signature are highlighted in red (n = 4). Two different combinations of siRNAs for YAP and TAZ were employed (#1, #2); 4 biologically independent samples for each RNAi experiment and controls were analyzed.
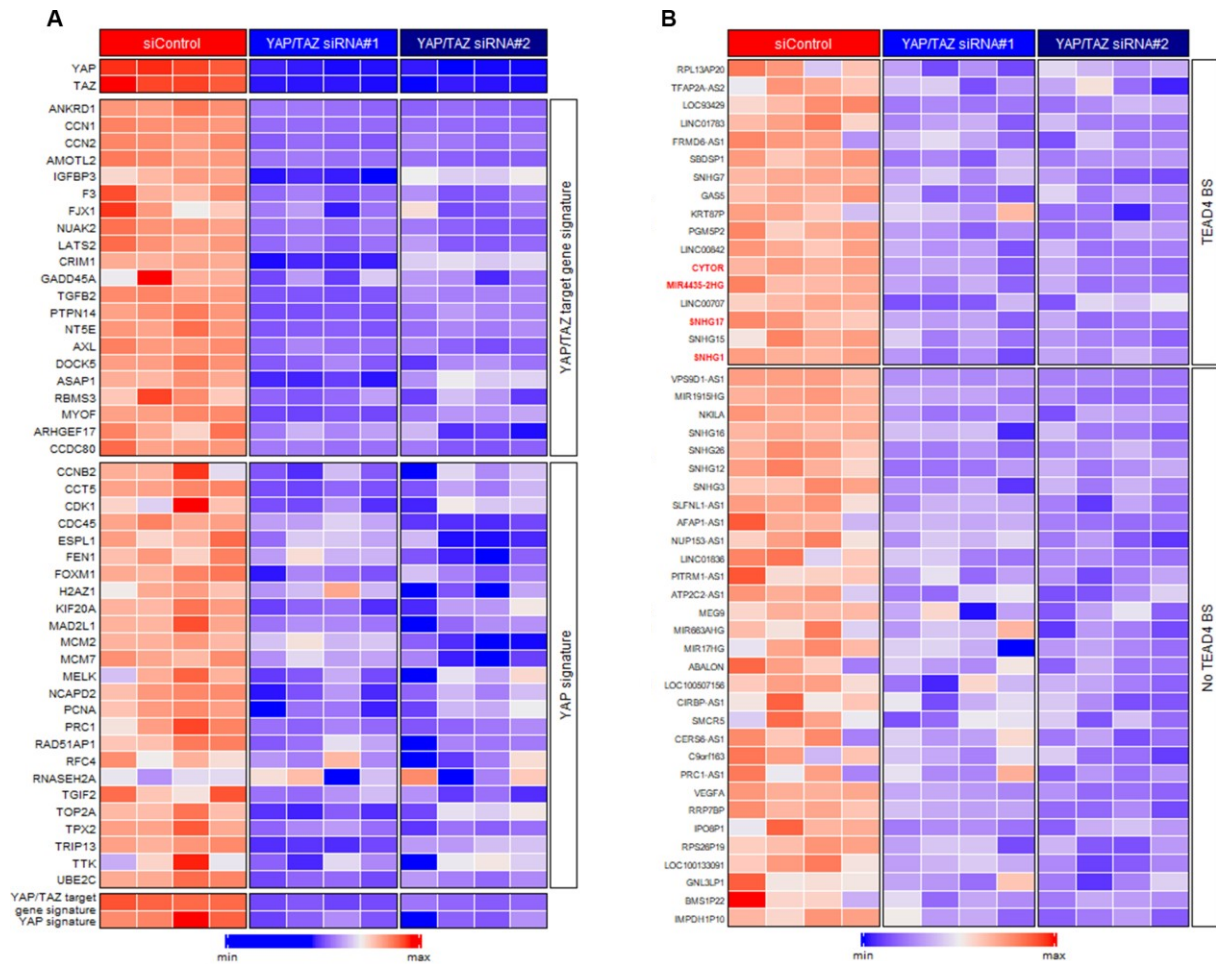
Figure Appendix 2

Figure Appendix 2| Identification of YAP/TAZ-regulated lncRNAs in LUAD cells. (A) Heatmap summarizing NGS data for YAP/TAZ and YAP/TAZ-known target genes in A549 cells after combined inhibition of YAP/TAZ for 24 h. Genes were retrieved from a previously published Hippo pathway signature (21/22 genes)[111] and a YAP target gene signature associated with chromosomal instability (CIN25; 25/25 genes)[108,187]. Two different combinations of different siRNAs for YAP and TAZ were employed (#1, #2); 4 biologically independent samples for each inhibition and control were analyzed. **(B)** Heatmap summarizing NGS data for differentially expressed lncRNAs in A549 cells after YAP/TAZ knockdown. lncRNAs (n = 48) were clustered according to the number of predicted TEAD binding sites. Because only TEAD4 ChIP-Seq data was available, all lncRNAs with 1 TEAD BS were considered for further analysis (n = 17). Selected candidate lncRNAs are highlighted in red. Two different combinations of siRNAs for YAP and TAZ were employed (#1, #2); 4 biologically independent samples for each inhibition and control were analyzed.
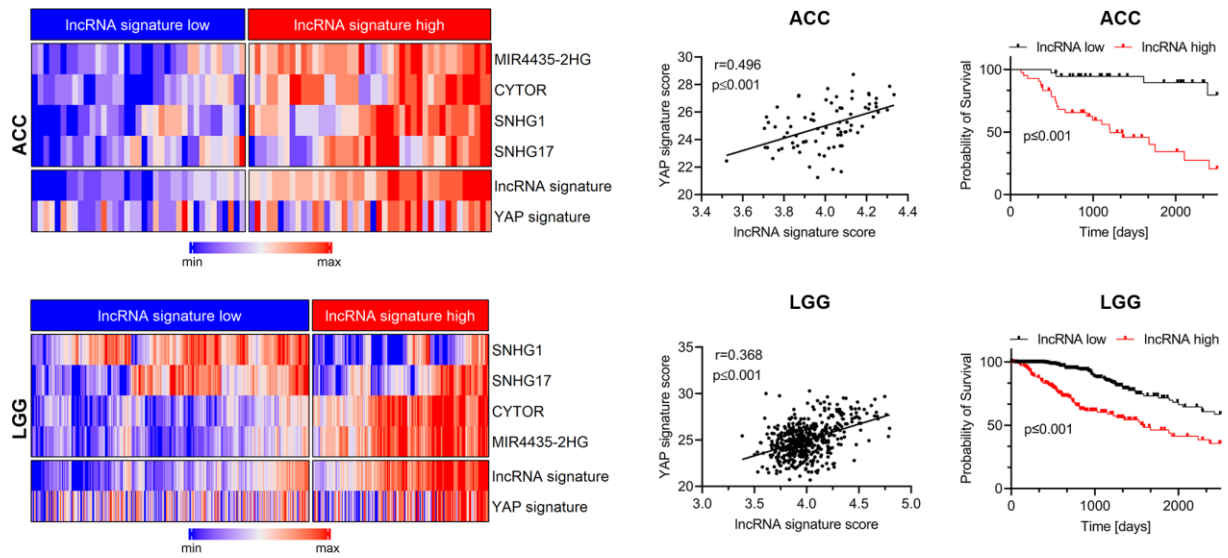
Figure Appendix 3

Figure Appendix 3 | Detection of the YAP/TAZ-regulated lncRNA signature in different tumor types. The presence of the 4 lncRNA signature was investigated in adrenocortical carcinoma (ACC) and low-grade glioma (LGG). Data illustrate a strong association between the presence of the lncRNA signature score and of the YAP-dependent CIN25 signature. For both tumor types, the respective heatmap after K-mean clustering, lncRNA/CIN25 signature correlation, and patient survival are shown (Kaplan-Meier survival curves with low and high lncRNA signature expression, log-rank test).

Eidesstattliche Versicherung gemäß §8 der Promotionsordnung

Hiermit erkläre ich, dass ich die vorgelegte Dissertation " A pan-cancer long non-coding RNA (lncRNA) signature defines oncogene activity in blood serum of cancer patients" selbstständig verfasst und keine anderen als die angegebenen Quellen und Hilfsmittel benutzt habe. Des Weiteren bestätige ich, dass ich an keiner anderen Stelle ein Prüfungsverfahren beantragt bzw. die Dissertation in dieser oder einer anderen Form bereits als Prüfungsarbeit verwendet oder einer anderen Fakultät als Dissertation vorgelegt habe.

Heidelberg, den

Fabian Rose